Characterization of cell mismatch in photovoltaic modules using electroluminescence and associated electro-optic techniques

Jacqueline Louise Crozier

Submitted in fulfilment of the requirements for the degree of

Magister Scientiae

in the Faculty of Science at the Nelson Mandela Metropolitan University

January 2012

Supervisor: Prof E.E. van Dyk

Co-Supervisor: Dr F.J. Vorster

Declaration

Full Names: Jacqueline Louise Crozier

Student No: 207094248

Qualification: Magister Scientiae

In accordance with Rule G4.6.3, I hereby declare that the above-mentioned treatise/ dissertation/ thesis is my own work and that it has not previously been submitted for assessment to another University or for another qualification.

Jacqueline Louise Crozier

Dated: 5 January 2012

Acknowledgements

My sincere thanks to:

- My supervisor, **Prof E.E. van Dyk** for his guidance, support and encouragement throughout my research.
- My co-supervisor, **Dr F.J. Vorster** for his advice and assistance.
- **Mr Johan Wessels** for his technical assistance.
- **Mr Peet Booysen** from Setsolar for his assistance with module samples.
- The colleagues and friends in the Physics department and PV research group for their input, assistance and companionship during this project.
- **Ms. Jualine Ferreira** and **Miss Mariska Muller** for their administrative help.
- **Centre for Renewable and Sustainable Energy Studies (CRSES)** and the **Nelson Mandela Metropolitan University** for their financial support.
- A special thanks to my parents and family for their support and encouragement during the course of my studies.

Abstract

Solar cells allow the energy from the sun to be converted into electrical energy; this makes solar energy much more environmentally friendly than fossil fuel energy sources. These solar cells are connected together in a photovoltaic (PV) module to provide the higher current, voltage and power outputs necessary for electrical applications. However, the performance of the PV module is limited by the performance of the individual cells. Cell mismatch occurs when some cells are damaged or shaded and produce lower current output than the other cells in the series connected string. The cell mismatch lowers the module performance and can result in further damage as the weak cells are reverse biased and dissipate heat. Bypass diodes can be connected into the module to increase the module current output and prevent further damage. Since cell mismatch results in a significant decrease in the performance of deployed modules it is important to fully understand and characterise its effect on PV modules.

PV modules can be characterised using various techniques, each providing important information about the performance of the module. Most commonly the current-voltage (I-V) characteristic curve of a module is measured in outdoor, fully illuminated conditions. This allows performance parameters such as short circuit current (Isc), open circuit voltage (Voc) and maximum power (Pmax) to be determined. In addition to this the shape of the curve allows device parameters like series and shunt resistances to be determined using parameter extraction algorithms like Particle Swarm Optimisation (PSO). The extracted parameters can be entered into the diode equation to model the I-V curve of the module. The I-V characteristic of the module can also be used to identify poor current producing cells in the module by using the worst-case cell determination method. In this technique a cell is shaded and the greater the drop in current in the whole module the better the current production of the shaded cell. The photoresponse of cells in a module can be determined by the Large-area Light Beam Induced Current (LA-LBIC) technique which involves scanning a module with a laser beam and recording the current generated. Electroluminescence (EL) is emitted by a forward biased PV module and is used to identify defects in cell material. Defects such as cracks and broken fingers can be detected as well as material features such as grain boundaries. These techniques are used to in conjunction to characterise the modules used in this study.

The modules investigated in this study each exhibit cell mismatch resulting from different causes. Each module is characterised using a combination of characterisation techniques which allows the effect of cell mismatch be investigated. EL imaging enabled cracks and defects, invisible to the naked eye, to be detected allowing the reduced performance observed in I-V curves to be explained. It was seen that the cracked cells have a significant effect on the current produced by a string, while the effect of delaminated areas is less severe. Hot spots are observed on weak cells indicating they are in reverse bias conditions and will degrade further with time. PSO parameter extraction from I-V curves revealed that the effect of module degradation of device parameters like series and shunt resistances. A module with cracked cells and degradation of the antireflective coating has low shunt resistance indicating current losses due to shunting. Similar shunting is observed in a module with delamination and moisture ingress. The extracted parameters are used to simulate the I-V curves of modules with reasonable fit. The fit could be improved around the "knee" of the I-V curve by improving the methods of parameter extraction.

This study has shown the effects of cell mismatch on the performance and I-V curves of the PV modules. The different causes of cell mismatch are discussed and modules with different cell configuration and damage are characterised. The characterisation techniques used on each module provide information about the photoresponse, current generation, material properties and cell defects. A comprehensive understanding of these techniques allows the cell mismatch in the modules to be fully characterised.

Contents

Declaration......ii

Acknowledgements......iii

Abstract......iv

Contents......vi

List of Tables......viii

List of Figures......viii

Chapter 1: Introduction......1

1.1. Overview of Photovoltaics in South Africa......1

1.2. Research Objectives......2

1.3. Outline......2

Chapter 2: Photovoltaic device physics......4

2.1. Introduction......4

2.2. Physics of Solar Cells......4

2.3. Solar Cell Materials......14

2.4. Photovoltaic (PV) Modules......14

2.5. Summary......15

Chapter 3: Characterisation Techniques......16

3.1. Current-Voltage Characteristics......16

3.2. Large-Area Laser Beam Induced Current (LA-LBIC)......28

3.3. Electroluminescence 28

3.4. Infrared Imaging 32

3.5. Summary 33

Chapter 4: Experimental Details 34

4.1. Introduction 34

4.2. Current-Voltage (I-V) Characterisation Setup and Methodology 34

4.3. Large Area Light Beam Induced Current (LA-LBIC) measurement system set-up and methodology 38

4.4. Electroluminescence (EL) set-up and methodology 40

4.5. Modules in study 41

4.6. Summary 44

Chapter 5: Results and Discussion 45

5.1. Introduction 45

5.2. Module 1 45

5.3. Module 2 49

5.4. Module 3 58

5.5. Modules 4, 5 and 6 66

5.6. Conclusions 75

Chapter 6: Summary 76

Chapter 7: References 79

Appendix A 83

Research outputs associated with this work 83

Appendix B 84

List of Tables

Table 4.1: Summary of Modules used in this study and manufacturer given parameters. 44

Table 5.1: Performance Parameters of Module 1 47

Table 5.2: The module parameters of Module 2. 50

Table 5.3: Average extracted parameters for a single cell. 51

Table 5.4: Device parameters for a single ideal multi-crystalline silicon cell. 59

Table 5.5: Performance Parameters of the measured and ideal I-V curve. 59

Table 5.6: Average extracted parameters for a single cell. 59

Table 5.7: The extracted series and shunt resistances for Modules 4, 5 and 6 74

List of Figures

Figure 2.1: Energy bands introduced in by a) Group V impurity and b) Group III impurity. 5

Figure 2.2: The Energy- Crystal Momentum diagram of absorption in: a) a direct band gap material, b) an indirect band gap material. 6

Figure 2.3: The Energy- Crystal Momentum diagram of radiative recombination in: a) a direct band gap material and in b)an indirect band gap material. 7

Figure 2.4: Isolated p- and n- materials with respective energy-band structure. 8

Figure 2.5: The p-n junction structure with energy band diagram at thermal equilibrium. 9

Figure 2.6: The equivalent circuit of an ideal solar cell 10

Figure 2.7: The structure of a p-n solar diode. 11

Figure 2.8: The equivalent circuit of a solar cell in a) dark and b) illuminated conditions. 12

Figure 2.9: The equivalent circuit of the two-diode model in
a) dark and b) illuminated conditions. 12

Figure 2.10: The equivalent circuit of one-diode model with additional breakdown voltage term. .13

Figure 2.11: Typical construction of a silicon PV module. 15

Figure 3.1: Light Current-Voltage Curve of Solar cell. 17

Figure 3.2: The I-V curve of a solar cell modelled with a series resistance parameter of 0.01Ω or 0.1Ω. 18

Figure 3.3: The I-V curves of two cells with different open circuit voltages are shown with the resultant I-V curve. 21

Figure 3.4: The I-V curves of two cells with different short circuit currents connected in parallel are shown with the resultant I-V curve.. 21

Figure 3.5: The equivalent circuit of two matched solar cells in a) short circuit and b) open circuit conditions. 22

Figure 3.6: The equivalent circuit of mismatched cells under a) short circuit and b) open circuit conditions. 23

Figure 3.7: The equivalent circuit of two solar cells with parallel bypass diodes in short circuit conditions with a) matched and b) mismatched currents. 24

Figure 3.8: The effect of mismatch in series string of three cells with one cell shaded 50%. 25

Figure 3.9: The effect of shading one cell in a 3 cell series string by 50% on the resultant I-V curve with bypass diodes connected across each cell. 26

Figure 3.10: The Dark I-V curve of a PV module. 27

Figure 3.11: The Dark I-V curve of a PV module on a logarithmic scale. 27

Figure 3.12: Illustration of the EL principle showing carriers injected into the solar cell by applying a forward bias. 29

Figure 3.13: The typical emission spectrum of silicon and the sensitivity of a Si-CCD camera...... 29

Figure 3.14: The distribution of carriers in the p layer of a p-n silicon cell. The effect of the applied forward voltage is illustrated. 31

Figure 4.1: a) The Outdoor I-V tracer system. b) Schematic of the component configuration. 35

Figure 4.2: The dark I-V system with components labelled. 37

Figure 4.3: Schematic of the dark I-V system a) for a single solar cell and b) for PV modules........ 37

Figure 4.4: The experimental setup of the LA-LBIC system. 39

Figure 4.5: The LA-LBIC system with laser mounted on carriage below PV module. 39

Figure 4.6: Schematic outline of EL experimental setup. 40

Figure 4.7: I-V curve with point of forward bias indicated. 40

Figure 4.8: Module 1 with the strings indicated. 41

Figure 4.9: Diagram of cells connected in series strings and the bypass diodes connected across the strings in parallel 41

Figure 4.10: Module 2 with visible delamination around the edges of the module. 42

Figure 4.11: An optical image of the custom-made 36 cell multi-crystalline silicon module with dimensions 110 cm x 12 cm. 43

Figure 4.12: Optical image of a) Module 4(reference), b) Module 5 and c) Module 6. 43

Figure 5.1: Photograph of 72 cell single crystalline silicon module with strings indicated. 46

Figure 5.2: I-V curves of the individual strings and the whole module with bypass diodes..............47

Figure 5.3: I-V curve of the undamaged module compared with the measured curves of the module with and without bypass diodes.47

Figure 5.4: a) Optical image and b) Infrared image of the same portion of the module with damaged portion of string C labelled i) and a hot spot in string B labelled ii)............................. 48

Figure 5.5: The I-V curves of module 2 with and without bypass diodes and the simulated curve of the undamaged module. 50

Figure 5.6: The measured I-V curve of module 2 compared with the curve simulated using the Mathematica model... 52

Figure 5.7: The dark I-V curve of module 2.. 52

Figure 5.8: Optical image of module 2 with cells B1, D4 and C9 highlighted.................................54

Figure 5.9: Optical image of cells a) B1, b) D4 and c) C9 with the direction of the line scan indicated. The line scans of cells d) B1, e) D4 and f) C9.. 55

Figure 5.10: (a) Optical image of EFG module with cells indicated. (b) EL image of cell C5 with defects highlighted, (c) EL image of cell C9 showing the effect of delamination....... 56

Figure 5.11: Infrared image of a portion of the EFG module .... .57

Figure 5.12: The measure I-V curve of the measured curved, the Mathematica modelled I-V curve and the ideal, simulated I-V curve .... .59

Figure 5.13: Dark I-V curve of module 3. 60

Figure 5.14: An optical image of module 3. 61

Figure 5.15: An EL image of the module under forward bias of 2 A. The white areas indicate high EL intensity. The arrow indicates the path of the LA-LBIC line scan. .... .61

Figure 5.16: Enlarged EL image of cells 1(left) to cell 7(right) with defects indicated. .... .61

Figure 5.17: Infrared image of module in forward bias with hot spot at cells 4 and 5. 62

Figure 5.18: Large Area LBIC scan of module. 63

Figure 5:19: The Isc values of the module with one cell shaded plotted against the number of the shaded cell. 64

Figure 5:20: I-V Curve of the whole module compared with the I-V curves of the module with cells 5, 12 and 14 shaded... 65

Figure 5.21: I-V curves of reference module and the individual strings. 67

Figure 5.22: The EL image of (a) the entire reference module with (b) a section enlarged to illustrate common cell defects. 68

Figure 5.23: I-V curve of Module 5 and the individual strings. 69

Figure 5.24: The EL image of (a) module 5 with EL images of defects enlarged b) degradation of anti-reflective, c) micro-cracks resulting in high current density and d) micro-cracks resulting in inactive areas. 70

Figure 5.25: I-V curve of module 6 and the individual strings.. 71

Figure 5.26: The EL image of the (a) entire module 6 with (b) the most damaged cell highlighted..72

Figure 5.27: The I-V curves of modules 4, 5 and 6 without bypass diodes..................................... 73

Figure 5.28: Dark I-V curves of modules 4, 5 and 6 7

Chapter 1

Introduction

1.1. Overview of Photovoltaics in South Africa

Solar cells are able to produce energy from the abundant resource of sunlight. The photo-electric effect was first observed by Becquerel in 1839 when a light-dependant voltage was measured from an electrolyte solution. This was later developed into a solid state system using semiconductor materials and by 1954 silicon was the preferred material [1]. Further developments in solar cell production and design in recent years has made solar energy a viable and sustainable option to traditional fossil fuel energy.

The radiant power per unit area emitted by the sun outside the earth's atmosphere is known as the solar constant. The solar constant used in PV research is 1.353 kW/m^2 [1] however, the earth's atmosphere reduces the solar constant through scattering and absorption processes. But even with these losses the daily irradiance on a sunny day can be in the region of 700- 1000 W/m^2. South Africa is in an ideal country to utilise solar energy as it has an above average number of sunlight hours in a year. Solar energy is a reliable resource that is easy to predict and forecast, unlike wind energy which is less predictable. PV power is already used very effectively in off grid applications providing electricity in rural areas. The large areas of stable land required for large scale photovoltaic installations are available in South Africa's, for example in the Northern Cape area. At the moment over 90% of South Africa energy is generated by the burning of coal and it is the sixth largest consumer of coal in the world [2]. Alternative energies need to be considered to lower the country's carbon emissions to be in line with international guidelines.

Key to the large-scale implementation of solar energy is PV modules that have reliable power outputs over a long period of time. Cell mismatch can severely lower the performance and effective lifetime of a PV module. A PV module consists of many solar cells that are connected in series to form a string, with each solar cell contributing to the total voltage of the string and the output current determined by the individual cell current outputs. It is important that the solar cells are well matched within each string in terms of current output as the overall PV module current output is limited by the weakest cell. A cell can produce lower current as a result of front-surface soiling, shading of cells, optical degradation, manufacturer defects and cracked cells [3]. In research done in the 90s, the 1000-Roofs-PV-Programme [4], the main reduction in power output was due to partial shadowing of the modules. Due to the growing demand and interest in photovoltaics (PV) there is a need to understand the factors that cause performance degradation and failure in these devices.

1.2. Research Objectives

In this study cell mismatch in a photovoltaic module will be investigated by using several characterisation techniques and comparing the results in order to fully understand the effects of shaded and damaged cells on the module performance. The effect of cell mismatch will be investigated in the measured current-voltage (I-V) characteristic curve by comparing it with the simulated curves and extracting the device parameters. Further aims involve comparing the results from electroluminescence (EL) imaging, Large-area Light Beam Induced Current (LA-LBIC) scans and thermal imaging to identify defects and assess their influence in the performance of the module. Modules with different cell materials and module configuration are used to understand the different causes of cell mismatch in PV modules.

1.3. Outline

This section outlines and summaries the following chapters providing an overview of the scope of the study.

Chapter 2: An introduction to photovoltaic device physics with a discussion of semiconductor properties and absorptions and recombination processes. The formation of a p-n diode from n- and p-type semiconductor materials is discussed and the equations modelling the current-voltage behaviour of a solar cell are introduced. The different semiconductor materials used for solar cells are discussed as well as the connection of cells into PV modules.

Chapter 3: The characterisation techniques used in the study are discussed in detail. Explanation of how the current-voltage characteristic (I-V) curve provides the performance parameters of the module and can indicate the presence of cell mismatch is provided. Other I-V techniques such as dark I-Vs, worst-case cell determination, parameter extraction and I-V curve modelling are also discussed. The effects of cell mismatch on the I-V curve of a module and the formation of hot spots is discussed in detail. The principles behind LA-LBIC, electroluminescence and thermal imaging are introduced.

Chapter 4: The experimental setup of the characterisation techniques and the modules used in the study are discussed. The setups and equipment used in the outdoor and dark I-V tracer system are discussed. The physics involved in the recombination processes essential for electroluminescence imaging are introduced. The setup and methodology of the large-area LBIC system is discussed. The modules used in the study are introduced and cell material and configuration are discussed.

Chapter 5: The results of the characterisation of the six PV modules used in the study are given in this chapter. The cell mismatch in each module is discussed with reference to the different characterisation techniques used.

Chapter 6: The results and conclusions of the studies are summarised in this chapter.

Chapter 2

Photovoltaic device physics

2.1. Introduction

Photovoltaic (PV) devices convert the energy from light into an electrical current using the photoelectric effect. The physics behind semiconductor diodes and semiconductor materials used in the solar cells are discussed in this chapter. The semiconductor materials used for PV devices and the construction of PV modules are also discussed.

2.2. Physics of Solar Cells

2.2.1. Semiconductor Properties

Atoms have electrons arranged in bands of specific energy levels. In semiconductor materials the conduction and valence bands are separated by an energy gap, E_g [5]. The density of states function N(E) gives an indication of the number of allowed states per energy level as seen in figure 2.1. At absolute zero the valence band of a semiconductor is completely occupied by electrons and the conduction band is completely empty. The position of the Fermi energy level, E_F, is important as it indicates the level at which, at zero degrees Kelvin, all the levels below are occupied and all the levels above are empty. In semiconductor materials the energy gap is small and electrons can be excited into the conduction band by amongst others an increase in temperature or from an interaction with a photon. The electron is excited to the conduction band leaving a hole in the valence band. The hole is considered a mobile positive charge and the electron a mobile negative charge.

Semiconductor material can be doped to introduce additional energy levels [1]. Impurity atoms can occupy positions in between the silicon atoms called an interstitial impurity. The impurity atom can also substitute for the silicon atom in the regular atomic arrangement called a substitutional impurity. By introducing a periodic table group V element, such as phosphorous, as a substitutional impurity in silicon, an extra electron is introduced in the crystal bond structure. The group V impurity makes four covalent bonds with the neighbouring silicon atoms however the fifth electron is not in a covalent bond and thus not in the valence band. The energy required to free this electron to the conduction band is 0.02 eV much less than the band-gap energy of silicon 1.1 eV [1]. This extra electron tied to the group V atom introduces a donor level, E_D, below the conduction band E_C, as seen in figure 2.1a). The material is known as n-type and has an excess of electrons. In a similar way p-type material is doped with a group III element which has fewer valence electrons then is necessary to form the four covalent bonds with the neighbouring silicon atoms. This introduces an extra hole and thus an acceptor level, E_A, above the valance band, as seen in figure 2.1b). Electrons in the valence band are excited into the acceptor level creating additional mobile positive holes in the valence band. In n-type semiconductor material the electrons are referred to as the majority carriers and the holes as the minority carrier while in p-type semiconductor material the holes are the majority carriers and the electrons are the minority carriers.

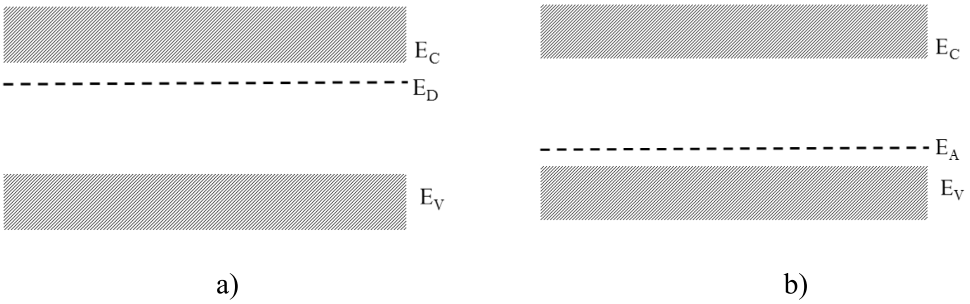

Figure 2.1: Energy bands introduced in by a) Group V impurity and b) Group III impurity.

2.2.2. Mobility of Carriers

Carriers can move though semiconductor material by two carrier transport mechanisms, drift and diffusion. Drift occurs as an applied electric field causes an electron to accelerate in a direction opposite to electric field [1]. However, the crystal structure of the semiconductor material results in collisions which prevent the drift velocity from increasing uniformly. The mobility of carriers is related to the strength of the electric field, the level of doping in the material, the quality of the semiconductor material and the temperature [1].

Diffusion occurs as carriers move from a high concentration to a low concentration in order to achieve equilibrium. The diffusion of carriers is important to the functioning of a p-n diode discussed in section 2.2.5.

2.2.3. Photon Absorption

Two primary photon absorption processes occur in semiconductor material used for solar devices, namely fundamental absorption and free carrier absorption [5]. Fundamental absorption occurs when an incident photon has energy equal to or greater than the band gap of the material generating electron-holes pairs. The energy that is greater than the band gap is lost thermally. Free carrier absorption occurs when the energy of the photon is absorbed by a free carrier increasing its kinetic energy but resulting in no additional energy band transitions.

Energy and momentum must be conserved in the absorption process. A photon has energy, equal to *hf* where *h* is Planck's constant and *f* is the frequency of the light, and momentum, equal to *h/λ* where λ is the wavelength [1]. Therefore a photon is a particle with high energy but low momentum. In a direct band gap material like GaAs the momentum remains the same and only the energy of a photon is needed for absorption as shown in figure 2.2(a). However in indirect gap materials like crystalline silicon the conservation of energy and momentum of an excited electron can only be achieved with a photon and a phonon, as shown in figure 2.2(b). A phonon is a fundamental particle with low energy and high momentum. The necessity of an extra particle makes absorption in in-direct semiconductor materials like silicon less probable.

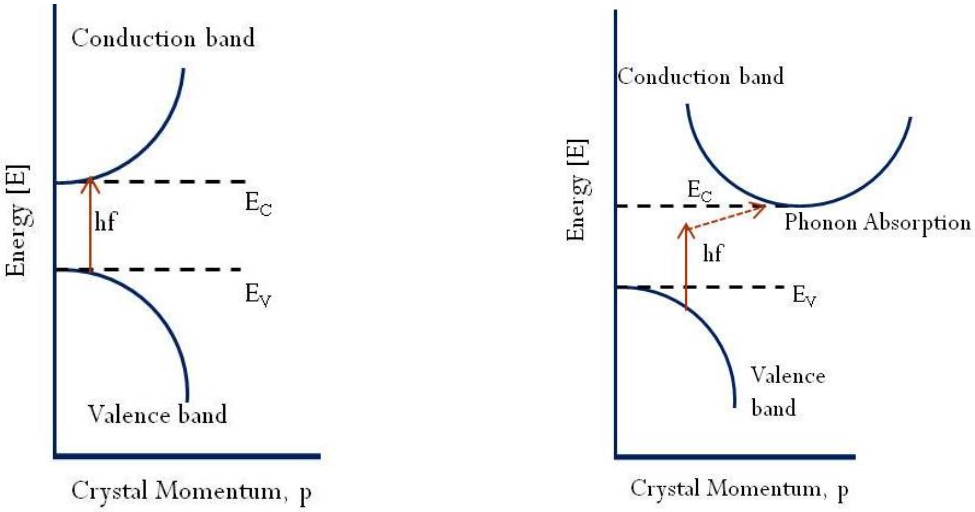

a) b)

Figure 2.2: The Energy- Crystal Momentum diagram of absorption in:

a) A direct band gap material,

b) An indirect band gap material.

The intensity of incident light decreases as it passes through a semiconductor material at a rate described by the absorption coefficient (α). The absorption coefficient depends on the structure of the material, crystalline or amorphous and indirect or direct band structure.

2.2.4. Recombination

Recombination occurs as the generated electron-hole pair decay and relax to their equilibrium states. Recombination can occur through different mechanisms.

Radiative Recombination

With radiative recombination the absorption process is reversed and the electron drops down from the higher energy state releasing energy in the form of light. Similar to the absorption process, energy and momentum must be conserved in the recombination process. Figure 2.3(a) shows the recombination process in a direct band- gap material. Recombination in indirect-band gap occurs with the assistance of a phonon, figure 2.3(b). This type of recombination is more probable in direct band-gap materials and occurs at a faster rate allowing these materials to be used in laser and light emitting diodes. Radiative recombination in indirect band-gap materials like silicon is not the primary recombination process but is vital for the electroluminescence characterisation technique.

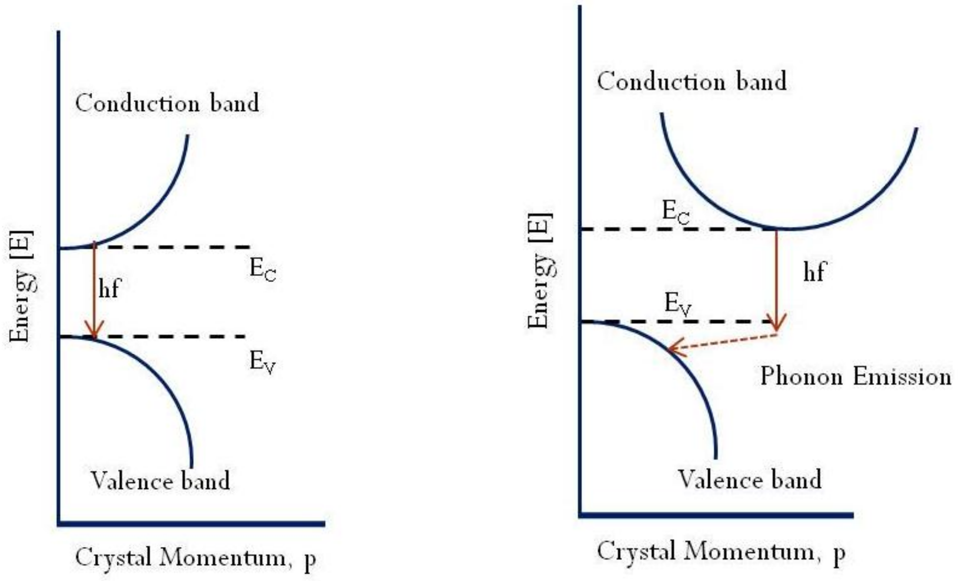

a) b)

Figure 2.3: The Energy- Crystal Momentum diagram of radiative recombination in:
a) a direct band gap material,
b) an indirect band gap material.

Auger Recombination

When an electron recombines with a hole, energy is given off in the form of kinetic energy to third carrier in the conduction band rather than as light. The third carrier then emits the excess energy as phonons and heat as it relaxes to the band edge[6]. This type of recombination is very dependent on the type and concentration of doping of the material, the band gap and the temperature.

Shockley-Read Hall recombination

Introduced dopants and impurities result in additional energy levels through which electrons and holes can recombine. This recombination mechanism was studied in detail be Hall, Shockley and Read, in 1952 and subsequently named after them [7].

2.2.5. P-N junction

A diode is made when the p- and n-type material are combined creating a concentration gradient for electrons and holes. Electrons diffuse from the n-type material, a region of high electron concentration, to the p-type material, a region of low electron concentration, and vice versa for the holes. Figure 2.4. shows isolated p- and n- type material and their corresponding energy-band diagrams with their respective Fermi energy levels, E_{Fp} and E_{Fn} , indicated. Figure 2.5 shows the p-n junction formed by bringing the p- and n- type materials together [1]. The Fermi level (E_F) must be constant in a material in thermal and chemical equilibrium so the conduction and valence bands adjust accordingly.

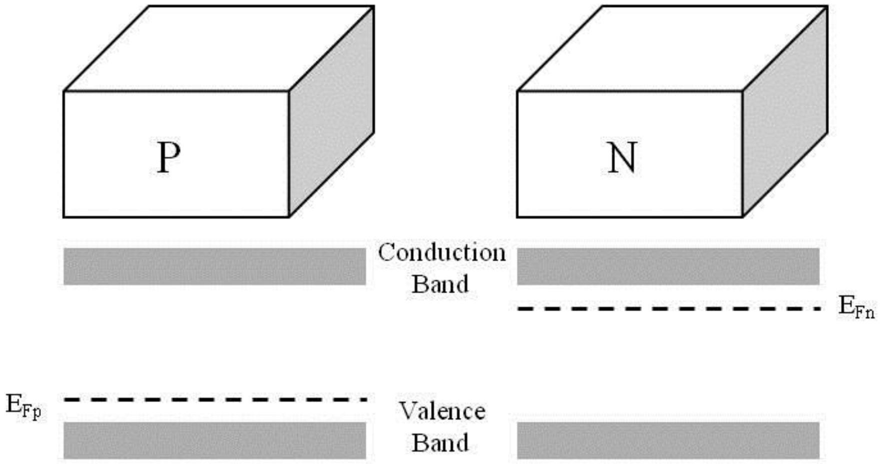

Figure 2.4: Isolated p- and n- materials with respective energy-band structure.

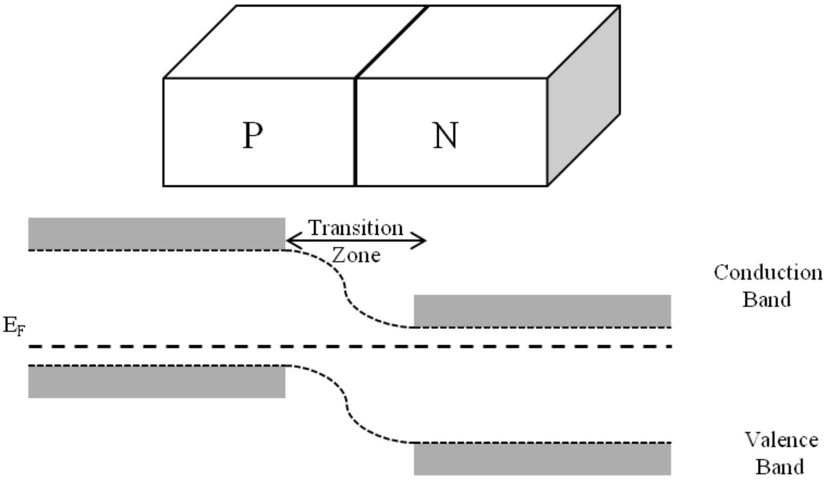

Figure 2.5: The p-n junction structure with energy band diagram at thermal equilibrium.

The equilibrium conditions of the semiconductor diode can be disturbed by changing the population of electrons and holes. This can be done by exposing the semiconductor to light or by applying an electrical bias [6]. Under illumination electron-hole pairs are generated, the concentration of majority carriers in each region is practically unaffected due to the large number of carriers, however, the minority carrier concentration is affected. Under zero bias there is electrochemical potential difference between the n- and p- regions and minority carrier concentration gradient occurs in the transition region. The carriers are collected and result in a current in the external circuit.

The current densities of the electrons and holes can be attributed to drift currents and diffusion currents. Drift currents occur as carriers flow due to an electric field in order to minimise their electric potential energy. Diffusion currents occur due to a carrier concentration gradient as carriers move to minimise their statistical potential energy [6].

Carrier collection occurs due to diffusion of minority carriers as electrons flow from the p-type to n-type region. Similarly the holes diffuse from n-type to p-type region. The electron and hole diffusion currents can cancel each other out unless the electron and hole concentration gradients are very different as achieved in device configurations such as a p-n junction. The lifetime of the minority carrier must be greater than the transit time towards the junction in order for collection to take place. The time before recombination takes place, and diffusion velocity of the minority carriers are important material properties indicating the efficiency of the carrier separation and collection processes. In crystalline indirect band gap materials like crystalline silicon the minority carrier lifetime and diffusion length must be large to obtain an efficient solar cell.

In indirect band gap materials like silicon the dark current of the solar cell can be described by the ideal diode equation, equation 2.1. This current is related to the diffusion current, J_{diff}, charge on the electron, q, diode voltage, V_D, Boltzmann's constant, k, and temperature, T.

$$I_D = I_{diff}\exp(\frac{qV_D}{kT} - 1) \qquad [2.1]$$

The equivalent circuit of an illuminated solar cell is given in figure 2.6. The current, I, generated by the solar cell flows through the external load R_L is related to the diode current, I_D, and the photogenerated current, I_L.

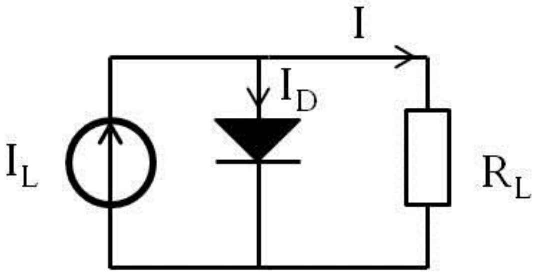

Figure 2.6: The equivalent circuit of an ideal solar cell.

The equation for a single diode equivalent equation for a solar cell under illumination is given in equation 2.2. The dark saturation current, Io, is the diode leakage current density in the absence of light. The dark saturation current is an important parameter differentiating one diode from another. It is related to the recombination of the device. Saturation current will increase with temperature and decrease as the quality of the material increases.

$$I = I_O\left[\exp\left(\frac{qV_D}{kT}\right) - 1\right] - \mathrm{I_L} \qquad [2.2]$$

Parasitic resistances affect the efficiency of the solar cell. These additional resistances are indicated in figure 2.7. Series resistance, R_S, results in ohmic losses due to the bulk material resistance and the contact resistance. The shunt resistance, R_p, occurs in parallel to the diode allowing for current leakages that lower the photogenerated current. The voltage (V) measured across the load is equal to the diode voltage (V_D) minus the voltage across the series resistor (I x R_S). These resistances limit the current generated by the introduction of an additional term in equation 2.3.

$$I = I_O\left[\exp\left(\frac{q}{kT}(V + IR_S)\right) - 1\right] + \frac{(V+IR_S)}{R_p} - \mathrm{I_L} \qquad [2.3]$$

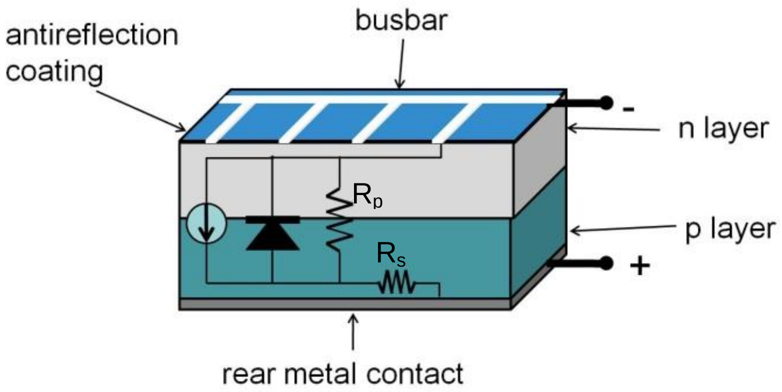

Figure 2.7: The structure of a p-n solar diode.

2.2.6. Solar Cell Models

The electrical behaviour of a solar cell can be successfully modelled by a diode equation based on an equivalent electrical circuit.

2.2.6.1. One-Diode Model

In dark conditions the one-diode solar cell can be represented by the circuit shown in figure 2.8(a). The solar cell is non-ideal and the performance is limited by parasitic resistances. The dark current-voltage behaviour of the solar cell is modified for non-ideal cells, equation 2.4, by the inclusion of the ideality factor, n. In an ideal solar cell n is equal to one but in reality n is typically between 1 and 2.

$$I = I_O\left[\exp\left(\frac{q}{nkT}(V - IR_S)\right) - 1\right] + \frac{(V - IR_S)}{R_p} \qquad [2.4]$$

In illuminated conditions the photogenerated current is represented by a current source as seen in figure 2.8(b). The equation for the illuminated current-voltage behaviour is given in equation 2.5.

$$I = I_O\left[\exp\left(\frac{q}{nkT}(V + IR_S)\right) - 1\right] + \frac{(V + IR_S)}{R_p} - \mathrm{I_L} \qquad [2.5]$$

The photogenerated current flows in the opposite direction to the dark current. Since the photogenerated current is greater than the dark current the equation can be rearranged to equation 2.6.

$$I = \mathrm{I_L} - I_O\left[\exp\left(\frac{q}{nkT}(V + IR_S)\right) - 1\right] - \frac{(V + IR_S)}{R_p} \qquad [2.6]$$

The two forms of the one-diode equation are equivalent but the convention in photovoltaics is such that the photocurrent is positive and thus equation 2.6 is used.

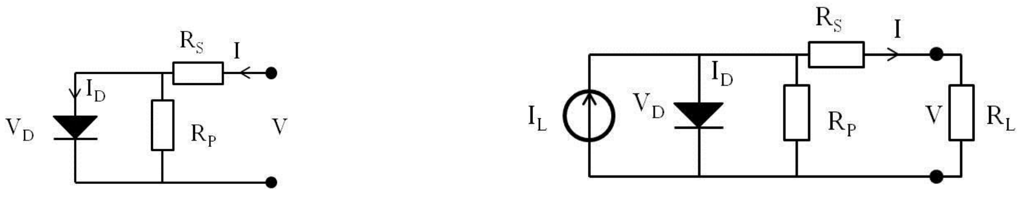

a) b)

Figure 2.8: The equivalent circuit of a solar cell in a) dark and b) illuminated conditions.

2.2.6.2. Two-diode Model

The two-diode model includes a second diode term to account for recombination processes. The equivalent circuit of the two-diode model in dark conditions is shown in figure 2.9(a). Equation 2.7 gives the current-voltage behaviour of the solar cell in the dark.

$$I = I_{O1}\left[\exp\left(\frac{q}{n_1 kT}(V - IR_S)\right) - 1\right] + I_{O2}\left[\exp\left(\frac{q}{n_2 kT}(V - IR_S)\right) - 1\right] + \frac{(V - IR_S)}{R_p} \quad [2.7]$$

Each diode is described with different saturation currents, I_{O1} and I_{O2}, and ideality factors, n_1 and n_2. The equivalent circuit under illuminated conditions is shown in figure 2.9(b). The equation for the illuminated solar cell is shown below. Equation 2.8 is shown in form similar to the dark equation while equation 2.9 is inverted to the conventional light I-V form.

$$I = I_{O1}\left[\exp\left(\frac{q}{n_1 kT}(V + IR_S)\right) - 1\right] + I_{O2}\left[\exp\left(\frac{q}{n_2 kT}(V + IR_S)\right) - 1\right] + \frac{(V + IR_S)}{R_p} - I_L \quad [2.8]$$

$$I = I_L - I_{O1}\left[exp\left(\frac{q}{n_1 kT}(V + IR_S)\right) - 1\right] - I_{O2}\left[exp\left(\frac{q}{n_2 kT}(V + IR_S)\right) - 1\right] - \frac{(V + IR_S)}{R_p} \quad [2.9]$$

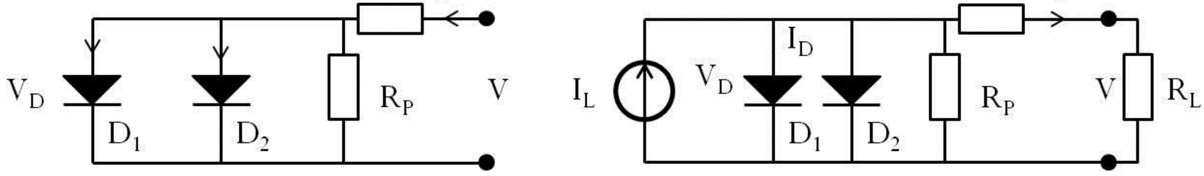

a) b)

Figure 2.9: The equivalent circuit of the two-diode model in a) dark and b) illuminated conditions.

2.2.7. Breakdown/Avalanche Voltage term

The reverse voltage behaviour of a solar cell becomes important when considering cell mismatch. A shaded cell produces a lower current which results in it being reverse biased which is discussed in more detail in section 3.1.4. The diode equation can be adapted to take into account the current in reverse bias conditions. The reverse current behaviour is accounted for by the inclusion of a voltage dependent leakage current, $I(V_p)$, term in the equivalent circuit, shown in figure 2.10. The current in the reverse voltage region is determined by the photo-generated current, the current through the shunt resistance and the breakdown current [8][9].

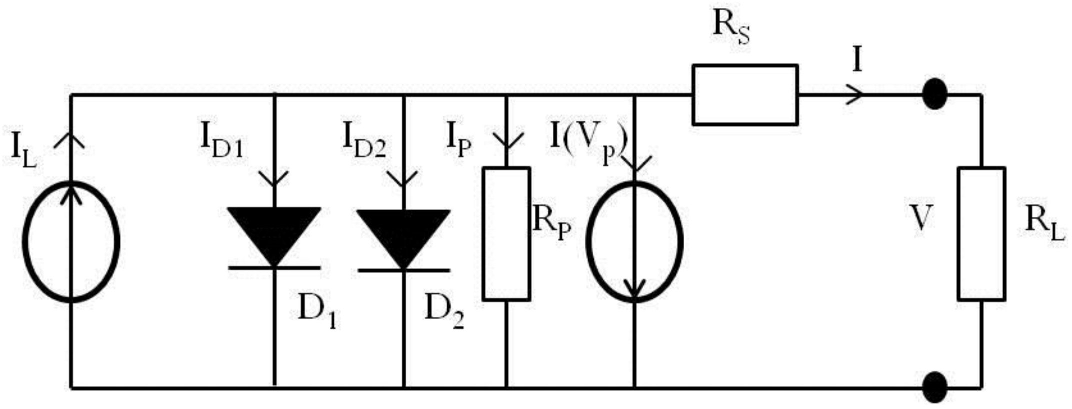

Figure 2.10: The equivalent circuit of one-diode model with additional breakdown voltage term.

The two-diode model is adapted with the inclusion of a term for diode breakdown and can be used for numerical simulation of mismatched cells [10]:

$$I = I_L - I_{O1}\left(\exp\left(\frac{V+IRs}{n_1 V_T}\right)-1\right) - I_{O2}\left(\exp\left(\frac{V+IRs}{n_2 V_T}\right)-1\right) - \frac{\mathrm{V}+\mathrm{IR_s}}{\mathrm{R_p}}$$

$$-\mathrm{a}(\mathrm{V}+\mathrm{IR_s})\left(1-\frac{\mathrm{V}+\mathrm{IR_s}}{\mathrm{V_{Br}}}\right)^{-\mathrm{m}} \qquad [2.10]$$

Where V_{Br} is the voltage breakdown, a is the fraction of ohmic current involved in avalanche breakdown and m is the avalanche breakdown exponent. Further discussion of the current-voltage characteristic curves and modelling using the diode equations is included in chapter 3.

2.3. Solar Cell Materials

Solar cells can be made from different semiconductor materials, such as single-crystalline, multi-crystalline and amorphous silicon. Other semiconductor materials are used for tandem solar cells or thin film solar cells which will not be discussed in this study.

Single-crystalline silicon is commonly used in electronic devices. It has a regular crystal structure with each silicon atom in a covalent bond with four neighbouring atoms. The covalent bonds provide electrons for conduction and doping of the material increases the free electron carrier concentration. The band gap energy needed to break the electron from the covalent bond is 1.1 eV [5]. Single-crystalline silicon has long range order in the crystal structure which means the atoms are arranged in a regular lattice. Multi-crystalline silicon material has larger grains resulting in a crystal structure with several different crystal planes present. Grain boundaries occur between the different structural orientations which result in regions which block minority carrier flow [1]. Single crystalline has a maximum recorded efficiency of 25% while the maximum efficiency of multi-crystalline is about 20% [11]. Amorphous silicon does not have long range order in its crystal structure and the arrangement of the atoms is not regular. Amorphous silicon-hydrogen alloys are used in photovoltaic devices with an efficiency of about 5 -10% [11]. These cells operate at a lower efficiency than crystalline silicon solar cells but the cell material is quicker and cheaper to produce.

2.4. Photovoltaic (PV) Modules

Solar cells are electrically connected together to form PV modules in order to increase the current, voltage and power produced. The cells are encapsulated in order to protect them from mechanical damage, provide electrical isolation and chemical stability[1]. The operating lifetime of modules can be limited by the degradation of the encapsulation which will be observed in the results of this study.

2.4.1. Module construction

The typical configuration of materials in PV modules is shown in figure 2.11. The layers of materials provide environmental protection. It is important that there is a barrier to prevent the infiltration of moisture into the module. Moisture ingress results in degradation of the cell material and the solder connections.

For the front surface material, glass is used as it has good structural strength and allows transmission of the wavelengths of light necessary for solar cell functioning. Glass has self-cleaning properties that prevent a build-up of dust and dirt which would shade the module. The losses due to reflection are counteracted by use of an antireflective coating, either silicon nitride or titanium oxide, sprayed onto the individual cells. The cells are encapsulated between two layers of ethylene/vinyl acetate (EVA). EVA is used because of its stability at high temperatures and under UV light. The back surface, commonly Tedlar, provides structural support and has a low thermal resistance thus be able to dissipate heat quickly. A frame is used to provide additional structural support and should provide a seal to prevent moisture ingress.

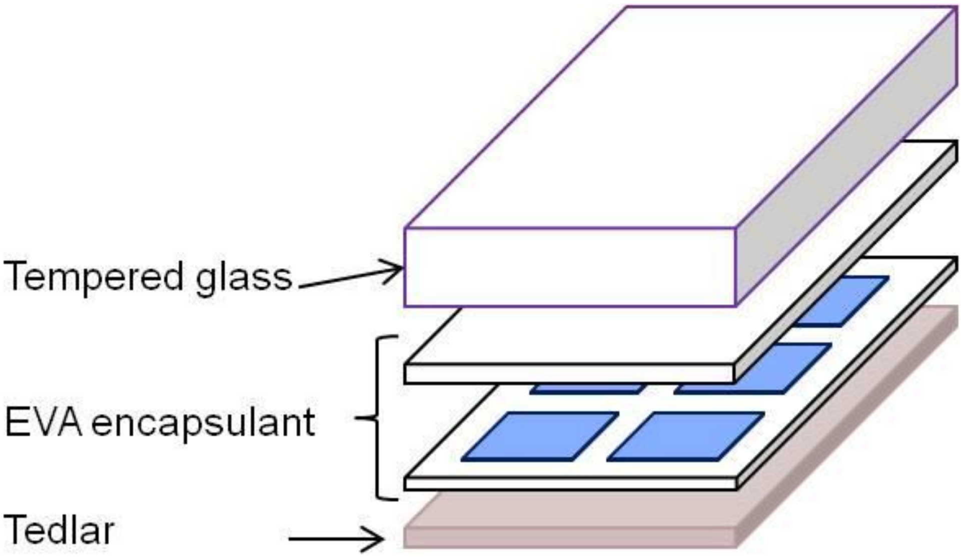

Figure 2.11: Typical construction of a silicon PV module.

2.5. Summary

Semiconductor materials are defined by a band structure that allows electrons to be excited from the valence to the conduction band. The incident light generates electron hole pairs that can move through an external circuit due to the photoelectric effect. A p-n diode is created by bringing together materials doped with extra electrons and extra holes then creating a diffusion gradient. The p-n diode forms the basis of a solar cell. The electrical behaviour of a solar cell is simulated using a diode equation with additional terms taking into account recombination effects, parasitic resistances and reverse voltage behaviour. The diode equation will be used in the simulation of I-V curves discussed further in section 3.1.2. The assembly of cells into a module increases the stability of the cells and allows them to be used in long-term outdoor applications. However, if the modules are not carefully constructed and air or dust is present between the layers module degradation can occur as seen in the modules introduced in chapter 4.

Chapter 3

Characterisation Techniques

3.1. Current-Voltage Characteristics

3.1.1. Parameters of a Solar Cell

The current-voltage (I-V) characteristics of a solar cell are represented by a diode equation (Eq. 2.6 and Eq. 2.9) and an equivalent circuit as discussed in chapter 2. They successfully describe the electrical behaviour of a solar cell [5].

The I-V characteristics of a solar cell or module are obtained experimentally using an outdoor current-voltage measurement system. This equipment is discussed in detail in section 4.1.1. The output current of an illuminated module is measured at different voltage points. The illuminated I-V curve occurs in the fourth quadrant, however, the convention is to use the absolute value of current and thus reflect the curve in the first quadrant [12]. Figure 3.1 shows the light I-V curve and power curve of a solar cell. The power output of the cell is at a maximum when the product of current and voltage is at a maximum. The P_{max}, I_{max} and V_{max} points are labelled on figure 3.1.

The temperature and irradiance conditions at the time of measurement influence the I-V curve. The irradiance affects the current generation of the module. Measurements should be taken at irradiance values greater than 700 W/m^2, thereafter the current is corrected to an irradiance of 1000 W/m^2.

Temperature affects the band gap of the semiconductor material. An increase in temperature results in a decrease in the band gap and an increase in minority carrier lifetime [13]. The increased temperature also increases the dark saturation current density thus reducing the Voc. At higher temperatures there is a slight increase in short circuit current (Isc) due to an increase in light-generated current. The open circuit voltage (Voc) is more significantly affected by an increase in temperature. For silicon the decrease in Voc is 2.3mV/°C [1]. The decrease in power of the entire module is 0.4-0.5 %/°C attributed to the significant variation in open circuit voltage with temperature [1]. The current and voltage correction factors are given by the manufacturer or can be determined experimentally [13]. The back of module temperature is measured during the I-V curve measurement and then the temperature is corrected to 25 °C.

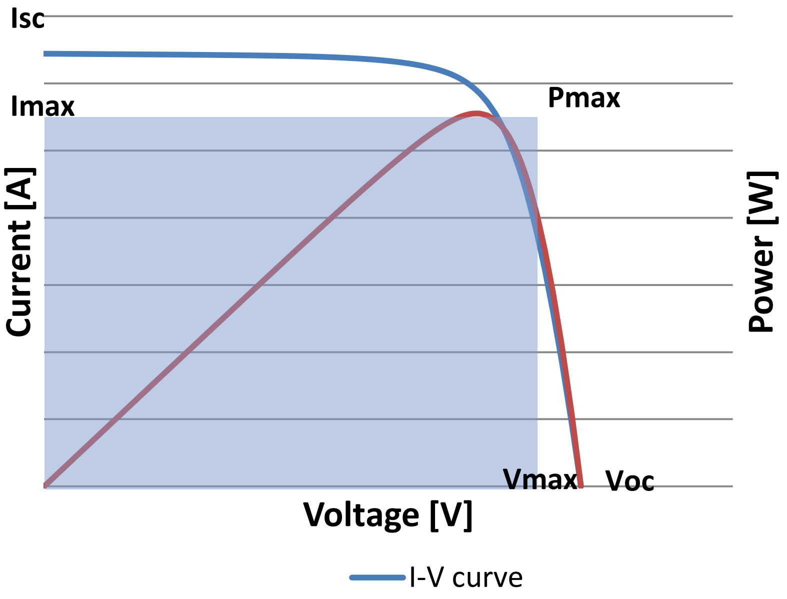

Figure 3.1: Light Current-Voltage curve of a solar cell.

Efficiency

The efficiency of a solar cell can be determined from the ratio of maximum power compared to the input power.

$$\eta = \frac{P_{output}}{P_{input}} = \frac{I_{max}V_{max}}{P_{input}} \qquad [3.1]$$

Light Generated Current

The short circuit current (Isc) is the current value that occurs when the voltage is zero. The Isc is equivalent to the photogenerated current (I_{ph}) unless the series resistance is high and there is a significant amount of leakage current flowing through the shunt resistance [5].

Open Circuit Voltage

The open circuit voltage (Voc) is a measure of the strength of the bias that occurs over the junction due to the photogenerated carriers [12]. Voc is related to the material properties of the device since due to its dependence on the ideality factor (n) and the saturation current (Io) of the diode.

Setting the current to zero in equation 2.2 allows open Voc to be defined in equation 3.2 [1].

$$V_{oc} = \frac{nkT}{q} ln\left(\frac{I_{ph}}{Io} + 1\right) \qquad [3.2]$$

Fill Factor

The fill factor (FF) is the ratio of the maximum power output to the product of short circuit current and open circuit voltage.

$$FF = \frac{P_{max}}{V_{oc}\, I_{sc}} \qquad [3.3]$$

Fill factor gives an indication of how the shape of the I-V curve varies from the ideal due to the effects of series and shunt resistances.

Series Resistance

In real solar cells series resistance occurs due to resistances along the current path to the external circuit of the collected carrier [5]. The series resistance includes the resistance in the bulk of the material, the emitter, the contacts and busbars. The presence of series resistance limits the current output and causes a drop in voltage at a specific current which lowers the fill factor of the curve [12].

Increasing the series resistance results in the I-V characteristic becoming flattened at the "knee" and at high series resistances the curve resembles the ohmic behaviour of a resistor. Figure 3.2 shows the effect of increasing the series resistance by a factor of 10, while keeping the other parameters constant.

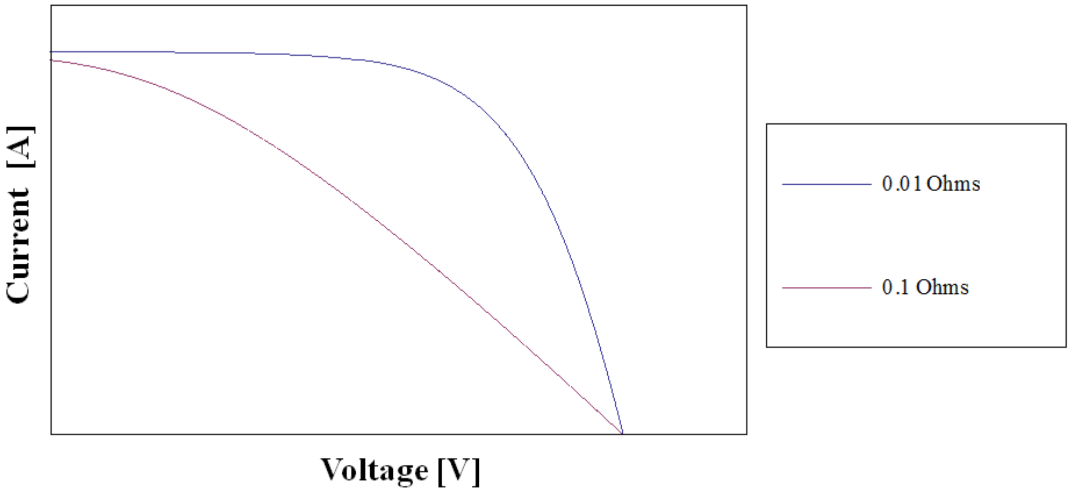

Figure 3.2: The I-V curve of a solar cell modelled with a series resistance parameter of 0.01Ω or 0.1Ω.

3.1.2. Modelling I-V curves

3.1.2.1. The diode equation

The electrical behaviour has been described previously, section 2.2.6, with an equivalent circuit and equivalent diode equation. The one-diode equation, equation 2.6, is commonly used for extracting parameters and for modelling solar cells in normal operating conditions [14]. The two-diode model, equation 2.9, takes into account recombination processes and can provide a better fit of the IV curve.

$$I = I_L - I_{O1}\left(\exp\left(\frac{V+IRs}{n_1V_T}\right)-1\right) - I_{O2}\left(\exp\left(\frac{V+IRs}{n_2V_T}\right)-1\right) - \frac{\mathrm{V+IR_s}}{\mathrm{R_p}} \qquad [3.4]$$

When series connected cells in a module are mismatched the poorly performing cells are driven into the negative voltage range. This requires a term in the two diode equation describing the voltage breakdown at negative currents. This was described by Bishop (1988) [8] and used in numerical modelling by Quaschning (1996) [10]. This model, equation 2.10, includes a non-linear multiplication term influencing the shunt resistance term. This adds to the leakage current term creating a current source in the equivalent circuit [16].

$$I = I_L - I_{O1}\left(\exp\left(\frac{V+IRs}{n_1V_T}\right)-1\right) - I_{O2}\left(\exp\left(\frac{V+IRs}{n_2V_T}\right)-1\right) - \frac{\mathrm{V+IR_s}}{\mathrm{R_p}}$$

$$-\mathrm{a(V+IR_s)}\left(1-\frac{\mathrm{V+IR_s}}{\mathrm{V_{Br}}}\right)^{-\mathrm{m}} \qquad [3.5]$$

The extra term accounts for the fact that at negative voltages the diode can breakdown and allow currents above the photogenerated current to pass. The breakdown voltage (V_{Br}) is determined by the reverse bias behaviour of the cell. Parameters a and m are correction factors [10].

The equation is rearranged in order to be solved by numerical methods.

$$0 = f(V,I) \qquad [3.6]$$

Where:

$$f(V,I) = I_L - I_{O1}\left(\exp\left(\frac{V+IRs}{n_1V_T}\right)-1\right) - I_{O2}\left(\exp\left(\frac{V+IRs}{n_2V_T}\right)-1\right) - \frac{\mathrm{V+IR_s}}{\mathrm{R_p}}$$

$$-\mathrm{a(V+IR_s)}\left(1-\frac{\mathrm{V+IR_s}}{\mathrm{V_{Br}}}\right)^{-\mathrm{m}} - \mathrm{I} \qquad [3.7]$$

The equation $f(V,I) = 0$ was solved for a given voltage. The root of this equation is the current. In this study the equation was solved by the Newton methods using a Mathematica routine, shown in appendix B.1.

3.1.2.2. Parameter Extraction

In order to successfully model the current-voltage characteristics of a solar module the parameters for the diode equation need to be determined. Various methods can be used to extract the parameters from measured I-V curves such as Interval division method based on a Newton iteration method [17]. In this study the Particle Swarm optimisation (PSO) was used to extract the parameters for the modelled curves. The PSO method is an evolutionary technique that was developed by Eberhart and Kennedy [18]. It simulates the social behaviour of animals like flocks of birds and schools of fish. A particle is assigned a random solution for the parameter and through iterations the parameters search for the combination of parameters that result in the best fit solution. This method was developed as a parameter extraction technique for I-V curves by Macabebe et al.[19] and further developed by Munji et.al[20]. The flow chart and necessary parameter definitions are included in appendix B.2.

3.1.3. Series and Parallel connected cells

Cells are connected together in a module in order to obtain a higher current and voltage output. In order to increase the voltage, cells are connected together in series, and to increase the current, cells are connected in parallel. The configuration of the cell connection is determined by the desired string or module output.

When cells are connected in a series string, the voltage of the entire string is the sum of the individual cells' voltages as shown in equation 3.8. The total current of the string is equal to the current of one cell in the string, equation 3.9. This equation is true under ideal operating conditions with all cells having identical I-V curves.

$$V_R = V_1 + V_2 \qquad [3.8]$$

$$I_R = I_1 = I_2 \qquad [3.9]$$

The I-V curves of two cells having non-identical I-V curves and the I-V curve of the combination is shown in figure 3.3. The voltages (0.6 V) of the two cells are added together at equal currents such that the Voc of the combined cells is 1.2 V. The Isc of the combined cells is the same as the Isc of the two cells. These curves were plotted using a modelling program called PVSim [21] which includes a statistical variation of parameters of the cells resulting in the I-V curves of cell 1 and cell 2 being slightly different.

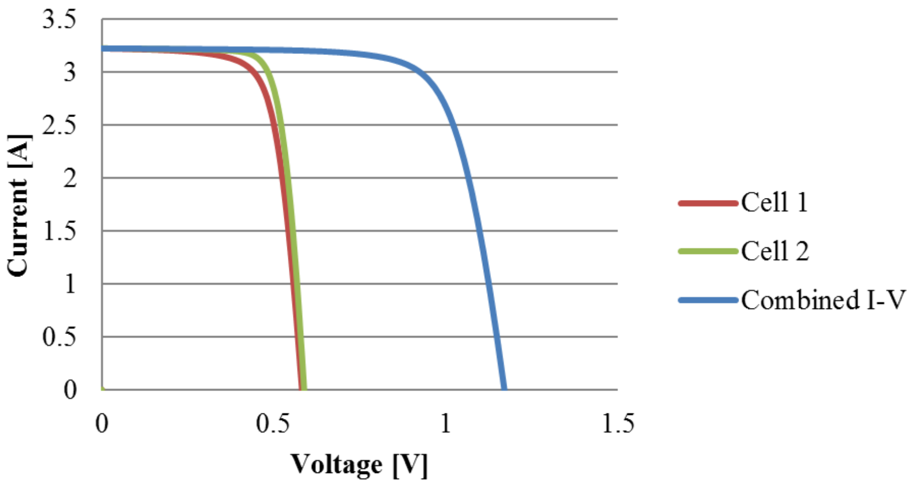

Figure 3.3: The I-V curves of two cells with different open circuit voltages are shown with the resultant I-V curve [21].

Alternatively, when cells are connected in parallel the currents add and the voltages are equal as seen in equations 3.10 and 3.11. The I-V curve of two cells connected in parallel is shown in figure 3.4. The current of the combined curve is equal to the sum of the two currents at a specific voltage.

$$V_R = V_1 = V_2 \qquad [3.10]$$

$$I_R = I_1 + I_2 \qquad [3.11]$$

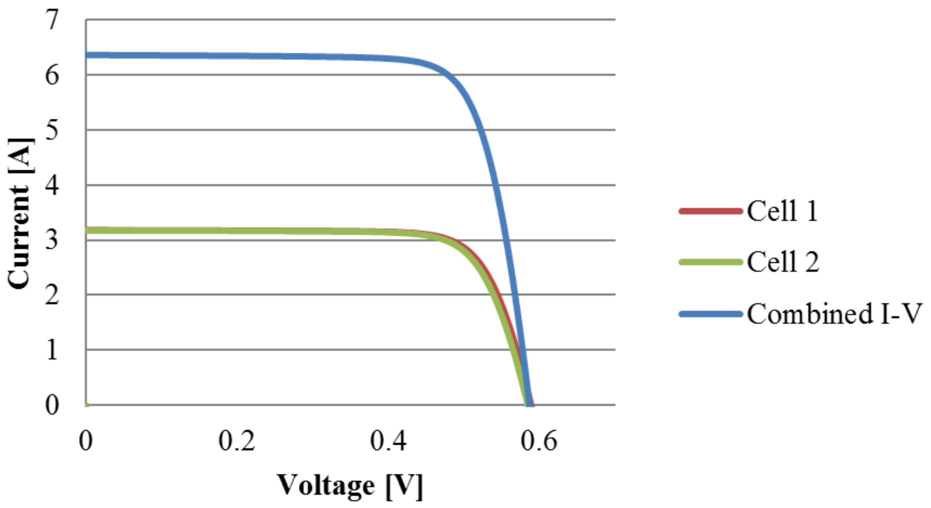

Figure 3.4: The I-V curves of two cells with different short circuit currents connected in parallel are shown with the resultant I-V curve [21].

3.1.4. Effects of Cell Mismatch

Cell mismatch occurs when a cell in a series connected string is shaded or damaged preventing it from generating current equal to the other cells in the string. This mismatch results in degradation to the module and a lower power output.

3.1.4.1. Formation and Prevention of Hot Spots

Figure 3.5(a) shows the equivalent circuit of the two cells connected in series in short circuit conditions. The two cells are both generating equal current, shown in green, which flows though the external circuit. There is no forward bias current flowing through the diode of the cell so the voltage across the each cell is zero [22]. Figure 3.5(b) shows the open circuit conditions of the two cells generating matched currents. No current flows through the external circuit so each cell is forward biased by its own photogenerated current. The open circuit voltage of the entire module is equal to the sum of the open circuit voltage of both cells.

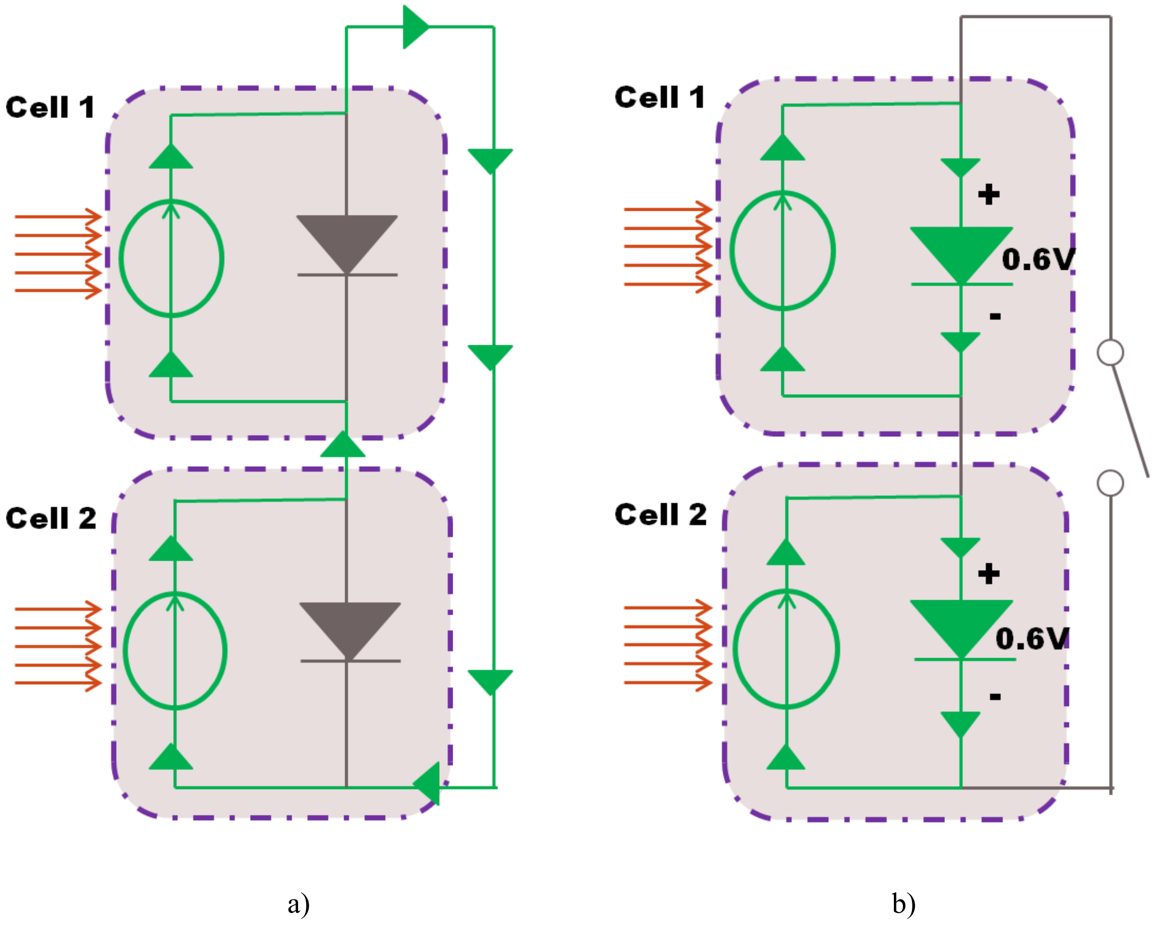

Figure 3.5: The equivalent circuit of two matched solar cells in a) short circuit and b) open circuit conditions

The same cell configuration in short circuit but with cell mismatch is shown in figure 3.6(a). Cell 2 is half shaded causing the photogenerated current to drop by 50%. The current generated by the weak cell is the maximum that can flow through the external circuit limiting the current output of the two cells. Cell 1 is not shaded but its total current produced is unable to flow through the external circuit so the extra current flows though the diode forward biasing the cell. In short circuit conditions the net voltage over the two cells must be zero. To maintain this condition the cell 2 must be reverse biased in magnitude equal to the forward bias of cell 1. When a cell is reverse biased it changes from a power generator to a current dissipater and may generate heat. This localised heat generation results in a hot spot which can cause damage to the cell material, melting the interconnection solder, discolouration in the EVA and cracks in the glass [23].

The short circuit is the worst case condition for mismatched cells since it results in the reverse biasing of the weak cells. In open circuit conditions the cells are forward biased by their photogenerated currents, illustrated in figure 3.6(b). The shading of the cell 2 results in it having a lower Voc which ultimately lowers the Voc of the combined cells. However over a large number of cells, typically 36 in a module, this drop in Voc is not significant. A mismatched cell lowers the performance of the entire module by limiting the current output and slightly decreasing the Voc of the module.

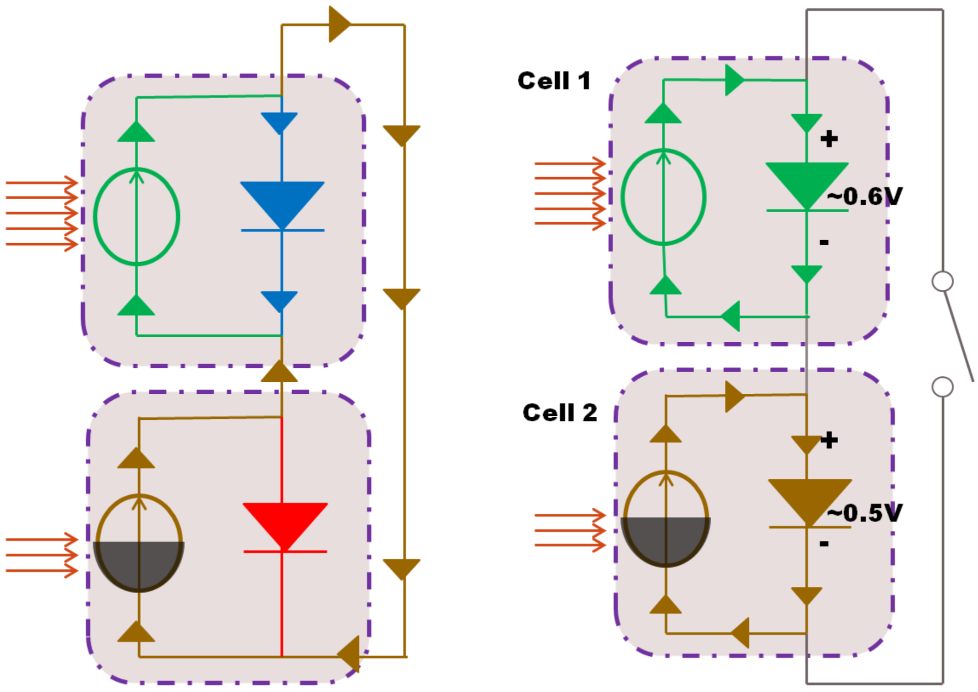

a) b)

Figure 3.6: The equivalent circuit of mismatched cells under a) short circuit and b) open circuit conditions.

Performance degradation due to cell mismatch and hot spot formation can be prevented by the use of bypass diodes. Bypass diodes are connected in parallel over the cells as indicated in figure 3.7(a). In matched current conditions the bypass diodes are reverse biased and have no effect [5]. However when there is cell mismatch, instead of the weak cell being reverse biased as in figure 3.6(a) the bypass diode is forward biased and conducts the "extra" current produced by the good cell as seen in figure 3.7(b). The weak cell is still reverse biased but only by about 0.5V, which is the activation voltage of the bypass diode. The current through the external circuit is now not limited by the weak cell once the bypass diode is activated. The effects of bypass diode activation on the I-V characteristic curve are discussed further in the next section.

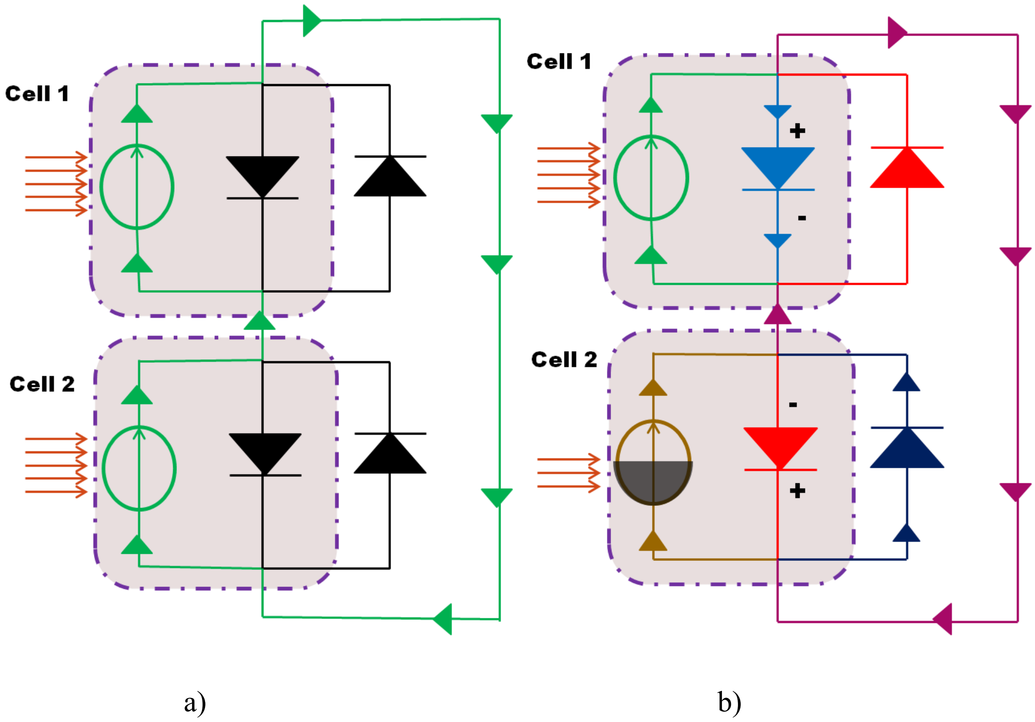

Figure 3.7: The equivalent circuit of two solar cells with parallel bypass diodes in short circuit conditions with a) matched and b) mismatched currents.

In this example a bypass diode is connected over each cell, however, this is not practical in large modules as a bypass diode over each cell would increase manufacturing costs. In practice bypass diodes are connected over series connected strings of cells. The configuration is dependent on the required output of the module and the expected shading conditions [16]. Anticipation of potential shading patterns is important for the module configuration as the worst performance is obtained if all strings are partially shaded simultaneously. It is preferable for the module performance that the shading falls on just one string with bypass diodes connected [25]. Shadows are more likely to fall vertically on a module caused by adjacent objects or buildings so the convention is to arrange the series strings vertically in the PV module.

3.1.4.2. Effect of Cell Mismatch on I-V curves

Cell mismatch has a substantial effect on the I-V curve of the whole module. A cell with a current output lower than the rest of the cells in the string is referred to as a "weak cell". When cells are connected in series the total current is limited by the weakest cell while the voltages add as normal. The combined output of the cells is dependent on the reverse voltage behaviour of the weak cell [26].

The effects of shading one cell in a series connection can be seen in figure 3.8. One cell in a series string of three cells is shaded 50%. This causes the current produced by this cell to drop by about 50% and the current of the resultant curve drops similarly. The voltages of the three cells add while the current is limited by the weak shaded cell.

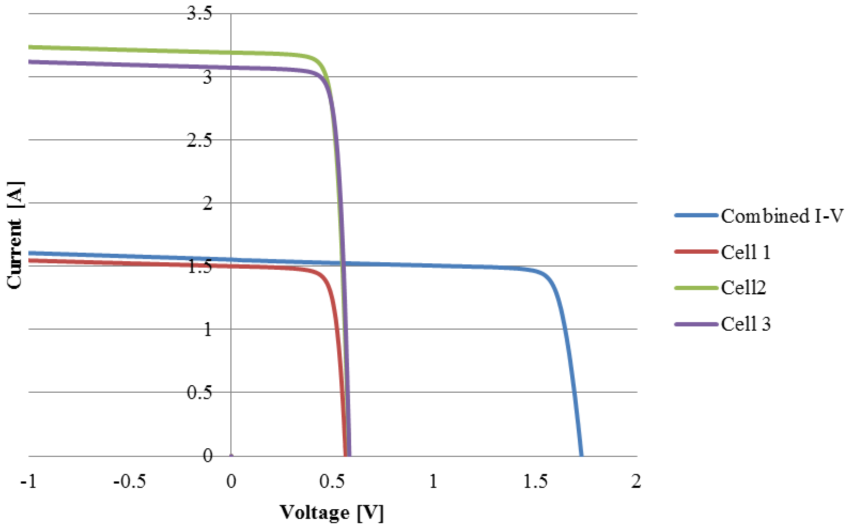

Figure 3.8: The effect of mismatch in series string of three cells with one cell shaded 50% [21].

The effects of mismatch can be mitigated by using bypass diodes connected in parallel over the cells. The bypass diode is activated when the reverse bias in the weak string is equal to the transmission voltage of the diode [25]. The activation of the bypass diode results in a step in the I-V curve. The position of the step is related to the behaviour of the weak cell in reverse bias [24] and the transmission voltage of the bypass diode. The effect of mismatch on three cells with bypass diodes connected in parallel across them where one cell is shaded 50% can be seen in figure 3.9. The resultant curve has a step related to the activation of the bypass diode over the shaded cell. This step up caused by the bypass diode activation results in a higher resultant curve of the combined cells.

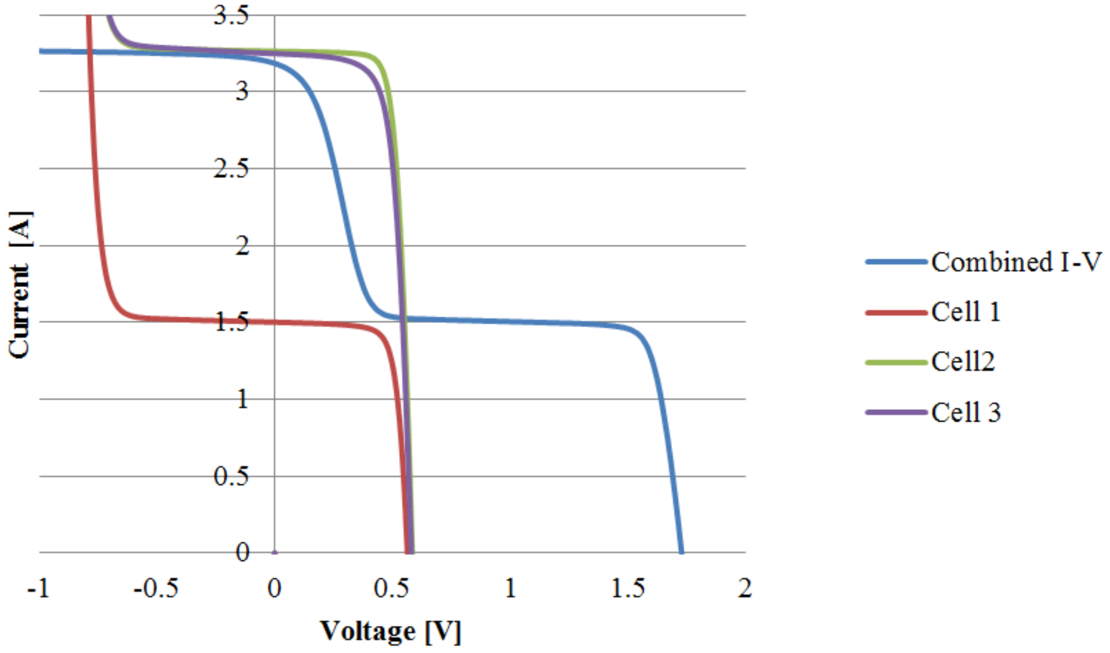

Figure 3.9: The effect of shading one cell in a 3 cell series string by 50% on the resultant I-V curve with bypass diodes connected across each cell [21].

3.1.5. Worst case cell determination technique

The worst case cell determination technique is used to non-destructively identify poorly performing cells in a module. This technique is fully described by Herrmann et. al. [27]. By taking the I-V curve of the module with individual cells shaded in turn, the weakest cell in the module is determined. A significant drop in current output of the module indicates that the shaded cell is performing well, while shading a weak cell has little effect on the module's I-V curve.

3.1.6. Dark I-V curves and Parameters

The I-V curve of a solar cell can be measured in the dark by injecting carriers rather than using photogenerated carriers in illuminated measurements. This technique is effective in removing subtle variations in the irradiance intensity that can occur in illuminated measurements. The behaviour of a solar cell in the dark is modelled by the dark diode equation (discussed in chapter 2, equation 2.4).

In the dark the solar cell behaves like a diode and provides information about the diode factor, the saturation current, series and shunt resistance of the cell [28]. The current-voltage exponential curve is shown in figure 3.10. The current-voltage curve can be plotted on a logarithmic axis as shown in figure 3.11. In the high voltage region a deviation from linear behaviour indicates higher series resistance while in the low voltage region deviation from linearity indicates high shunt resistance. The curve shape associated with high and low series and shunt resistance is indicated on figure 3.11.

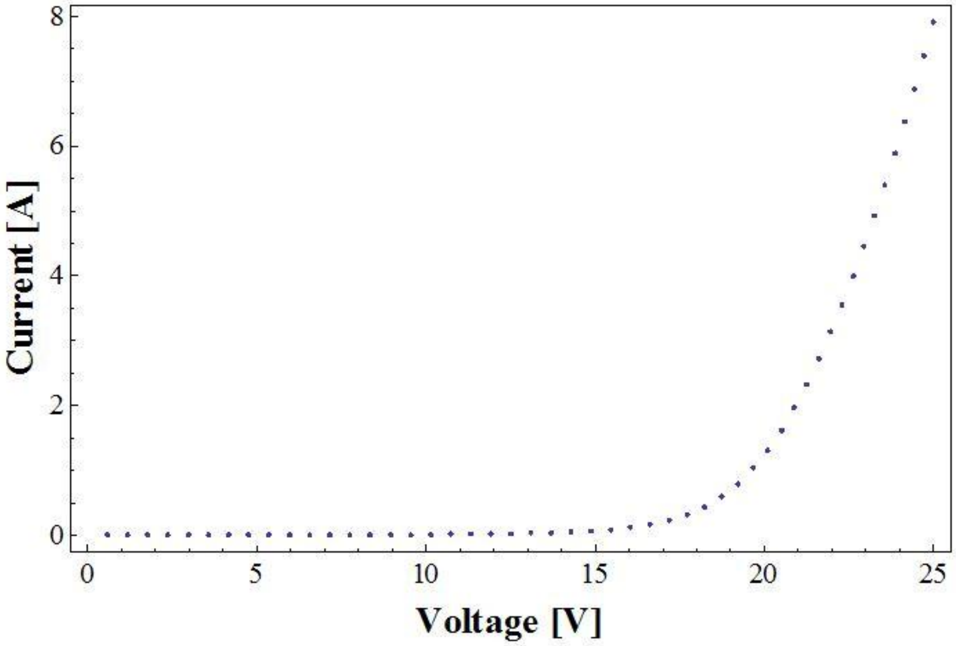

Figure 3.10: The Dark I-V curve of a PV module.

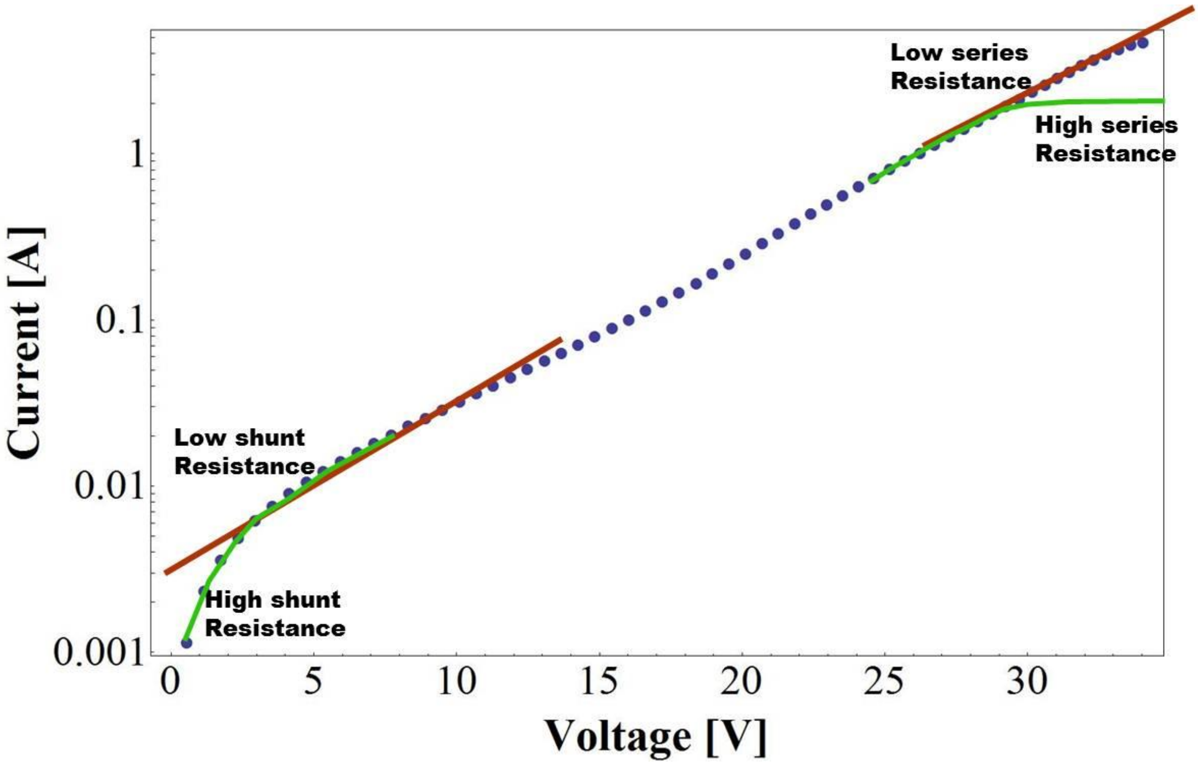

Figure 3.11: The Dark I-V curve of a PV module on a logarithmic scale.

3.2. Large-Area Laser Beam Induced Current (LA-LBIC)

3.2.1. Principles of LA-LBIC

The Laser Beam Induced Current (LBIC) measurement method of solar cell characterisation uses laser light as a light source to induce a current in the solar cell. By scanning the light beam probe across a solar cell the photogenerated current measured at each point gives an indication of the spatial distribution of the photoresponse of the cells. The region of the cell affected by the laser beam is related to the size of the spot and the wavelength of the laser. The effective spot size increases within the material as the carriers move at a rate determined by the materials minority carrier diffusion length [29][30][31]. The wavelength of the laser determines the depth of the sample that is analysed typically the depth is in the range of microns [32]. The LBIC technique is used to scan a small cell sample in a raster pattern and provide a spatial image of the current distribution in the cell [32][33]. It is able to detect cell defects such as grain boundaries in multi-crystalline silicon and determine material properties such as minority carrier diffusion length and lifetime [34].

On a PV module scale, LBIC measurements can be used to characterise interconnected cells and identify cells with poor photoresponse [30]. The Large-area LBIC (LA-LBIC) technique characterises the entire module by measuring the relative photoresponse of the cells in the module. The beam size of the laser is about 1 mm so a fairly large generation volume is involved. The current that is generated by one portion of one cell flows through the entire module and is thus affected by the other cells in the module and the series resistance of the contacts. For this reason the LA-LBIC technique provides information about the relative photoresponse of the cells rather than about specific cell defects. The current amplitude is plotted against the cell number, allowing the relative performance of cells to be determined.

3.3. Electroluminescence

3.3.1. Introduction

Electroluminescence (EL) is a non-destructive characterisation technique that provides spatial information about the solar cell material properties. This technique has been used to provide quantitative measurements of minority carrier lifetime, diffusion length [35][36][37] and series resistance[38]. The minority carrier diffusion length and lifetime are related to the collection efficiency of the cell material and are thus important material properties. EL is also a useful tool in identifying damaged or cracked cells which are responsible for cell mismatch in a module.

3.3.2. Principles of EL

The principle of EL is illustrated in figure 3.12. A solar cell is forward biased thus injecting carriers into the junction. These carriers then move through the material until they recombine. The radiative recombination of carriers emits energy in the form of electroluminescence. The intensity of the EL signal is related to the material properties such as the surface recombination velocity and recombination due to defects [35] as well as extrinsic defects induced during manufacturing.

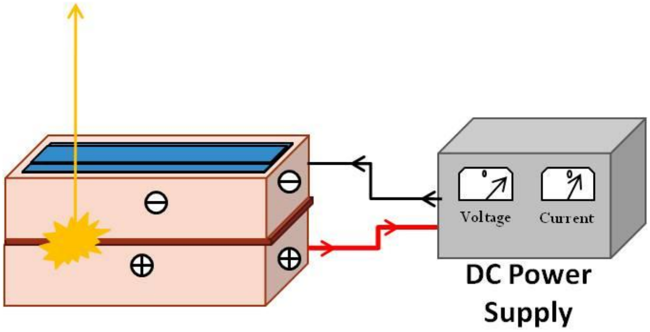

Figure 3.12: Illustration of the EL principle showing carriers injected into the solar cell by applying a forward bias.

The EL signal intensity is detected using a cooled Si-CCD camera which provides a greyscale spatial representation of defects in the cell. Figure 3.13 shows the emission spectrum of silicon at room temperature (R.T.) with the EL peak indicated and the sensitivity of a Si-CCD camera. The camera is sensitive to a region between 300-1100 nm which overlaps the bases of the electroluminescence peak for silicon at 1150 nm[39].

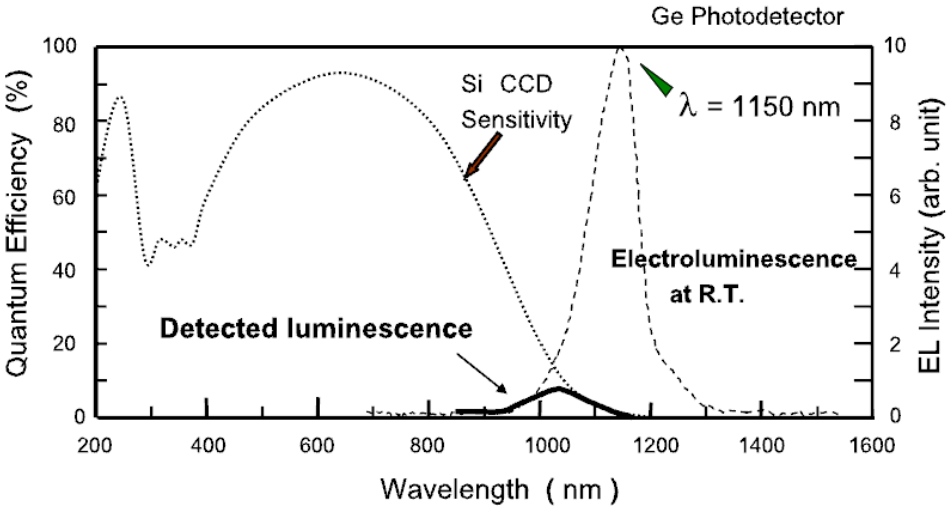

Figure 3.13: The typical emission spectrum of silicon and the sensitivity of a Si-CCD camera [39].

3.3.3. Intrinsic Material defects

Electroluminescence is the result of radiative recombination and the intensity of the signal can be related to the material properties that affect recombination. The rate of recombination is related to the minority carrier lifetime and diffusion length. EL can provide a complementary method to LBIC in mapping these properties in the solar cell. Experimentally it has been shown to provide information about the material properties faster than LBIC techniques in a correctly calibrated system [37]. To explain the dependence of EL signal on the cell's material properties the distribution of minority carriers (electrons) in the p layer of the p-n junction is considered. The number of minority carriers (n) in the p layer of the cell can be expressed as a function of distance (x) from the junction edge where L_e is the effective diffusion length and n_0 is the number of excess minority carriers at the junction edge [36].

$$n(x) = n_0 \exp(-\frac{x}{L_e}) \qquad [3.12]$$

It can be assumed that the localised effective diffusion length (L_e) varies across the surface of the cell but is constant along the depth from the junction to the surface [35]. Thus the total number of electrons, N, in the p layer is determined by the integration of equation 3.12 over the thickness of the cell, W.

$$N = n_0 \int_0^W \exp(-\frac{x}{L_e})\, dx = \; n_0 L_e [1 - \exp\left(-\frac{W}{L_e}\right)] \qquad [3.13]$$

The distribution is illustrated in figure 3.14 [35]. The term exp(-W/L_e) can be approximated to less than 1 so the expression can be reduced to equation 3.14.

$$N = n_0 L_e \qquad [3.14]$$

The intensity of the EL signal (I_L) is proportional to the number of minority carriers and the diffusion length at a certain carrier injection level, n_0.

$$I_L \propto N \propto \; n_0 L_e \qquad [3.15]$$

Further discussion of the mathematical proofs and experimental techniques involved in obtaining spatial diffusion length maps from EL images are covered by Würfel et al [37].

The EL signal is proportional to the forward current density [36]. At higher current density the EL signal is brighter especially along the busbars and contacts were recombination occurs more frequently with higher current densities. The intensity of the EL signal also increases at higher temperatures. Properties such as minority carrier length and lifetime depend on the energy levels in the material which are affected by temperature thus a change in temperature affects the recombination around intrinsic defects such as crystallographic defects and grain boundaries. This technique may also be used to differentiate extrinsic and intrinsic cell defects since defects such as micro-cracks have no temperature dependence [35].

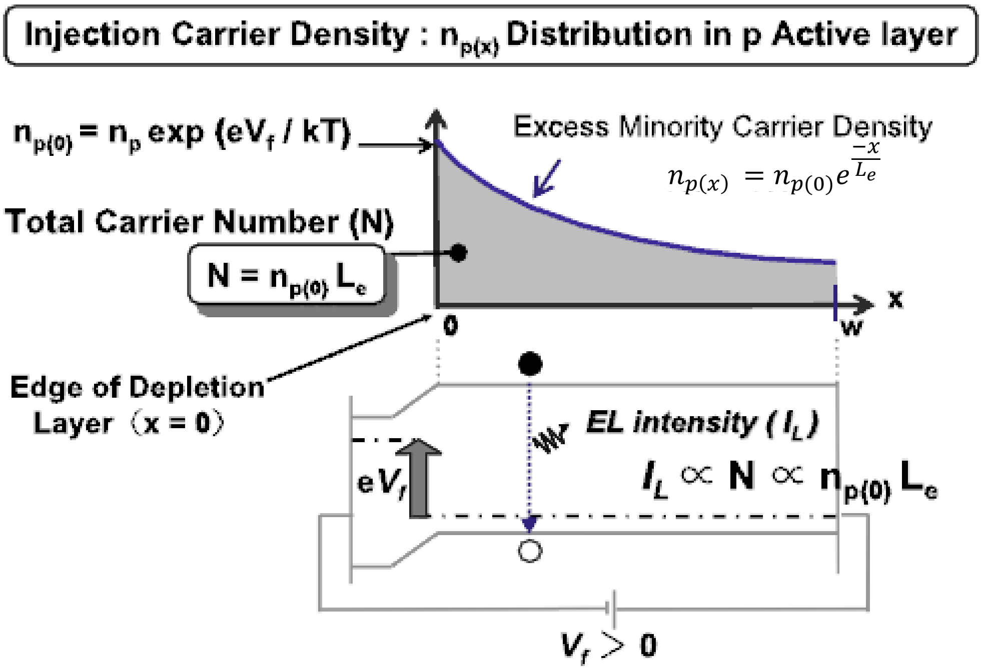

Figure 3.14: The distribution of carriers in the p layer of a p-n silicon cell. The effect of the applied forward voltage is illustrated [35].

3.3.4. Extrinsic cell defects

Micro-cracks

Silicon solar cells are made of thin, fragile wafers making the occurrence of micro-cracks fairly common. Micro-cracks can occur in the manufacturing process of the cell or in the assembly process of the module. They can be detected using an optical microscope but this is a time consuming process. EL provides a quick way of identifying cracks in cells and modules.

The effect of these cracks on the module power output depends on the extent of the cracks and whether the cracks remove portions of the cells from electrical contact. A crack in the cell material prevents electrical contact to the area and either fewer carriers are generated or none at all. The lack of radiative recombination in these areas renders these defects visible in the EL image.

The classification of micro-cracks is discussed by Kőntges et al [40] and divided into 3 classes:

i. Class A: Micro-cracks are visible in the EL but do not cause inactive areas of the cell.
ii. Class B: Micro-cracks result in an area of the cell that is darker in the EL image but varies with applied current density.
iii. Class C: Micro-cracks completely remove areas of the cell from electrical contact which appear completely dark in the EL image.

The effect on the power output of class A micro-cracks is minimal but has been shown that with time and thermal cycling class A micro-cracks can develop into B or C micro-cracks [40].

The orientation of the micro-crack also determines the effect it has on the power output. Cracks running parallel to the busbar are common [41] and can result in a large portion of the cell being inactive. Monitoring the occurrence of cracks due to the mechanical strain the module is placed under during manufacturing and use, using EL images provides information about the module degradation.

Broken fingers and poor cell contacts

Fingers are contacts that run perpendicular to the busbars across the cell. A break across the finger results in that area of the cell having decreased electrical contact. These defects are visible in the EL image as the area around the broken finger appears darker in the image.

The busbars and solder strapping in a cell provide the electrical contact to the cells. The contact between the solder strapping and the cell is dependent on the manufacturing processes used. Carriers are injected into the junction along the busbars so there is a high probability that radiative recombination will occur in these regions and a bright EL signal along the busbar results. This can be minimised in single cells by insuring good electrical contact but in modules the contacts are fixed.

An especially bright EL signal can be confirmed to be a poor contact with a high series resistance by using infrared imaging. A poor contact would result in a hot spot visible in the IR image.

3.4. Infrared Imaging

Infrared energy is emitted by an object proportional to its temperature. Thermal imaging cameras are able to detect the infrared electromagnetic radiation and focus the image using appropriate optics onto an infrared detector. The infrared image uses a colour scale to differentiate between temperatures. Thermal imaging is used in conjunction with EL images to differentiate between intrinsic material defects such as grain boundaries and extrinsic defects such as manufacturing faults, broken contact fingers or cracks. Variations in the module temperature, hot-spots, indicate poorly performing cells.

A hot-spot occurs when that cell is performing worse than the other cells in the series string. It becomes reverse biased and starts to dissipate power and heat up. The degradation that occurs due to hot-spot formation was discussed in detail in section 3.1.4.1.

3.5. Summary

A photovoltaic module can be characterised using different techniques, with each technique providing different information about the operating behaviour of the module. The I-V characteristic curve is obtained experimentally using I-V tracer equipment. This curve illustrates the maximum power output, the short circuit current and open circuit voltage of the module. The efficiency and fill factor can be determined from these parameters. Cell mismatch occurs when cells in the module are not producing similar currents due to mechanical defects or shading. Cell mismatch affects the performance of the module and can be mitigated by the use of bypass diodes. Device parameters extracted from the I-V curve using PSO extraction techniques can be used to model the solar cell. The LA-LBIC technique is used to determine the relative photoresponse of the cells in a module. A line scan of a module can provide information about cells in the module that have poor photoresponse. EL images provide a visible indication of the performance of cells and allow defects in a module to be quickly identified. EL imaging can be used in conjunction with infrared imaging to identify the cause of hot-spots. Localised areas of heating can be due to poor electrical contacts or severely cracked cells. The techniques discussed in this chapter are applied and discussed further in chapter 4.

Chapter 4

Experimental Details

4.1. Introduction

Module characterisation techniques provide information about the performance of the module and identifies cell mismatch. The experimental setup used in these characterisation techniques is explained further in this chapter.

4.2. Current-Voltage (I-V) Characterisation Setup and Methodology

4.2.1. Outdoor I-V Measurement System

The outdoor I-V measurement system measures the I-V characteristic curve of PV modules in outdoor conditions. Figure 4.1 (a) shows the set-up of the I-V tracer. The components of the system are indicated in the schematic, figure 4.1 (b), and are discussed below.

Agilent N3301A DC Electronic Load

The electronic load is used to step though a range of voltages allowing the current to be measured at each step. Electronic loads have a higher maximum power range than DC power supplies and thus are effective for characterising PV modules. However they are unable to sink current to zero volts for the short circuit current. In order to cover this 0-3 V region an additional linear power booster is used.

Agilent 34410A Digital Multi-meters

Three digital multi-meters (DMM) are used in the system to ensure accurate module testing. A precision shunt is placed in series with the output current. The voltage across the shunt resistor is measured by DMM 1 and since the resistance of the shunt is known the output current can be determined. The supply voltage is measured using DMM 2 as the electronic load can be inaccurate.

DMM 3 is used in conjunction with reference cell or pyranometer to measure irradiance. The sampling interval is set in the I-V tester software but is related to the sampling rate of the DMM. This model is capable of taking 10 000 readings per second at 5½ digits resolution.

Agilent 33220A 20Mhz Function/Arbitrary Waveform Generator

The function generator is used to simultaneously trigger the electronic load and measurements from the multi-meters.

Agilent 34970A Data Acquisition/ Switch Unit

This unit is used to for logging the data from the digital multi-meters and relaying it to the PC via a USB interface.

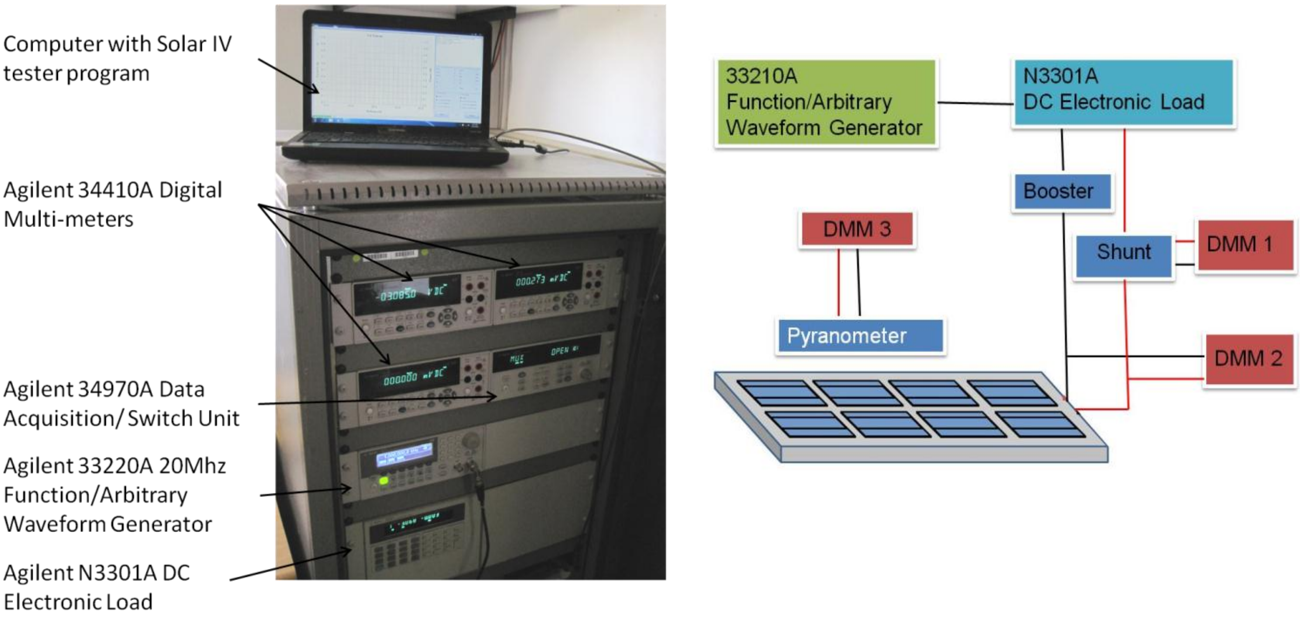

a) b)

Figure 4.1: a) The Outdoor I-V tracer system. b) Schematic of the component configuration.

The back of module temperature is measured using a thermocouple attached to the back of the module. The average temperature during the measurement is used to make temperature corrections. The voltage has significant temperature dependence while current is less significantly affected. The current (α), voltage (β) and power (γ) correction factors are given by the manufacturer. They can also be determined by measuring the parameters at different temperatures and then extracting the coefficient with regression analysis [13]. The temperature is corrected to 25 °C and the irradiance (Irrad) is corrected to 1000 W/m^2. The equation for corrected current (I_c), equation 4.1, combines both temperature and irradiance corrections, where I_m is measured current and T is the measured temperature. Equation 4.2 shows the calculation of the corrected voltage (V_c) from the measured voltage (V_m).

$$I_c = [I_m + \alpha(25 - T)] \times \frac{1000}{Irrad} \qquad 4.1.$$

$$V_c = [V_m + \beta(25 - T)] \qquad 4.2.$$

4.2.2. Dark I-V System

The Dark I-V system is used to determine the dark current-voltage characteristic of a PV module. The system setup has been fully described in previous research [19]. The system, seen in figure 4.2, with the schematic of the components illustrated in figure 4.3. The components of the system are discussed further.

Power Supplies

An Agilent E3646A programmable power supply is used for testing single solar cells. It has a range of 8 V and 3A. For the higher voltages needed for PV modules the Agilent power supply is used in conjunction with an Elteknix power supply, that has a range of up to 60V and 30 A. The set up for solar cells and PV modules is illustrated in figure 4.3. a) and b) respectively.

Digital Multi-meters

Agilent 34401A multi-meters are used to measure the voltage across the solar cell or PV module. Another is used to measure the voltage across the shunt resistor and thus determine the current.

Resistor box

The voltage is measured across a shunt, with a known resistance, to determine the current in the circuit.

Computer

The computer is used for logging data. The reading from the multi-meters are conveyed to the computer via a GPIB bus. A Labview program is used to acquire data and plot the current voltage curve on a log scale.

Module Compartment

The module is placed in a compartment such to ensure dark conditions. Under these conditions the PV modules can handle much higher voltages before saturation occurs.

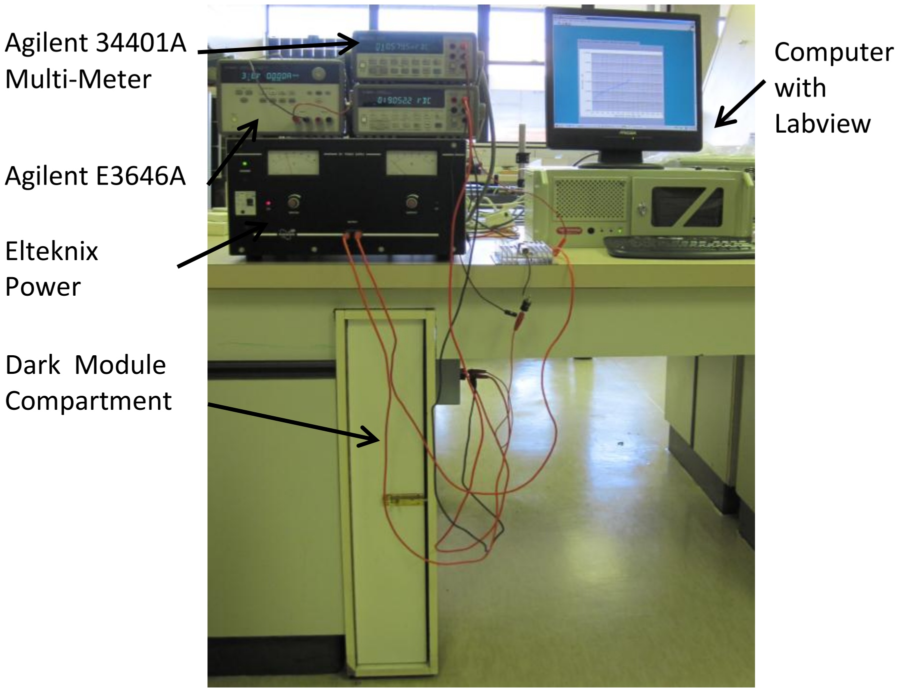

Figure 4.2: The dark I-V system with components labelled.

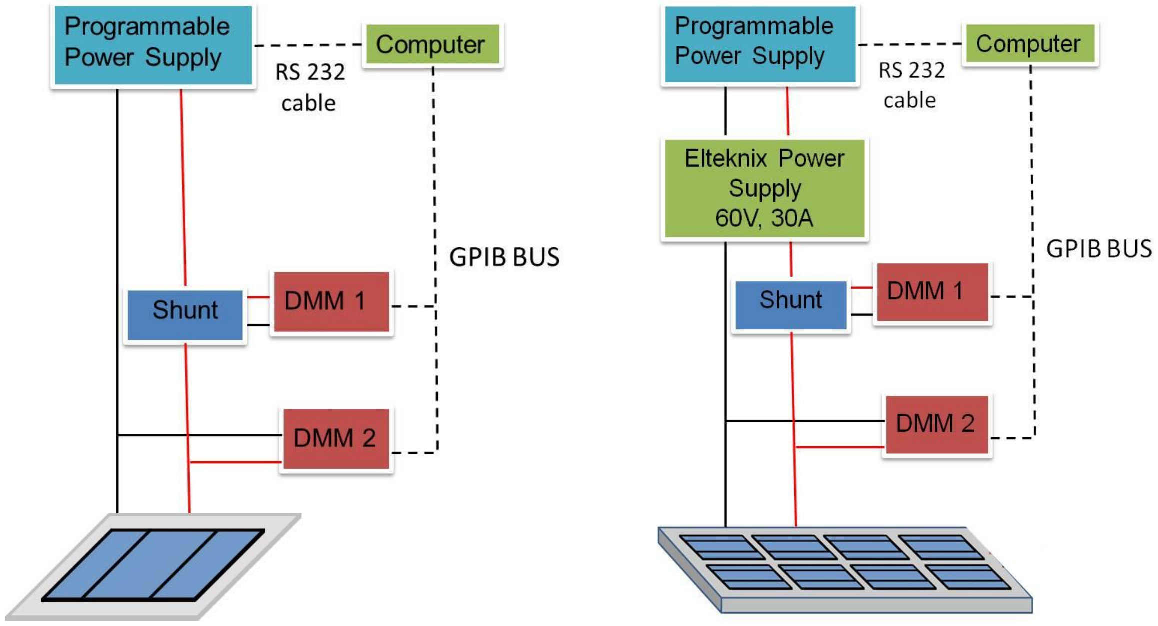

a) b)

Figure 4.3: Schematic of the dark I-V system a) for a single solar cell and b) for PV modules.

4.2.3. Worst-case cell determination

When a cell is shaded it is unable to generate current which results in cell mismatch. The degree of cell mismatch caused in the module I-V curve compared to the entire module I-V curve gives an indication of whether a good current generating cell has been shaded. This is the principal behind worst-case cell determination [27]. When a good cell is shaded the performance and I-V characteristic of the module is worse than the entire module. However, if a bad cell is shaded there is little change in the I-V curve shape since the cell wasn't contributing much current to start with.

The module is placed on a two-axis tracker so it is perpendicular to the incident solar irradiance. The measurements are performed at solar noon to ensure the best possible irradiance and spectral response. Rubber strips cut to the size of the cell are placed over each cell in turn and the I-V curve is measured using the outdoor I-V tracer described in section 4.1.1. The I-V curves are corrected for temperature and irradiance and then compared to the I-V curve of the entire module.

4.2.4. I-V curve modelling

The modelling of the I-V characteristics of a single solar cell is done using a Mathematica programme. The I-V curve is modelled using the diode equation which is solved using Newtonian methods, discussed in 3.1.2 and appendix B.1. The input parameters used in the diode equation are extracted from the measured curve using a Particle Swarm Optimisation (PSO) programme [19]. The I-V curve of an ideal module can be built up from the curve of a single cell if the assumption that all the cells are identical is made. The voltage is multiplied by the number of cells and the current is the same which gives the I-V curve of the entire module.

4.3. Large Area Light Beam Induced Current (LA-LBIC) measurement system set-up and methodology

The LA-LBIC system has a laser beam that acts as a light source in order to generate current from specific areas of the cell. A laser with a wavelength of 660 nm and power of 5 mW focussed to a spot with a diameter of about 1 mm was used. The photoresponse was measured and amplified using a current amplifier. Due to the low current, in the region of micro amps, and nature of the LBIC measurement technique the LBIC signal is proportional to the photoresponse of the cell material and not necessarily the current produced by the cell in the operational fully illuminated module. Thus it is possible for a cell can have high photoresponse in the LA-LBIC scan but produce a low current when connected in the entire module. Line scans were taken down the length of the module thus allowing the variations in photogenerated current of different cells to be observed. Figure 4.4 shows the experimental set up of the LA-LBIC equipment. The laser is mounted on a stage which can move in the x-y plane based on the commands from the drivers and Labview programme. The current measured by the current amplifier is represented as a graph in Labview with the current amplitude on the y-axis in arbitary units while the x-axis is a measure on position. For practical reasons the laser carriage is mounted below the module as illustrated in figure 4.5.

Line scans are done on the modules by scanning along the length of a string. The line scans can be performed along different positions on the cell. Inaccuracies in the motorised carriage system prevent the system from currently being used to raster scan and provide area maps of the cells.

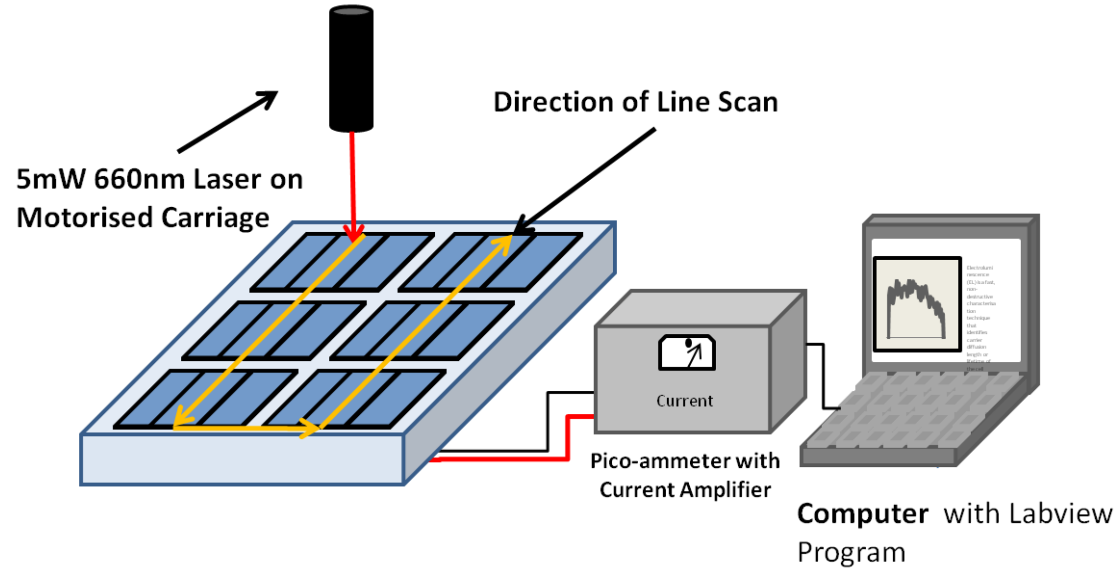

Figure 4.4: The experimental setup of the LA-LBIC system.

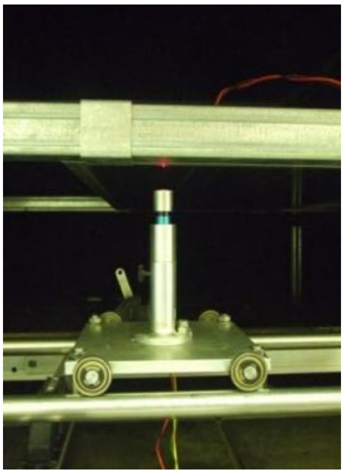

Figure 4.5: The LA-LBIC system with laser mounted on carriage below PV module.

4.4. Electroluminescence (EL) set-up and methodology

EL was used to non-destructively evaluate the extent of the degradation in PV modules. The modules under investigation were forward biased to a current greater than the short circuit current of the module. The emitted luminescence of a silicon sample has a peak at about 1150 nm and a portion of this peak is detected by the coolSamBa HR-830 Si CCD camera which has a range of 300-1000 nm [35]. The CCD camera is cooled to 50 °C below ambient and has a resolution of 3300 x 2500 pixels. The data acquisition time is in the range of 1.5 to 2.5 seconds. The experimental set-up is illustrated in figure 4.6. The DC power supply forward biases the module to a point on the I-V curve about one and half times its Isc indicated on figure 4.7, generally in the region of 30 V and 5 A.

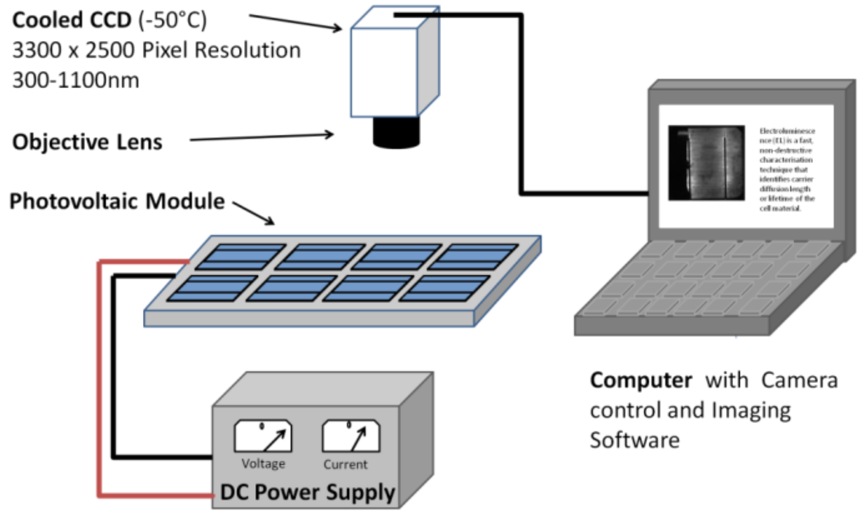

Electroluminescence (EL) is a fast, non-destructive characterisation technique that identifies carrier diffusion length or lifetime of the cell material.

Figure 4.6: Schematic outline of EL experimental setup.

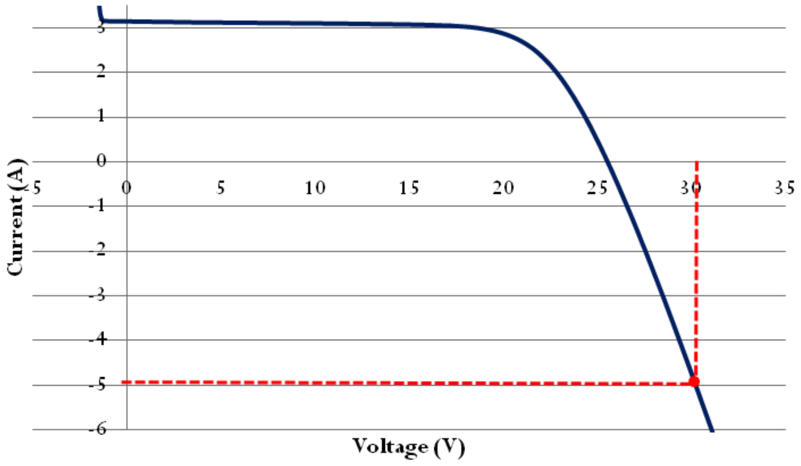

Figure 4.7: I-V curve with point of forward bias indicated.

In order for the electroluminescence to be detected the setup must be placed in a dark room as any light source will affect the results. The CCD camera is connected to the computer with image capturing software, which is supplied with the camera. Further image processing and analysis is done using free ImageJ software [42].

4.5. Modules in study

4.5.1. Module 1

This module has 72 single crystalline cells connected in 3 series strings. Figure 4.8 shows the module with the strings indicated. The module has degraded and there is visible delamination affecting about 4 cells in stings B and C. The interconnection of the strings can be varied depending on the voltage output required, 12 or 24 V. For this study we used the 24V connection with 3 bypass diodes placed in parallel over the three strings as seen in figure 4.9.

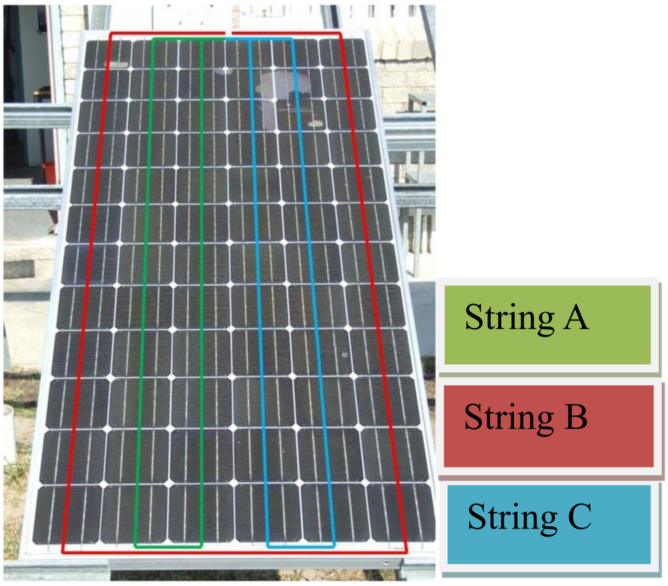

Figure 4.8: Module 1 with the strings indicated. There is visible damage to cells in strings B and C.

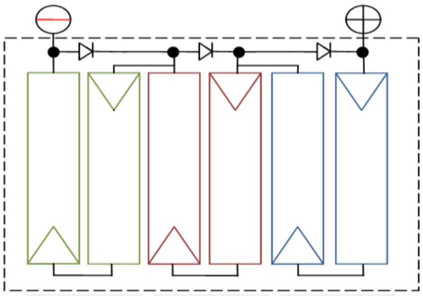

Figure 4.9: Diagram of cells connected in series strings and the bypass diodes connected across the strings in parallel.

This module has a specified power output of 110 W with an Isc of 3.45 A and Voc of 43.5V. The effects of the damage on the module's I-V characteristics are investigated using I-V tracer equipment. Thermal imaging and LA-BIC techniques were used to further identify cell mismatch in the module.

4.5.2. Module 2

The Edge-defined film-fed (EFG) module has 36 cells connected in series. The module is configured with two strings of 18 cells. Bypass diodes can be connected in parallel over each string. There is visible delamination around the edges of the module as seen in figure 4.10. Previous studies on this module have shown that the encapsulant delaminated and moisture ingress has occurred [43].

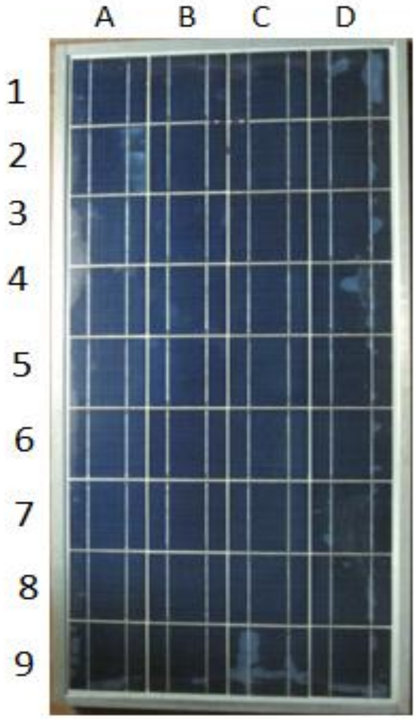

Figure 4.10: Module 2 with visible delamination around the edges of the module.

The Module has a manufacturer specified power output of 49 W and an Isc of 3.2 A and Voc of 20V. The effect of the delamination was determined by taking I-V curves in light and dark conditions and by using EL, LA-LBIC and thermal imaging techniques.

4.5.3. Module 3

Module 3 is multi-crystalline silicon with one string of 36 cells in series. The module was custom made with cells having dimensions 2.5 cm x 7.5 cm. As can be seen in figure 4.11 the module consists of a single string of cells so it is not possible to introduce bypass diodes into the configuration. This module was characterised using outdoor I-V curve, dark I-V curve, worst-case cell determination, LA-LBIC scans and thermal and EL imaging.

Figure 4.11: An optical image of the custom-made 36 cell multi-crystalline silicon module with dimensions 110 cm x 12 cm.

4.5.4. Module 4, 5 and 6

Modules 4, 5 and 6 are single crystalline silicon modules with the same cell material and configuration, shown in figure 4.12. The modules have 44 cells connected in two strings of 22 cells with bypass diodes connected in parallel across the strings. The specified power output is 65 W. Modules 5 and 6 have a visible grey-white discolouration that affects both modules to an equal extent. This is thought to be due to degradation in the anti-reflective coating on the cell surfaces. The effects of this degradation can be determined by comparing these modules with module 4 that has no visible degradation. Module 4 acts as a reference module for comparison with modules 5 and 6.

The illuminated I-V curves of these modules were obtained using the I-V tracer equipment. These results were compared with EL and thermal images to identify the cause of the cell mismatch. The results of the modules were compared in order to determine the effect the degradation on the module performance.

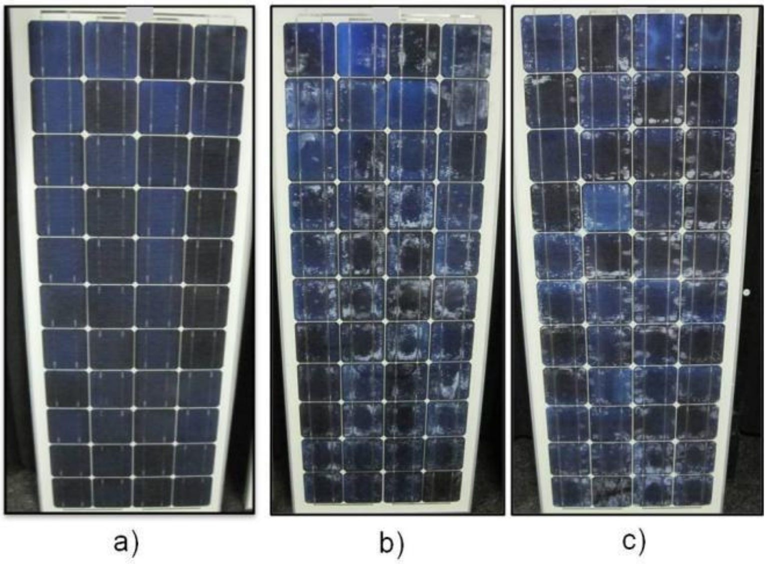

a) b) c)

Figure 4.12: Optical image of a) Module 4(reference), b) Module 5 and c) Module 6.

4.6. Summary

The characterisation techniques discussed in this section were used in this study to characterise cell mismatch in PV Modules. Cell mismatch results in lower power performance which can be observed in the I-V curves of the modules. Dark I-V measurements and worst-case cell determination techniques provide further information about the I-V characteristics of the module and the individual cells. In order to identify the cause of this cell mismatch other techniques such as LA-LBIC, Thermal and EL imaging are necessary. These techniques are applied to several modules, summarised in table 4.1, and the results are discussed in chapter 5.

Table 4.1: Summary of Modules used in this study and manufacturer given parameters.

Module No.	No. of cells	Material	Voc	Isc	P_{max}
1	72	c-Si	44 V	3.5 A	110 W
2	36	EFG Si	20 V	3.2 A	49 W
3	36	m-Si	20 V	0.8 A	12 W
4	44	c-Si	25 V	3.6 A	65 W
5	44	c-Si	25 V	3.6 A	65 W
6	44	c-Si	25 V	3.6 A	65 W

Chapter 5

Results and Discussion

5.1. Introduction

The results of measurements on the modules introduced in chapter 4 are discussed in this chapter. The details of these modules are listed below:

Module 1: 72 Cell Single crystalline Silicon

Module 2: 36 Cell Edge-defined Film-Fed (EFG) Silicon

Module 3: 36 Cell Custom-made Single crystalline Silicon

Module 4: 44 Cell Single crystalline Silicon

Module 5: 44 Cell Single crystalline Silicon

Module 6: 44 Cell Single crystalline Silicon

The results of modules 4, 5 and 6 are compared as the modules are the same cell material and they have identical cell configuration.

5.2. Module 1

5.2.1. Introduction

Module 1 is a single crystalline silicon module with 72 cells connected in three strings. The module has been damaged and areas of delamination are present in two of the three strings. The effect of this damage on the performance of the module was determined by the current voltage characteristic and infrared imaging.

5.2.2. Current-Voltage (I-V) Characteristics

The visual inspection of the module, shown in figure 5.1, shows that string C has the most significant damage. String B has some damage while string A has no visible damage. The I-V curves of the module and the individual strings were measured using the outdoor I-V measurement system. Figure 5.2 shows the I-V curves of the three strings compared with the I-V curve of the entire module with bypass diodes. Bypass diodes are connected in parallel over each string as discussed in section 4.5.1. String C is the weakest string in the module so without the bypass diodes the current output of the entire module is limited by this string. However, the bypass diode is activated by the reverse biasing of string C resulting in a step in the module curve and an observed increase in current as the connection of bypass diodes allows the Isc of the module to increase to close to the Isc of string A. String A has the best individual I-V curve and it gives an idea of the current output of the rest of the strings if no damage had occurred. The ideal, undamaged curve of the module can be generated by assuming all strings would have a performance of string A. This I-V curve is shown in figure 5.3 along with the I-V curves of the module with and without bypass diodes. Table 5.1 details the performance parameters of the simulated, undamaged module and the actual module with and without bypass diodes. The presence of bypass diodes prevents the current from being limited by the Isc of the weakest string, 2.50 A, causing a step in the I-V curve which increases the Isc of the module to 3.46 A. However, the bypass diodes do not increase the power output of the module substantially and in both configurations the power output is much lower, between 37 and 39 W, than the ideal 72 W.

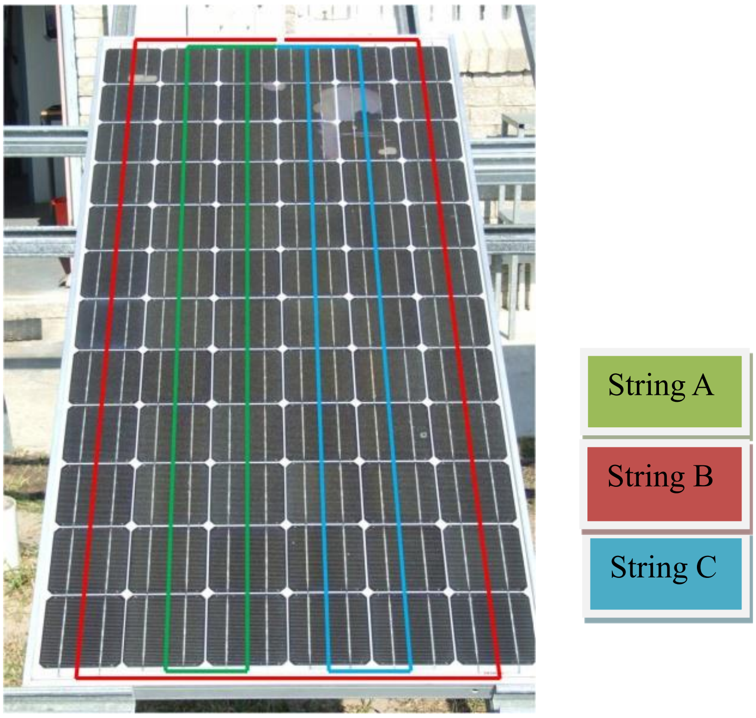

Figure 5.1: Photograph of 72 cell single crystalline silicon module with strings indicated.

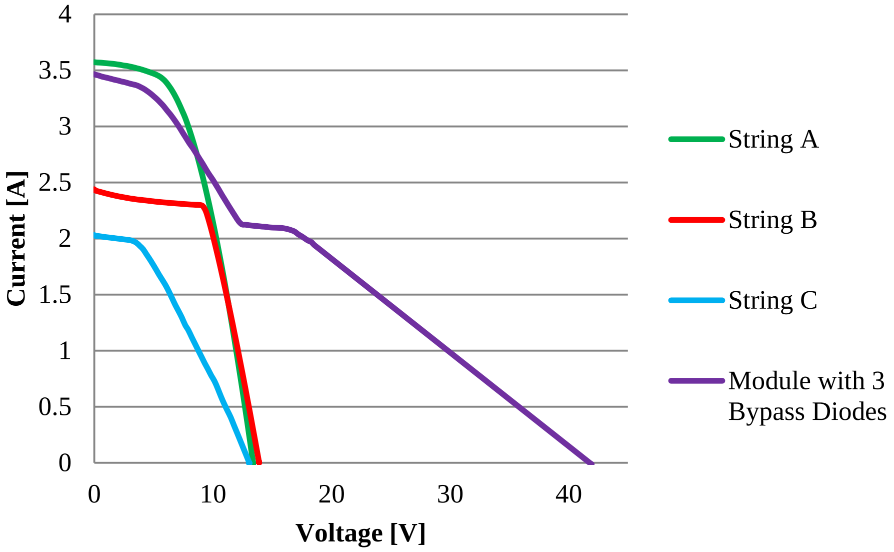

Figure 5.2: I-V curves of the individual strings and the whole module with bypass diodes.

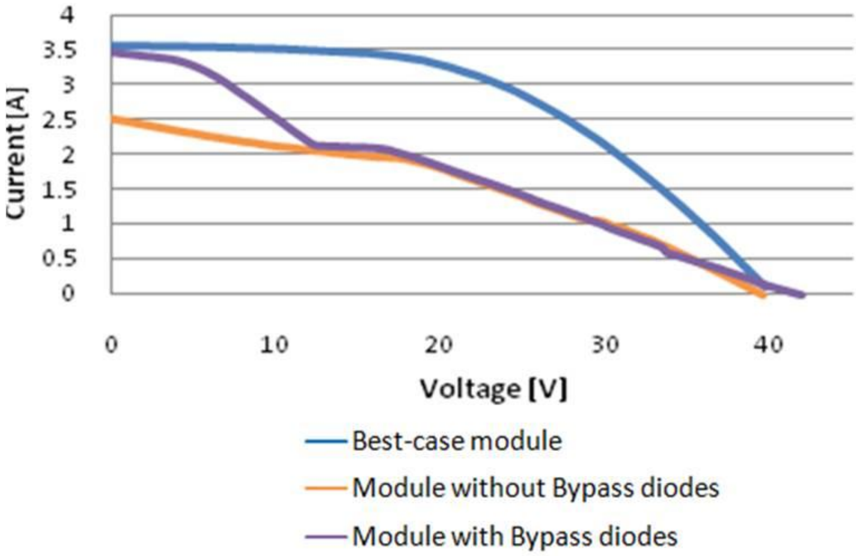

Figure 5.3: I-V curve of the undamaged module compared with the measured curves of the module with and without bypass diodes.

Table 5.1: Performance Parameters of Module 1.

	Isc [A]	Voc [V]	Pmax [W]
Ideal Module	3.57	39.9	72.0
Module with Bypass diodes	3.46	41.7	38.2
Module without Bypass diodes	2.50	39.1	37.3

5.2.3. Infrared Imaging

The cell mismatch present in the module results in hot spots which can be seen using infrared imaging techniques. An infrared image of the damaged area of the module is shown in figure 5.4. along with the optical image. The module has bypass diodes connected across the strings so while the damaged string is not reverse biased by more than +/-0.5 V, the activation voltage of the bypass diodes, the damaged cells will still be reverse biased and dissipating heat. The damaged area in string C is highlighted in region i) in both images. The initial cause of damage to these cells is not known but could be attributed to a micro crack in the cell that degraded further with thermal cycling resulting in a severely cracked cell. The heat generated by this cell caused the delamination, the encapsulant has separated from the cell and the cell is visibly cracked. The cracked cell area is visible as a cold area in the infrared image. The rest of the cell heats up to over 40°C as the cell is reverse biased. This heating causes the further damage to the cell and the delamination spreads across the surrounding cells. However, the presence of micro-cracks in the module could not be confirmed with electroluminescence (EL) imaging as the EL equipment was not available at the time.

The infrared image of the module shows a hot spot in string B, labelled ii), which is not visible on the front of the module. This hot spot could with time spread and result in delamination and possibly cracked cells like what is seen in string C. Evidence of the hot spot is visible on the back of the module where a bubble has occurred in the encapsulant.

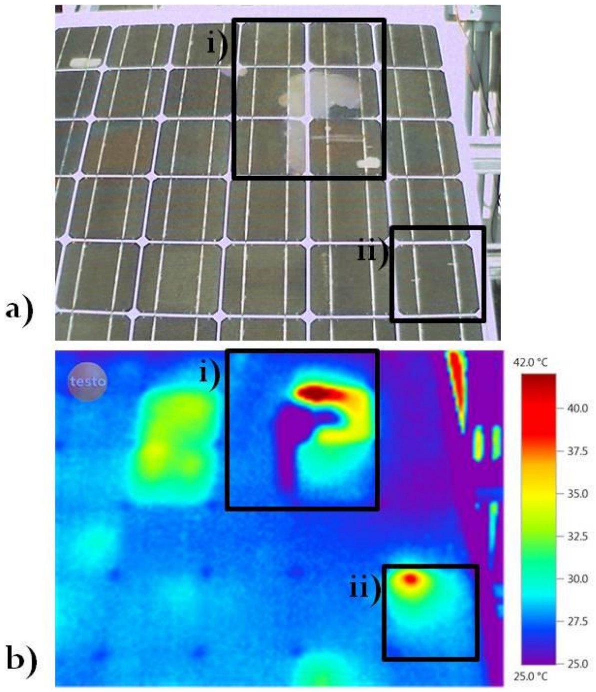

Figure 5.4: a) Optical image and b) Infrared image of the same portion of the module with damaged portion of string C labelled i) and a hot spot in string B labelled ii).

5.2.4. Discussion of Results

The visible damage to this module has caused the power output to drop from a potential 72W to 38W. Since the damage occurs on two of the three strings it is too severe to be offset by the use of bypass diodes. The bypass diodes increase the Isc value but don't substantially increase the power output. The damage to the module results in hot spots which are visible in the infrared images of the module. These hot spots can result in further damage to the module as they cause further delamination and cell degradation. The bypass diodes are helpful in preventing hot spot formation and further degradation.

5.3. Module 2

5.3.1. Introduction

Module 2 is a 36 cell EFG silicon module with visible delamination around the edges of the module. This module was used in a previous study exposing it to outdoor use and thermal cycling which resulted in the delamination and moisture ingress in the module[43]. The effect of this delamination on the performance of the module is investigated using current-voltage characteristics, LA-LBIC, EL and infrared imaging techniques.

5.3.2. Current-Voltage (I-V) characteristics

5.3.2.1. Illuminated I-V curve

The I-V curve of module 2 was measured pre-deployment before any degradation had occurred [43]. Defects could have occurred before deployment in the manufacturing, transport or installation processes. Recently the I-V curve was measured again without bypass diodes and with bypass diodes connected in parallel over each of the two strings. The ideal I-V curve of a 36 cell module is simulated using PVSim [21]. All the curves are shown in figure 5.5. The I-V curve of the module after deployment with bypass diodes has a step indicating the activation of a bypass diode. The bypass diode is activated when a string in the module is producing less current than the other string. The bypass diode is, however, unable to increase the current output of the module significantly possibly since both strings are affected by the delamination. The defects and cell mismatch in the module will be discussed further in the EL imaging section. The module parameters of the undamaged module and the module with and without bypass diodes are given in table 5.2. Comparison of the measured and simulated curves and parameters shows a drop in maximum power output from 49 W to 39W. This is due to the performance degradation resulting from the delamination or from other defects. The shape of the curve is also affected, resulting in a decrease in the fill factor. Previous studies [43] have shown that the presence of delamination and the resulting moisture ingress cause an increase in parasitic resistances. The effect of series resistance can be seen in the slope of the graph between the Vmax and Voc point. The series resistance increases since the busbars and contacts are degraded by the presence of air and moisture ingress.

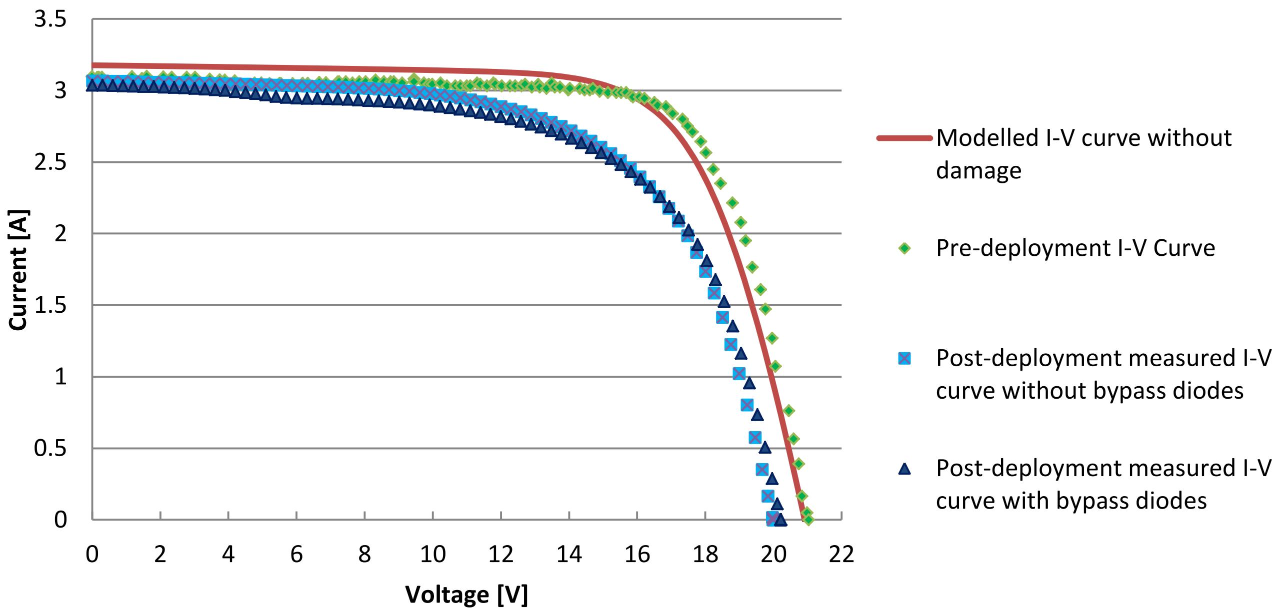

Figure 5.5: The I-V curves of module 2 with and without bypass diodes and the simulated curve of the undamaged module.

Table 5.2: The module parameters of Module 2

	Voc [V]	Isc [A]	FF [%]	Vmax [V]	Imax [A]	Pmax [W]
Module Pre-deployment	21.04	3.10	75	16.85	2.89	48.64
Simulated undamaged module	20.99	3.17	75	17.01	2.92	49.69
Module Post-deployment without bypass diode	19.99	3.06	63	15.22	2.55	38.96
Module Post-deployment with bypass diode	20.21	3.03	62	15.53	2.48	38.54

5.3.2.2. Parameter extraction and modelled I-V curve

The average parameters of a single cell are determined using the Particle Swarm optimisation (PSO) parameter extraction programme. The programme determines the parameters that allow the two-diode equation to best fit the measured curve. It determines values for series resistance (Rs), shunt resistance (Rp), diode saturation current (Is), ideality (n) and photogenerated current (Iph). The parameters are extracted from the measured pre-deployed module and from the post-deployment, delaminated module. These parameters are given in table 5.3.

Table 5.3: Average extracted parameters for a single cell.

	Rs (Ω)	Rp (Ω)	Is1 (A)	n1	Is2 (A)	n2	Iph (A)
Pre-deployed Module	0.0047	140.61	0.00019	3.36	2.09×10^{-7}	1.72	3.06
Post-deployment Module	0.0052	34.24	0.00023	2.26	1.92×10^{-7}	3.14	3.03

The extracted parameters are the average for a single cell, so the series and shunt resistances are 36 times greater for the entire module. Comparison of the parameters for the pre-deployed module and the module in its current state after several years of outdoor exposure and storage shows a decrease in shunt resistance with time. The shunt resistance is originally 5062 Ω and drops down to 1224 Ω indicating that degradation of the cell material has resulted in losses due to shunting. The series resistance has increased slightly since deployment from 0.17 Ω to 0.19 Ω for the entire module. It is expected for the series resistance to increase with time as degradation in the contacts and bulk material contributes higher resistances. The ideality factors, n1 and n2, are greater than what is typically expected possibly due to the parameter extraction methods or due to the averaging process.

The parameters for the current delaminated module are entered into the Mathematica simulation programme, described in appendix 1, and the module curve is acquired. The simulated I-V curve and the measured I-V curve are shown in figure 5.6. The simulated curve fits the measured curve well apart from a poor fit around the knee. The PSO program calculates the device parameters of a single cell. These are used to simulate the curve of a single cell which is then used to construct the entire module curve. The PSO curve fitting program runs until a fit with a R^2 value of greater than 0.9999 is achieved. However, a good R^2 value can be achieved even if there is a poor fit around the "knee" of the I-V curve. For example there can be good fit in the short circuit and open circuit regions but the knee has a poor fit. The ideality factor affects the region of the curve between the knee and Voc so poor fit around the knee can result in inaccurate ideality values being extracted.

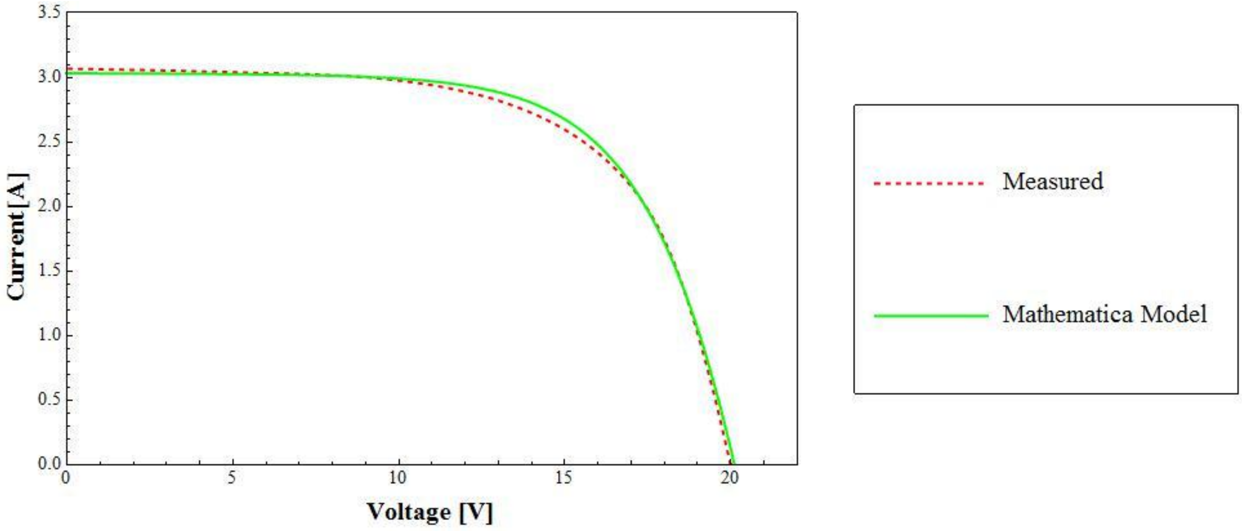

Figure 5.6: The measured I-V curve of module 2 compared with the curve simulated using the Mathematica model.

5.3.2.3. Dark I-V curve

The dark I-V curve of module 2 is shown in figure 5.7. The different regions in the curve are affected by different loss mechanisms. The low voltage region is affected by shunt resistance and the linear shape of this graph in this region suggests a large shunt resistance. The high voltage area is governed by series resistance. In this region the graph does not deviate from the linear shape indicating that low series resistance in the module. If the series resistance was higher the curve would flatten off as the current is limited. This is supported by the results from the light I-V parameter extraction.

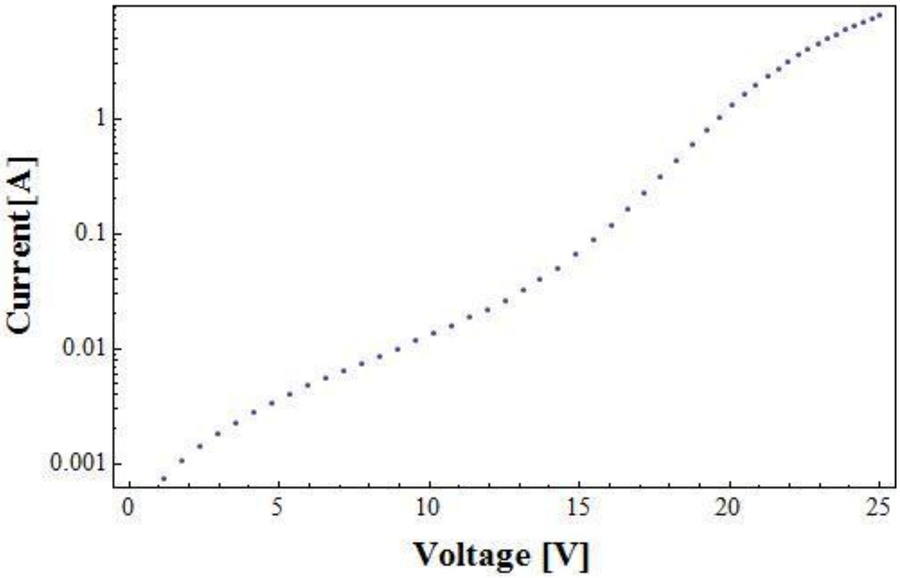

Figure 5.7: The dark I-V curve of module 2.

5.3.3. Large Area Light Beam Induced Current (LA-LBIC)

A LA-LBIC line scans gives an indication of the relative photoresponse of the individual cells in a PV module. The effect of the delamination on the photoresponse of the cells in the module can be determined using this technique. The LA-LBIC line scan measures the amplified current as a function of position. In figure 5.8 three cells with delamination have been highlighted in the module. An enlarged view with the direction of the line scan indicated of cells B1, D4 and C9 are shown in figure 5.9 a), b) and c), respectively. The LA-LBIC line scans of cells B1, D4 and C9 are shown in figure 5.9 d), e) and f), respectively. In all three cells the delamination results in a drop in current amplitude. The areas with white delamination result in a slightly lower current output than the grey areas of delamination. The delamination results in a drop in current of between 5 and 10 %. This is due to degradation of the cell material due to exposure to air and moisture ingress from the delamination. Also the discolouration, white or grey, in the encapsulant layer acts to shade the cell causing a lower photoresponse in that area. The laser beam has a spot size of 1mm however reflections within the material result in a slightly larger effective beam size.

5.3.4. EL and infrared images

EL and infrared imaging is also used to assess the effects of the damage to Module 2. Figure 5.10 (a) shows the optical image of module 2 with cells C5 and C9 indicated. Figure 5.10(b) and 5.10(c) show the EL images of the C5 and C9, respectively.

Despite there being no optically visible damage to cell C5, the EL image shows that the cell has cracked. This crack decreases the electrical contact to a portion of the cell and thus lowers the intensity of the EL signal. The nature of the EFG growth process results in striation-like variations in the cell material which are visible in the EL image. The eight back contacts that are present in each EFG cell are visible as areas of lower EL signal intensity. This is due to the high collection efficiency in these areas due to the back contact.

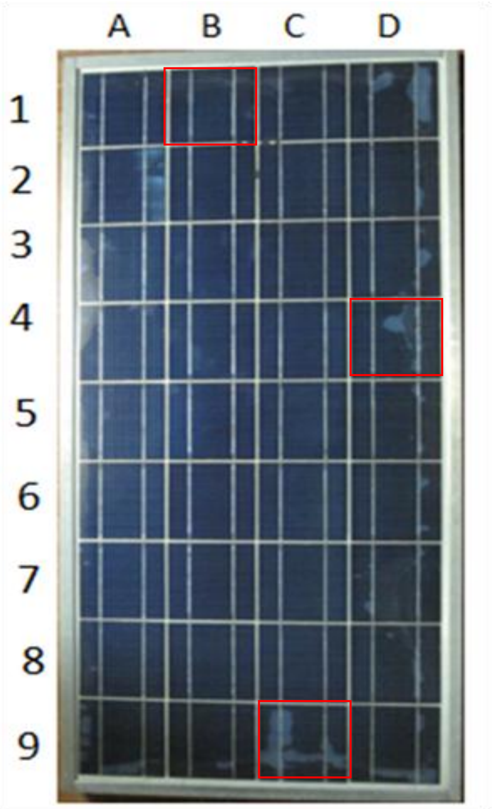

Figure 5.8: Optical image of module 2 with cells B1, D4 and C9 highlighted.

Cell C9 is severely affected by delamination which has spread along the busbar and affects about half of the cell. The EL image shows very low signal intensity over the areas of the cell affected by delamination meaning that the exposure to moisture has degraded the cell material and what little luminescence that is produced is blocked by the encapsulant discolouration.

Figure 5.11 shows the infrared image of the bottom-right corner of the module under forward bias conditions. The ambient temperature of the room is below 20°C. A hot spot is visible over cell C9 identifying it as a damaged cell. This suggests that cell C9 is a poor current producing cell since it is being reverse biased and dissipating heat. This supports what is seen in the optical and EL images. The cells that are good current producing cells are operating at lower temperatures in the region of 22-24°C.

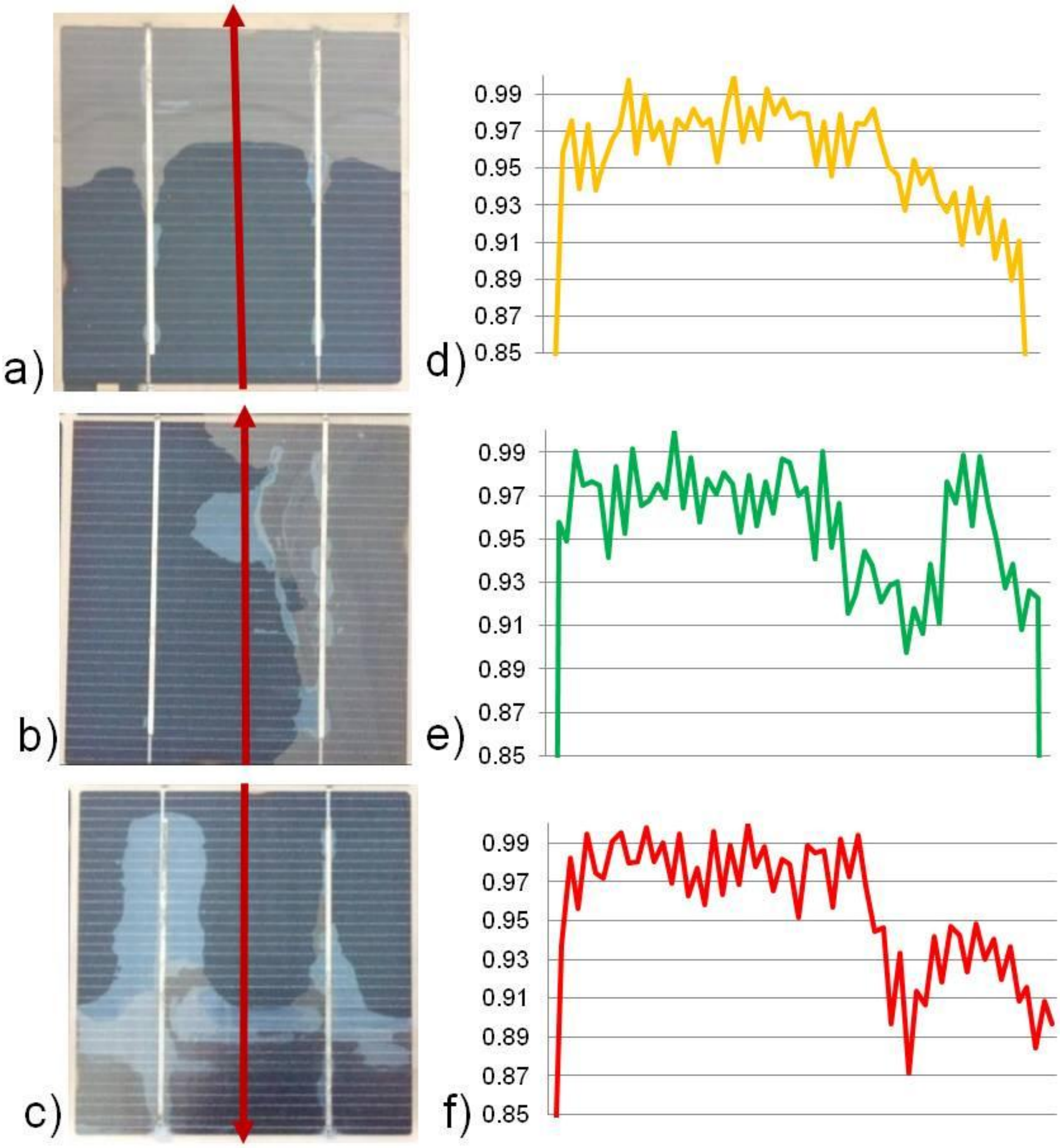

Figure 5.9: Optical image of cells a) B1, b) D4 and c) C9 with the direction of the line scan indicated. The line scans of cells d) B1, e) D4 and f) C9.

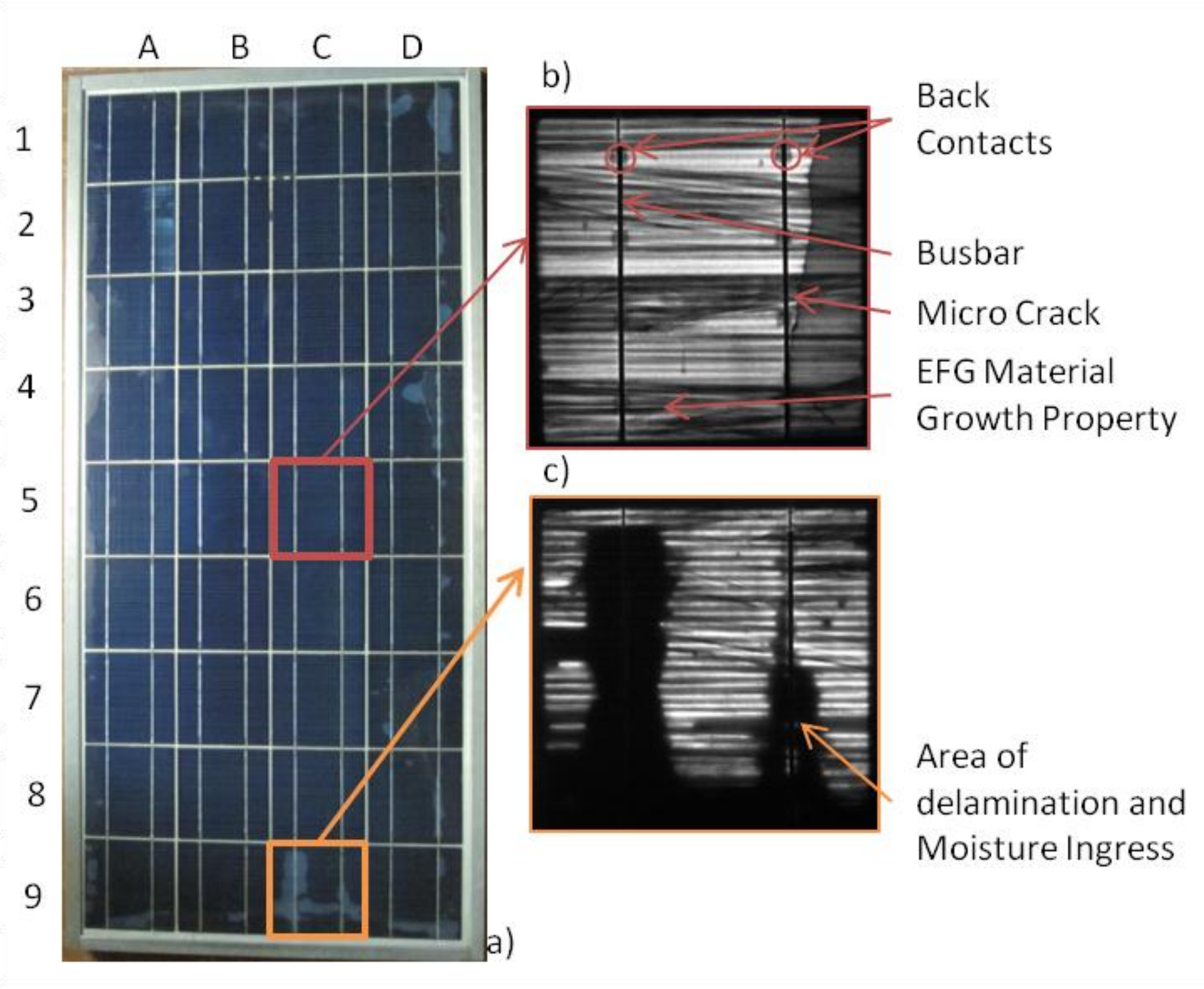

Figure 5.10: (a) Optical image of EFG module with cells indicated. (b) EL image of cell C5 with defects highlighted, (c) EL image of cell C9 showing the effect of delamination.

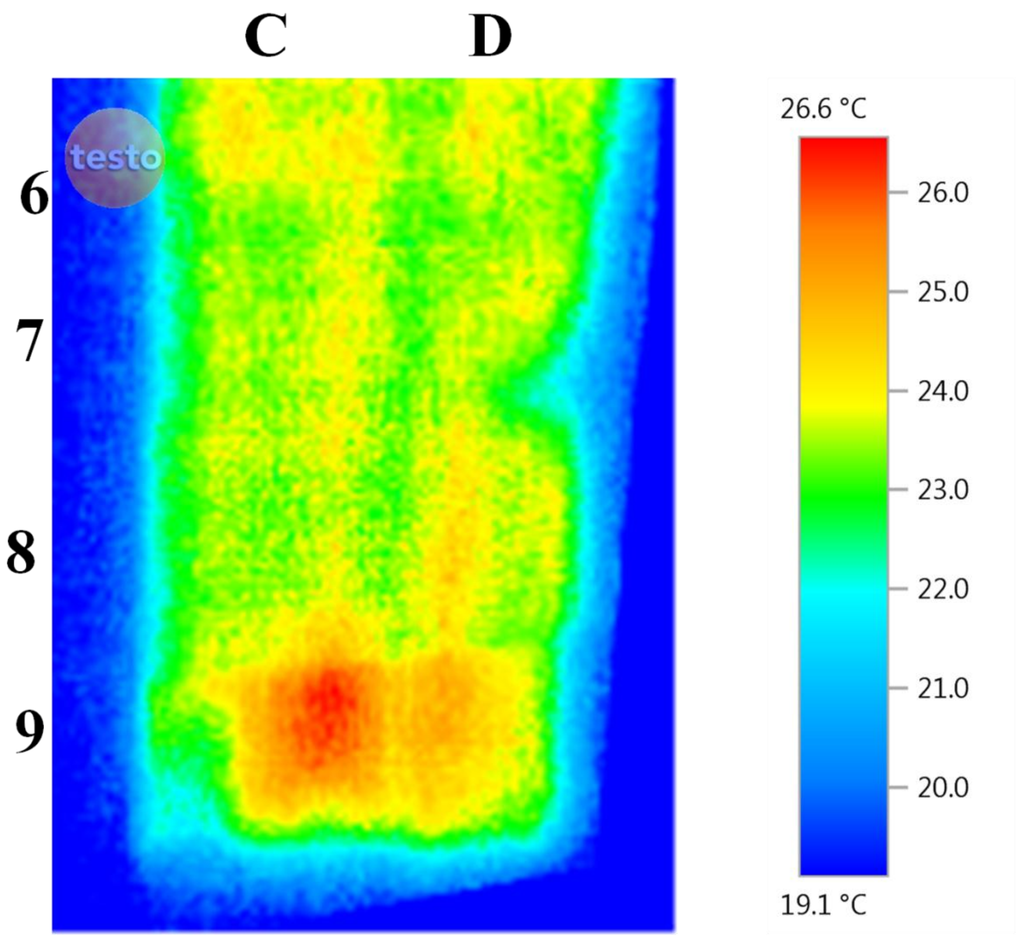

Figure 5.11: Infrared image of a portion of the EFG module.

5.3.5. Discussion of Results

The effects of the delamination in the module are visible in the I-V curve of the module where the power output is much lower than the pre-deployed I-V curve. Since the delamination affects both strings in the module the presence of bypass diodes did not significantly increase the power output of the module. An I-V curve of the module is modelled using extracted parameters, with reasonably good fit. The extracted parameters and the dark I-V curve indicate a high shunt resistance and low series resistance. The effects of shunting and series resistance have increased since deployment resulting in significant performance losses. The LA-LBIC line scans and EL images indicate that the areas affected by the delamination have a lower photoresponse and current output. The delamination in module 2 has resulted in significantly lowering the module performance. This illustrates the importance of the module manufacturing and laminating process as the cell material is itself undamaged.

5.4. Module 3

5.4.1. Introduction

Module 3 is a custom-made 36 cell multi-crystalline silicon module. It consists of a single string of cut cells which was commissioned for a low concentrator PV application. When a module is placed under a higher concentration of sunlight the loss mechanisms such as series and shunt resistance are amplified so full module characterisation is necessary. This module was characterised using I-V curve, worst-case cell determination, LA-LBIC, EL and Infrared Imaging.

5.4.2. Current-Voltage characteristics

5.4.2.1. Illuminated I-V curve

The I-V curve of module 3 was measured using the outdoor I-V tracer equipment. The measured I-V curve is compared with the ideal I-V curve and the simulated curve using extracted parameters. These three I-V curves are shown in figure 5.12.

The custom-made module does have manufacture specified performance parameters so an ideal I-V curve for the 36 cell module has to be simulated using ideal device parameters. The parameters used for the ideal module curve are shown in table 5.4 and are based on values used for modelling multi-crystalline silicon cells [15]. The current, voltage and power values of the measured and ideal modules are given in table 5.5. The fill factor indicates the deviation of the shape of the I-V curve from the ideal shape. In this module the I-V curve the measured fill factor is 49% which is low compared to the ideal curve, 79%. This indicates the presence of performance limiting features such as high series resistance and shunting.

The device parameters are extracted from the measured curve using the PSO programme and then used to construct the I-V curve of the entire module using the Mathematica programme. The modelled I-V curve uses PSO extracted parameters listed in table 5.6. The fit of the curve using average device parameters is not very good for reasons discussed in 5.3.2.2. The comparison of the measured and simulated I-V curves illustrates the slight variation of the extracted parameters. The series resistance of the entire module is 5.04 Ω and the shunt resistance is 533 Ω. This indicates that significant losses are occurring due to high series resistance and shunting. The series losses are observed in the shape of the I-V curve.

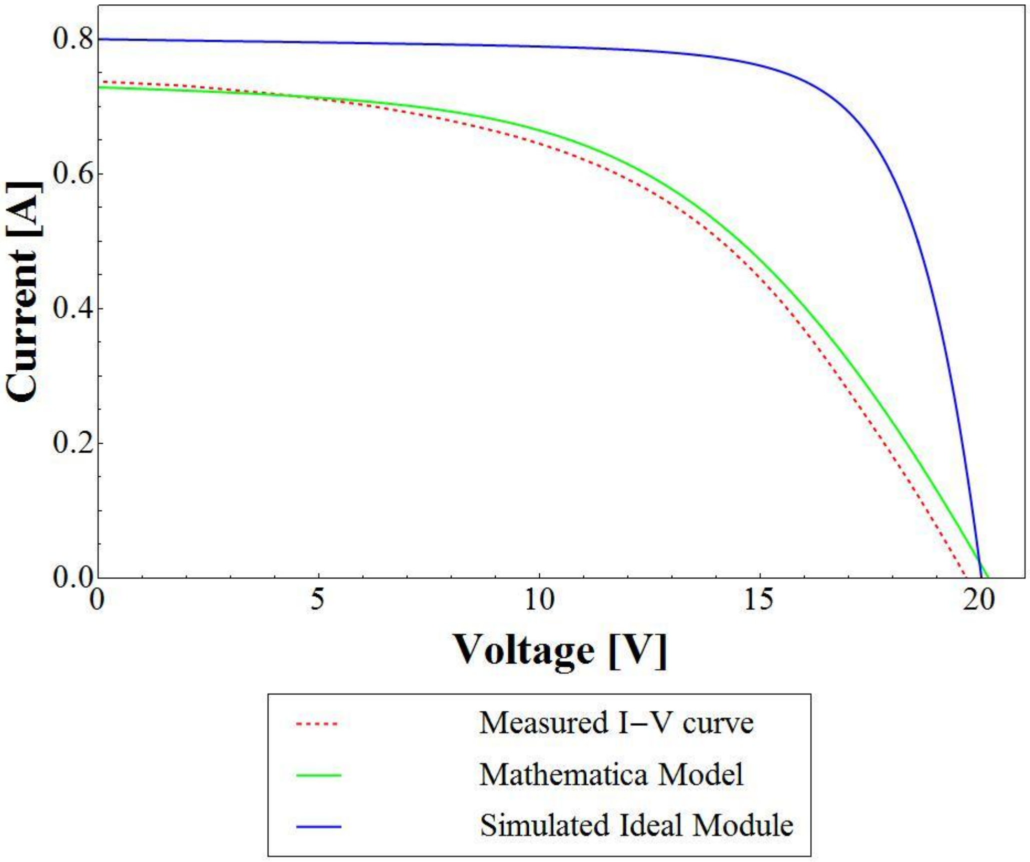

Figure 5.12: The measure I-V curve of the measured curved, the Mathematica modelled I-V curve and the ideal, simulated I-V curve.

Table 5.4: Device parameters for a single ideal multi-crystalline silicon cell

	Rs (Ω)	Rp (Ω)	Is1 (A)	n1	Is2 (A)	n2	Iph (A)
Simulated cell	0.0052	34.24	0.00023	2.26	$1.92\text{x}10^{-7}$	3.14	3.03

Table 5.5: Performance parameters of the measured and ideal I-V curve

	Isc [A]	Voc [V]	FF [%]	Pmax [W]
Measured	0.74	19.8	49	7.21
Ideal	0.8	19.9	79	11.86

Table 5.6: Average extracted parameters for a single cell

	Rs (Ω)	Rp (Ω)	Is1 (A)	n1	Is2 (A)	n2	Iph (A)
Simulated cell	0.14	14.80	0.00023	2.38	2.41x10-7	2.41	0.73

5.4.2.2. Dark I-V curve

The dark I-V curve of module 3 is shown in figure 5.13. The shape of the curve in the low voltage region suggests the low shunt resistance values and thus losses due to shunting. The series resistance affects the high voltage region. In this case the linear shape of the curve in this region suggests low series resistance. This is contrary to the results of the light I-V curve parameters extraction.

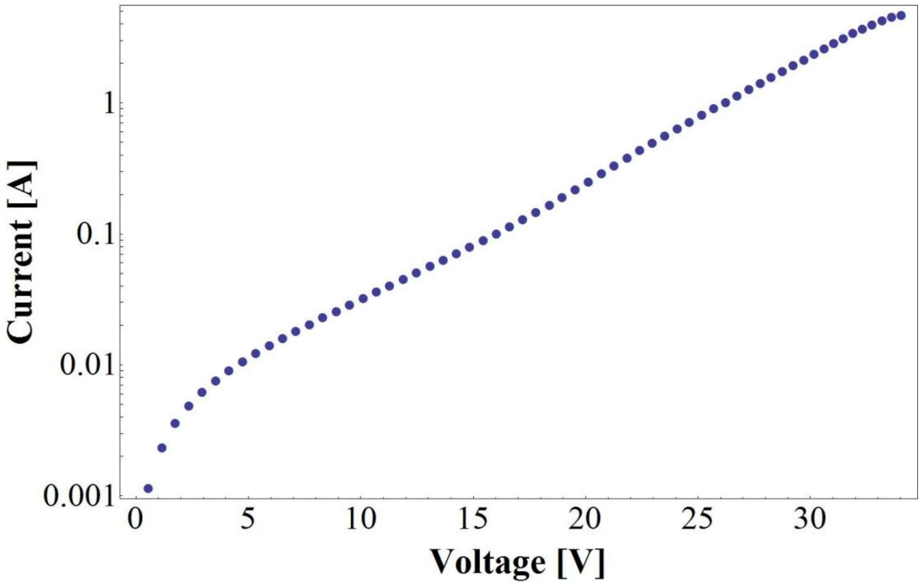

Figure 5.13: Dark I-V curve of module 3.

5.4.3. EL and IR images

The module has no visible defects or damaged areas in the cells or contacts, as seen in figure 5.14. However, the EL image, figure 5.15, of the entire module shows defects in the module. The intensity of the EL signal varies throughout the entire module. The changes in intensity are due to intrinsic defects in the cell material or due to extrinsic defects such as micro-cracks that may have occurred during manufacturing. Since cell 12 produces no EL signal it is identified as being completely inactive and the weakest cell in the module. This could be due to the solar cell device, itself, being faulty or having poor junction characteristics, resulting in it not functioning as a p–n junction device.

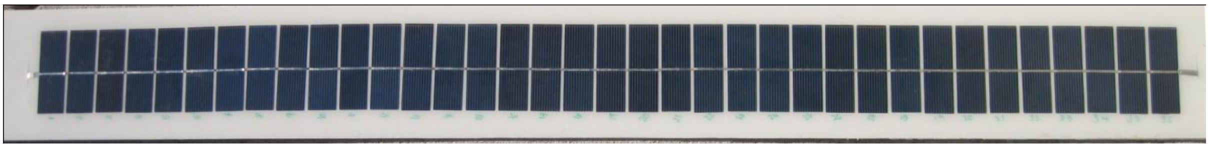

Figure 5.14: An optical image of module 3.

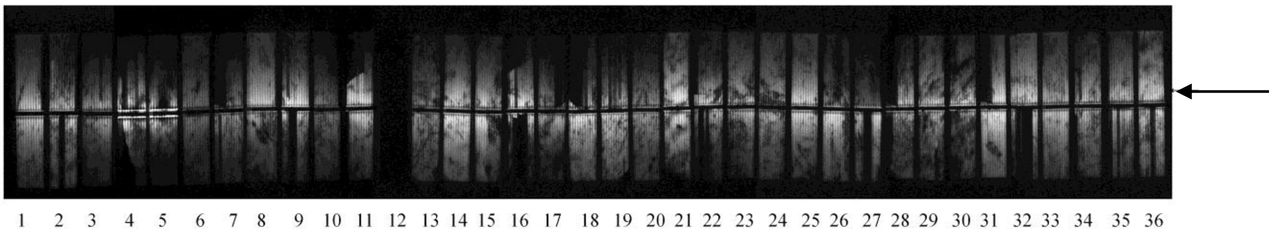

Figure 5.15: An EL image of the module under forward bias of 2 A. The white areas indicate high EL intensity. The arrow indicates the path of the LA-LBIC line scan.

Figure 5.16 shows a close-up view of cells 1–7. The variations in the EL intensity observed indicate variations in the cell material corresponding to grain boundaries in the cell material, cracks and broken contact fingers as labelled in figure 5.16. These defects are prevalent throughout the module, as shown in figure 5.15, and give rise to considerable cell mismatch. The fourth feature observed is a high intensity EL signal along the aluminium busbar on cells 4 and 5. This effect is identified as poor electrical contact between the solder strapping and the busbar. This poor contact gives rise to a high series resistance which lowers the collection efficiency of the area, resulting an increase in recombination and the bright EL signal.

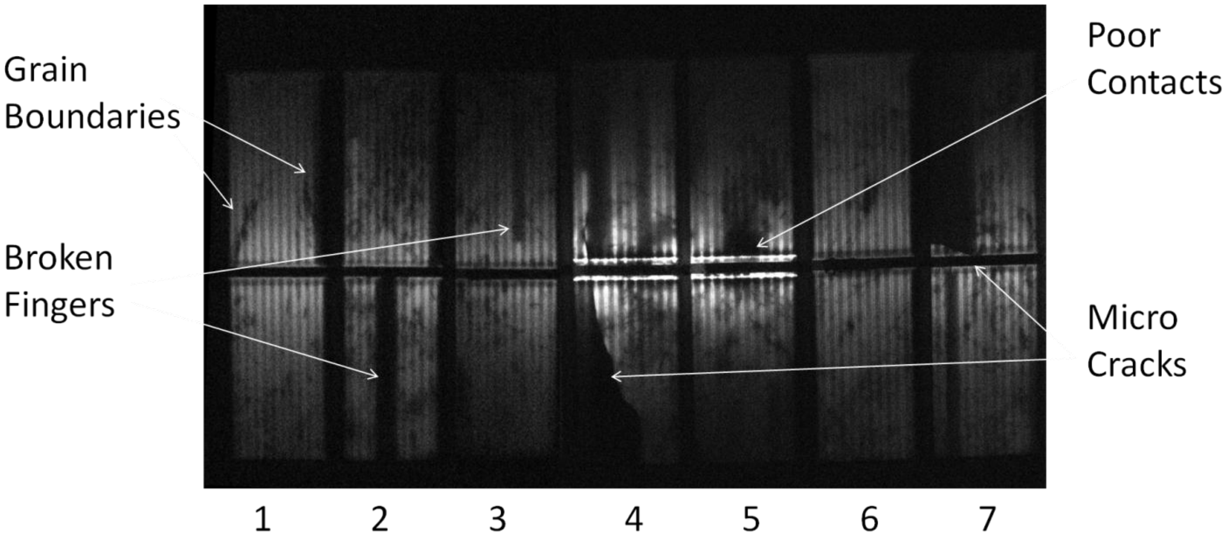

Figure 5.16: Enlarged EL image of cells 1(left) to cell 7(right) with defects indicated.

Figure 5.17 shows an IR image of the module under forward bias. There is a hot spot present over the busbars of cells 4 and 5. When figure 5.17 is compared with figure 5.15 it can be seen that the hotspot occurs in the same area identified as having high series resistance in the EL image. In addition, there are also bubbles visible along the busbar in this region. These bubbles are possibly due to air trapped under the solder straps during the manufacturing process.

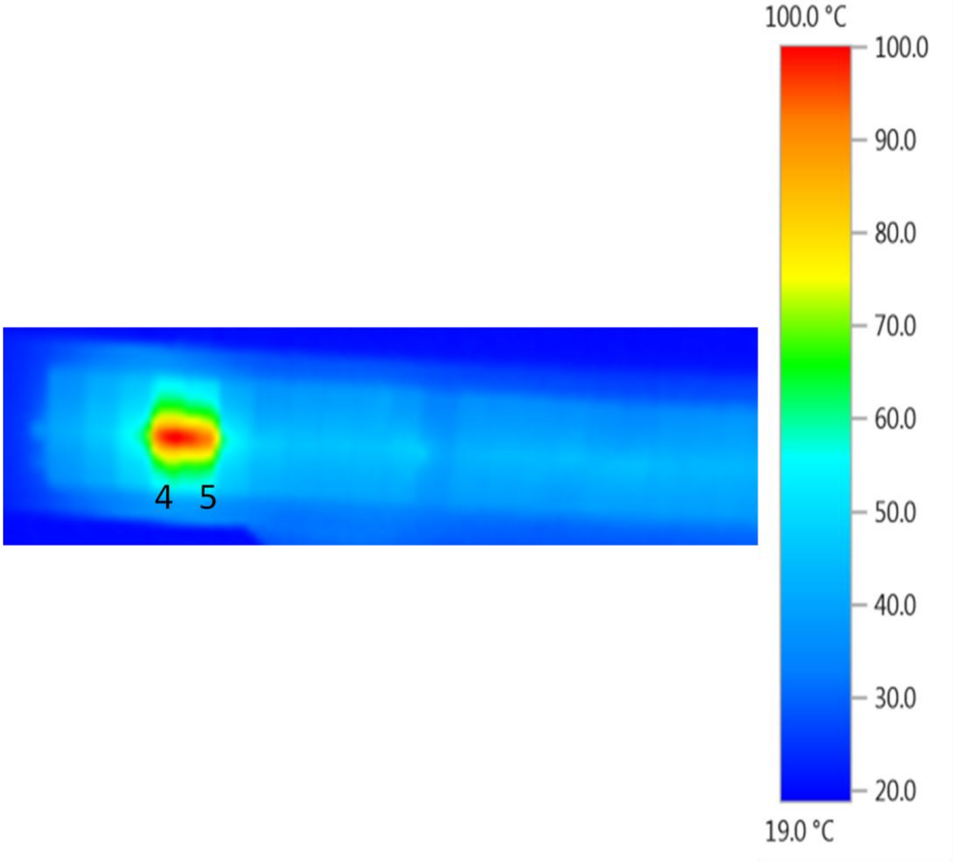

Figure 5.17: Infrared image of module in forward bias with hot spot at cells 4 and 5.

5.4.4. LA-LBIC line scans

The large area LBIC line scan of the module shown in figure 5.18 depicts the photo-induced current along a line across the cells in the module. The line scan was taken across the cells as indicated by the arrow in figure 5.15. As expected from the EL images, cell 12 has a current magnitude of almost zero supporting the argument that the cell is not functioning as a p–n junction. Other cells in the module, namely cells 10, 17 and 27, also produce a low LBIC signal. These cells have a lower EL intensity compared with other cells in the module as seen in figure 5.15. This indicates that these cells have a poor performance, also possibly due to the cell material. The highest LBIC signal is produced by cell 5. This cell was identified in the EL image, figure 5.16, as having poor busbar contacts. This suggests that although the cell is poorly contacted it is still a cell with a good photoresponse. It should be noted, however, that the laser beam probe of the LA-LBIC system, being 660nm, only collects information from within the penetration depth of about 3.5 μm and that defects deeper in the cell are not detected. In addition the LA-LBIC scan is taken at a bias close to short circuit current while the EL images are taken at a forward bias, which could result in the difference in the two results. The LBIC laser current is very small so not affected by the high series resistance observed in the contacts of cell 5 in the EL image.

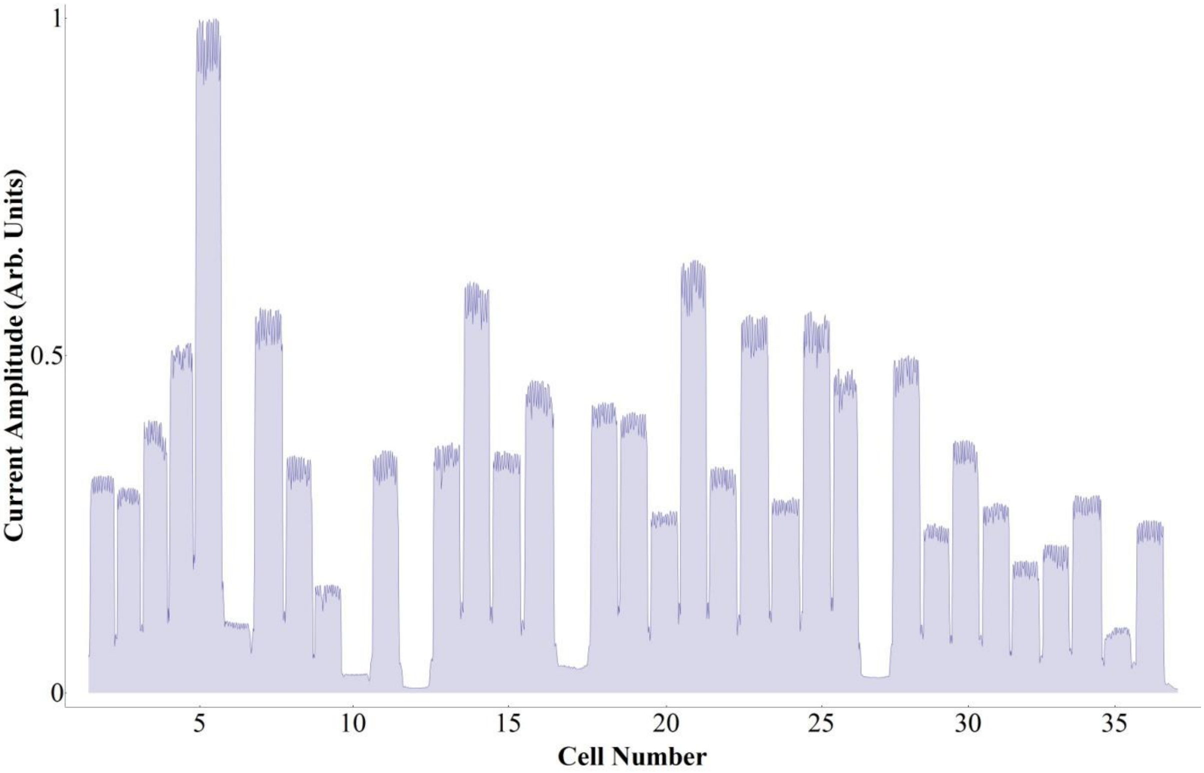

Figure 5.18: Large Area LBIC scan of module.

5.4.5. Worst-case cell determination

When one cell in a series configuration is shaded, it is possible to determine the current contribution of that cell by measuring the drop in the Isc in the I–V curve. The shaded cell is unable to produce current, so if a good current producing cell is shaded it will result in an I–V curve with a low Isc. If the Isc in the I–V curve is unaffected then the cell shaded is a weak current producing cell.

In figure 5.19 the Isc values measured, with one cell shaded, are plotted against the number of the shaded cell. From this graph one can identify the cells with the highest and lowest current contribution within the operating module. Figure 5.20 shows the I–V curves of the whole module and the module with cells 5, 12 and 14 shaded. These cells represent high, low and average photoresponse as measured by LA-LBIC.

Cell 14 is identified as a good cell because when it is shaded the Isc drops from 0.69A to 0.49A. This is the largest current drop compared to the other cells. The I–V curve of the module with cell 14 shaded shows the drop in current as well as a change in the shape of the curve. The I–V curve no longer has the characteristic shape of a diode but approaches the straight line shape of a resistor. The suggestion that this cell is the best cell in the module can be supported by the EL images, where cell 14 has no obvious defects apart from grain boundaries in the cell material. Cell 12 is identified as a poor cell as the Isc is virtually unaffected when it is shaded. The I–V curve shows that shading cell 12 does not severely affect the I–V curve of the whole module. The Voc is decreased by the voltage produced by one cell but otherwise the shape of the curve remains roughly the same as that of the whole module curve.

The I–V curve with cell 5 shaded confirms that it is a low current producing cell due to the poor contacts observed with the EL.

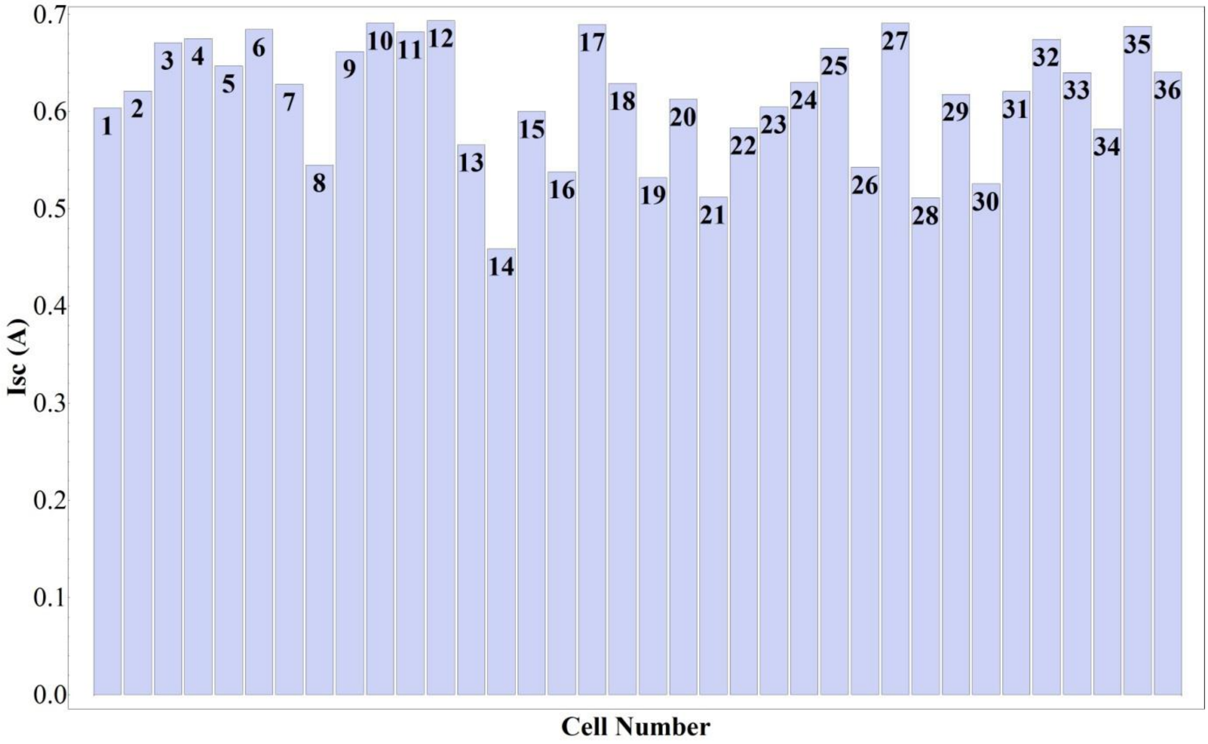

Figure 5:19: The Isc values of the module with one cell shaded plotted against the number of the shaded cell.

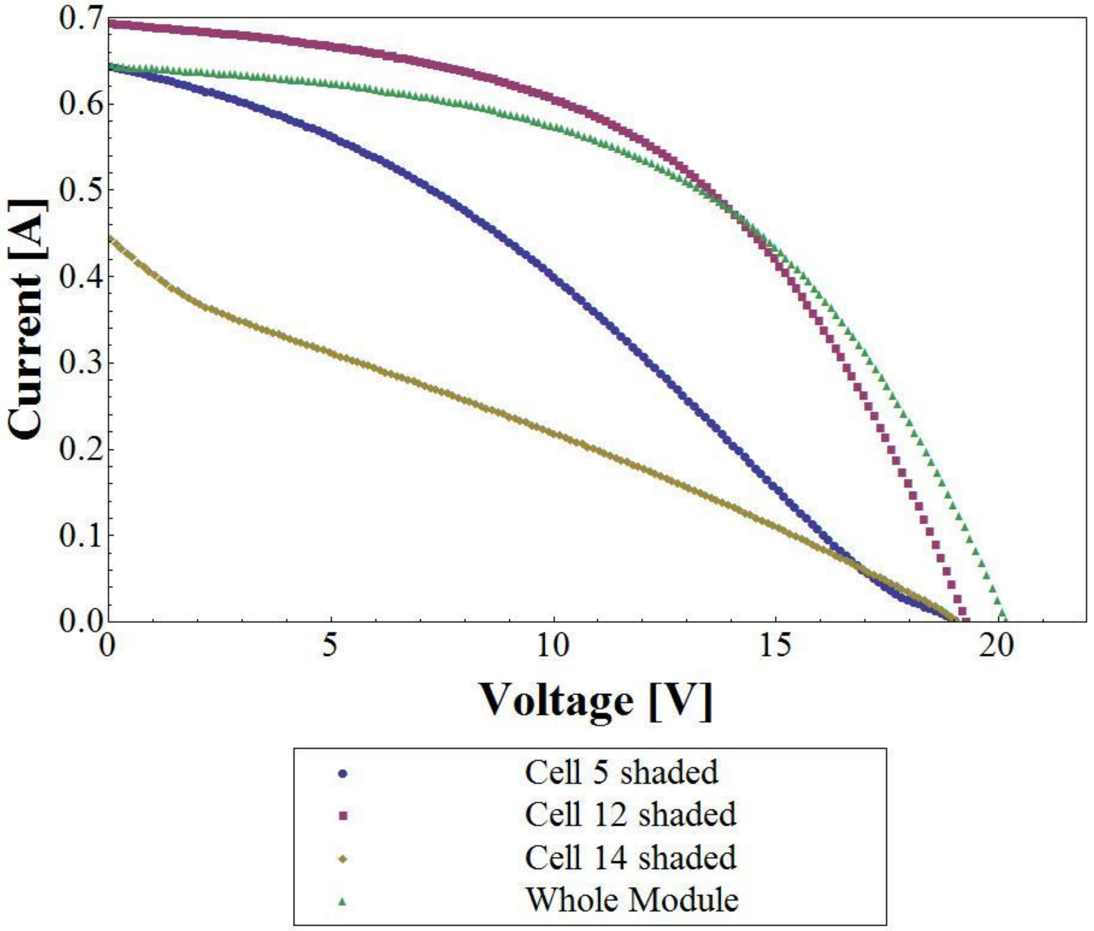

Figure 5:20: I-V Curve of the whole module compared with the I-V curves of the module with cells 5, 12 and 14 shaded.

5.4.6. Discussion of results

There are several techniques for characterising a module and determining the extent of mismatch in that module. I-V curves, parameter extraction, EL imaging, IR Imaging, LA-LBIC techniques were used to characterise this module. The I-V curve indicated performance degradation in the module since the power output was lower than expected. The shape of the curve indicated the effects of parasitic resistances. The extracted parameters also suggested significant parasitic resistances. These resistances were confirmed by the EL image of the module showing high series resistance over the busbars of some cells. These areas corresponded with a hot spot visible in infrared image due to the resistive heating at the busbar. From the I-V curve the current-producing ability of individual cells cannot be determined. An inactive cell can be identified in the EL image as a low intensity signal and will also produce a low current in a LA-LBIC scan and contributes minimal current to the series string as seen when shading that cell in the module. However, when trying to identify the best cells in the module these techniques differ. It cannot be identified from the EL image since a cell with no mechanical damage can have subtle variations in the cell material itself. High current magnitudes in the LA-LBIC scan are related to the photoresponse of the cell material but their scope is limited to the surface region and the penetration depth of the light beam probe. However, by combining these techniques one is able to get a better overall picture of the module than a single technique used in isolation.

5.5. Modules 4 ,5 and 6

5.5.1. Introduction

Modules 4, 5 and 6 are 44 cell single crystalline silicon modules. They all have the same cell type and configuration and thus allow the cell mismatch in the three modules to be compared. Module 4 acts as a reference as it has no visible damage while module 5 and 6 have a grey-white discolouration affecting the majority if the cells. These modules are characterised using I-V curves and EL imaging techniques.

5.5.2. Module 4 (Reference)

5.5.2.1. Illuminated I-V curves

Module 4 has no visible damage or degradation as discussed in section 4.4.4 and seen in the optical image of the module, figure 4.9(a). The I-V curve of the reference module with bypass diodes and the individual strings is shown in figure 5.21. The I-V curve shows that the performance of the two strings is evenly matched. From the I-V curve it is clear that the voltages of the two strings add at equal currents, resulting in the I-V curve of the whole module which does not show any signs of mismatch.

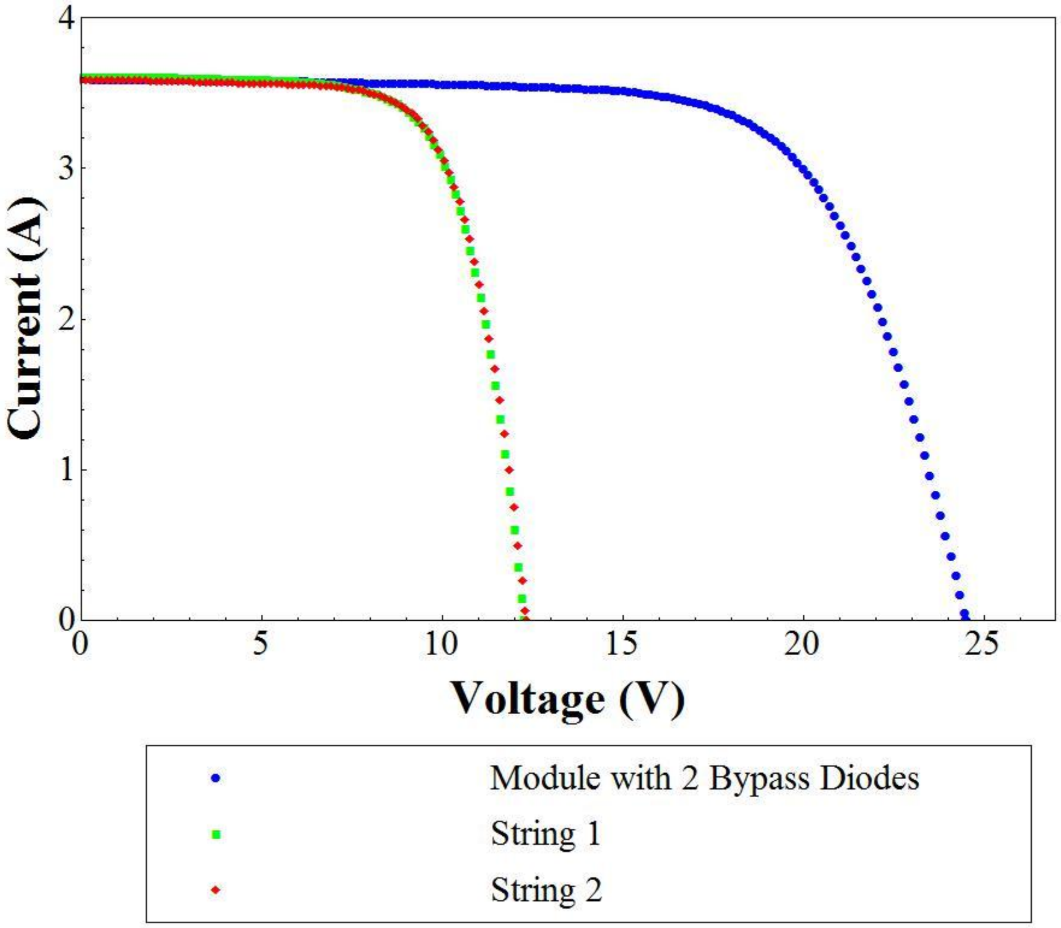

Figure 5.21: I-V curves of reference module and the individual strings.

5.5.2.2. EL Images

The EL image of the reference module, figure 5.22(a), corroborates the results of the I-V curve as there are no large severely damaged areas visible and the two cell strings are evenly matched. Common cell defects that affect small areas can be detected in the module and are highlighted in figure 5.22(b). Finger defects in the module are indicated in figure 5.22(b). A break across the finger results in the area between the fingers of the cell having decreased electrical contact and appearing darker in the EL image. Finger defects occur in the majority of the cells in this module possibly due to problems in the manufacturing process. Micro-cracks in the module are highlighted in figure 5.22(b). The micro-cracks indicated by label (ii) are visible in the EL but do not cause inactive areas in the cells. These are class A micro-cracks [40]. This type of crack most likely occurred during the manufacturing process and would not be detected in the I-V module testing process as they do not result in a significant drop in cell performance. With time and thermal cycling these cracks have the potential to spread and result in performance degradation. The micro-crack labelled (iii) is a class C [40] micro-crack since it completely removes an area of the cell from electrical contact resulting in a completely dark area in the EL image. This inactive area indicates that this area of the cell has poor photoresponse lowering the performance of the cell.

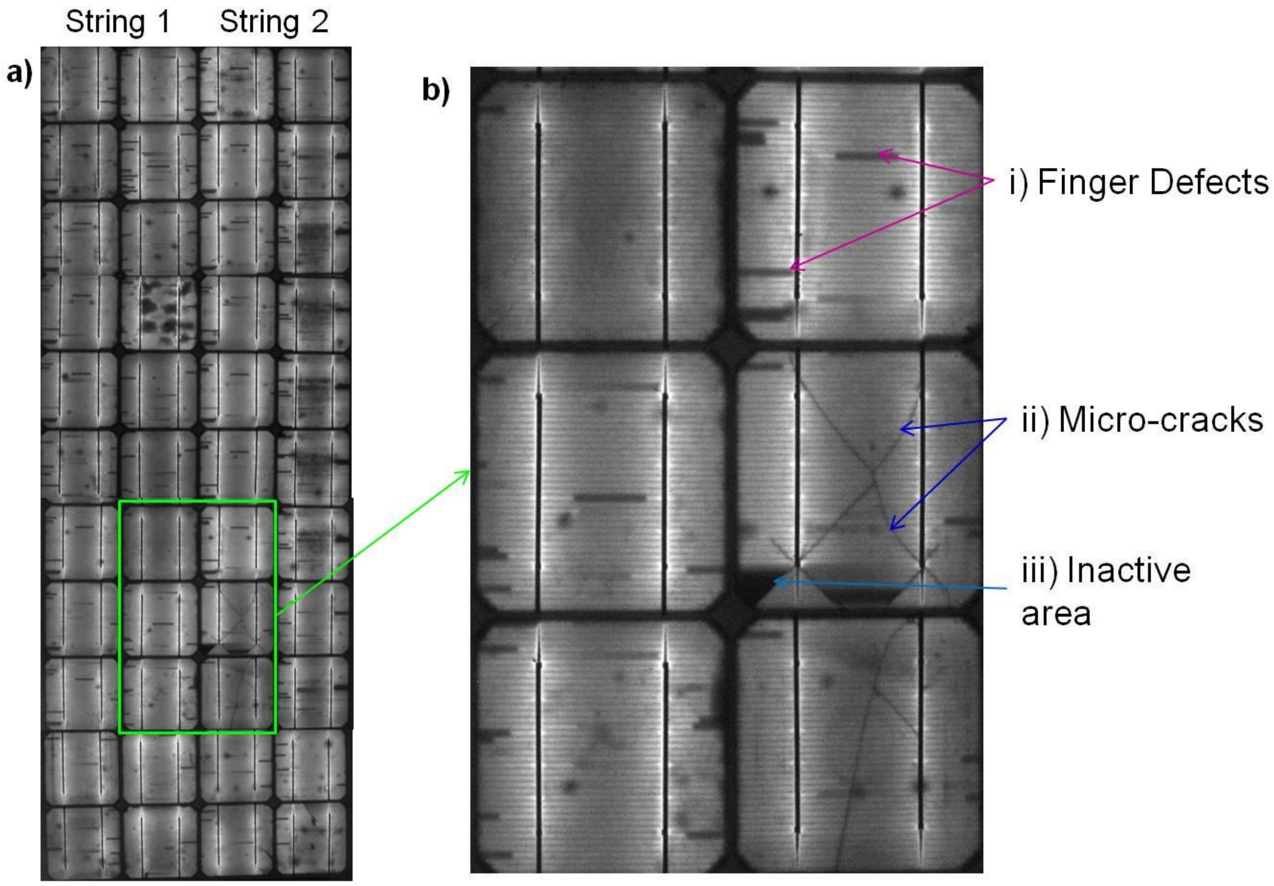

Figure 5.22: The EL image of (a) the entire reference module with (b) a section enlarged to illustrate common cell defects.

5.5.3. Module 5

5.5.3.1. Outdoor I-V curves

The I-V curve of module 5 and the cell strings is shown in figure 5.23. String 1 has a lower Isc and power output than string 2. This results in current mismatch between the two strings which causes the bypass diode across string 1 to be activated. The step in the I-V curve of the module is due to the activation of the bypass diode when the current mismatch between the two strings results in the reverse biasing of string 1 by greater than the activation voltage of the bypass diode.

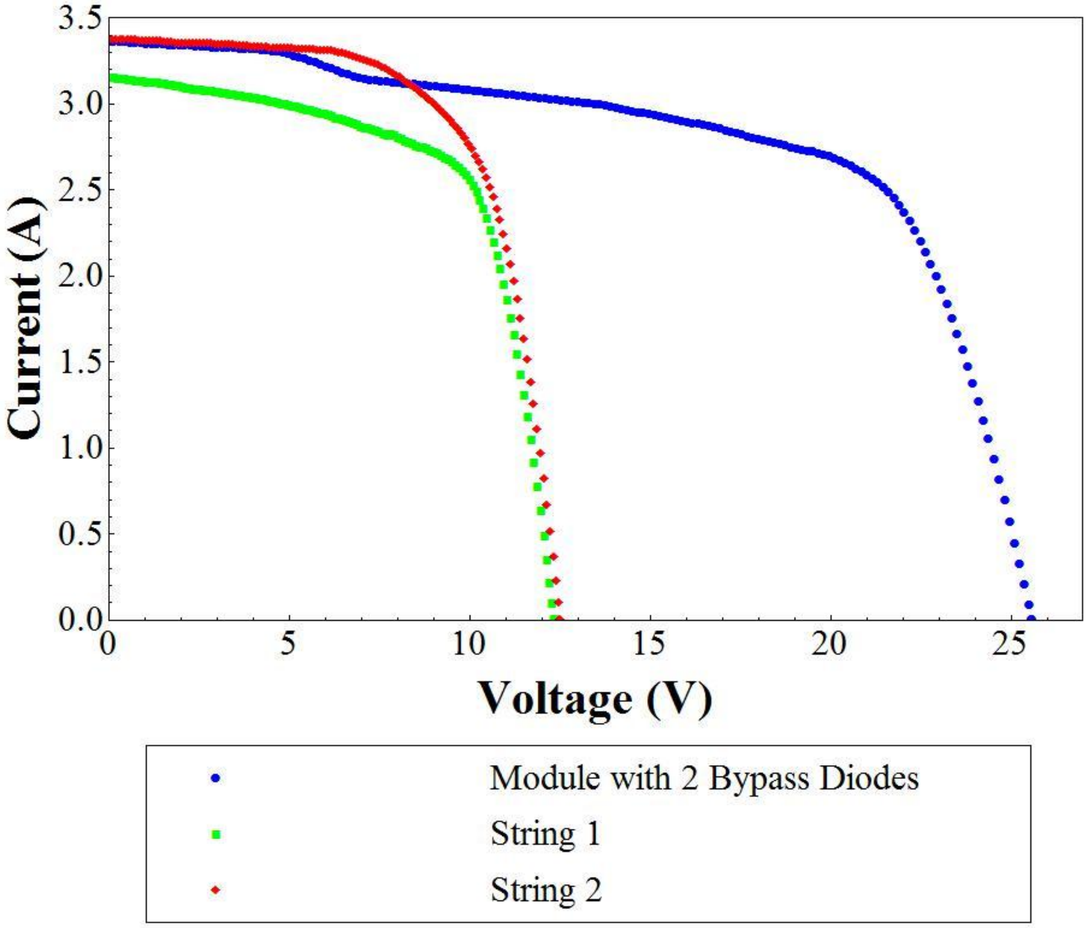

Figure 5.23: I-V curve of Module 5 and the individual strings.

5.5.3.2. EL Images

The EL image of module 5 is shown in figure 5.24(a) with several defects highlighted and enlarged in figures 5.24(b), (c) and (d). In figure 5.24(b) the effect of the degradation in the anti-reflective coating is visible in the EL image. Areas that have been discoloured correspond with areas of lower EL signal intensity. This could mean that the cell material in these regions is damaged or that the discolouration of the anti-reflective coating blocks the EL signal from being detected. Either way this degradation results in poor photoresponse and, ultimately, performance degradation in the affected areas. Figure 5.24(c) highlights a cell where a micro-crack has prevented electrical contact between the one side of the cell and the other. The high current density in the one third of the cell results in a higher intensity EL signal. Figure 5.24(d) highlights the area of the module where several cells and been cracked. These cracks cause large inactive areas which result in lower performance of these cells. The cause of this damage is most likely due to mechanical damage as the cracks line up with scratches that have been observed along the back surface of the module. The EL images explain the mismatch seen in the two strings as there are more damaged cells in string 1 than in string 2.

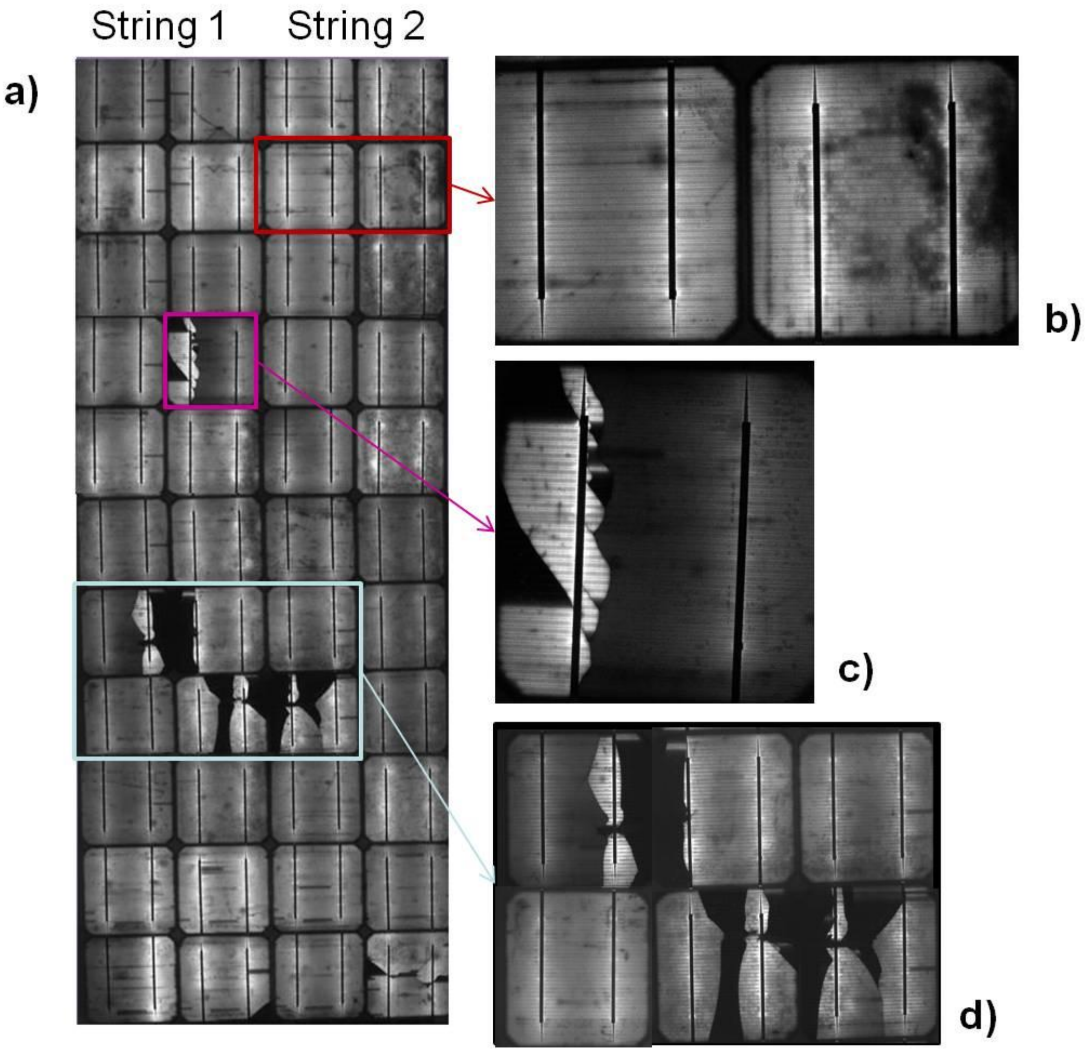

Figure 5.24: The EL image of (a) module 5 with EL images of defects enlarged b) degradation of anti-reflective, c) micro-cracks resulting in high current density and d) micro-cracks resulting in inactive areas.

5.5.4. Module 6

5.5.4.1. Outdoor I-V curves

The I-V curve of module 6 and the individual strings is shown in figure 5.25. The strings both have similar current output but the shape of the I-V curve of string 1 indicates the significant influence of the shunt resistance of one string on the I-V curve of the module. In an ideal solar cell the shunt resistance is infinite. The shunt resistance results in the slope of the graph changing in the region between short circuit and the maximum power point or “knee” of the I-V curve.

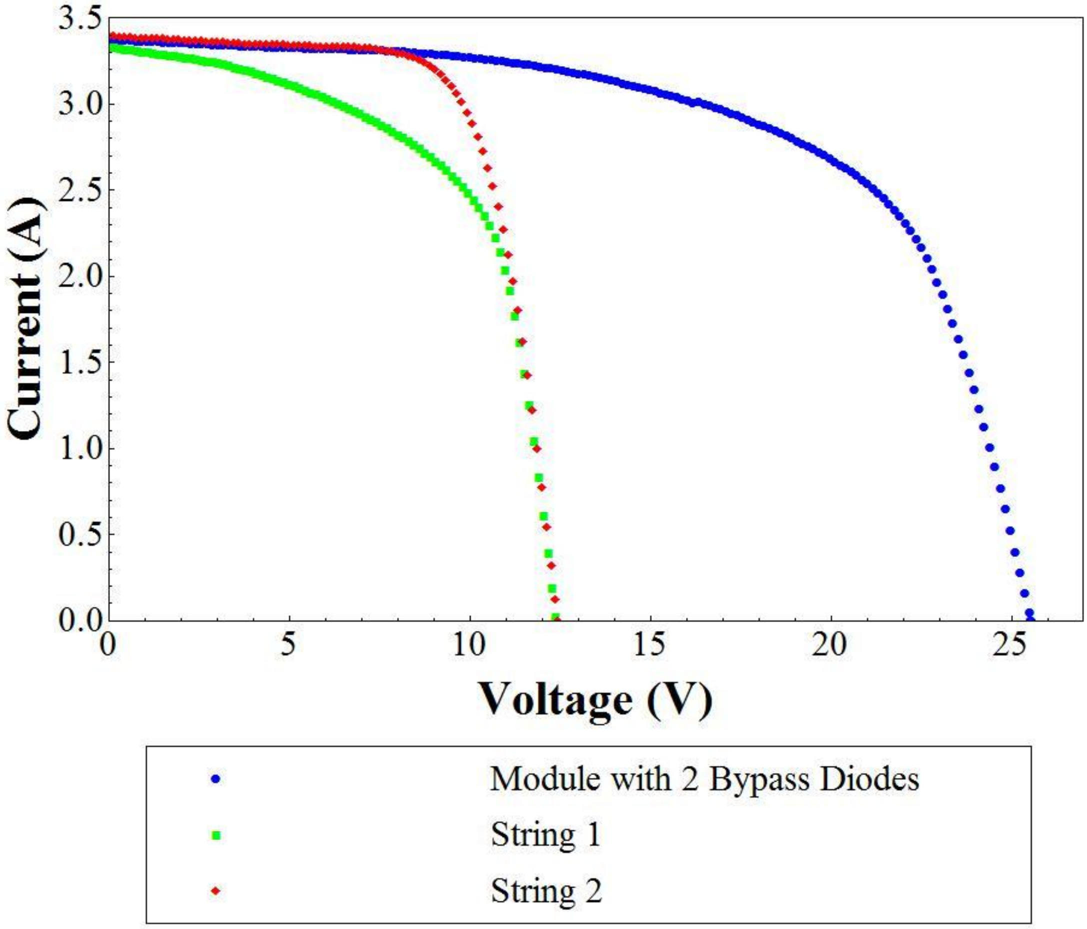

Figure 5.25: I-V curve of module 6 and the individual strings.

5.5.4.2. EL Images

The EL image of module 6 is shown in figure 5.26(a). Highlighted in the figure 5.26(b) is the most damaged cell in the module. This cell has cracks which result in large inactive areas which lower the performance of the module. The I-V curve of the string containing this cell suggests that the damage to this cell results in lowering of the shunt resistance of the cell, causing more photogenerated current to bypass the cell’s diode junction.

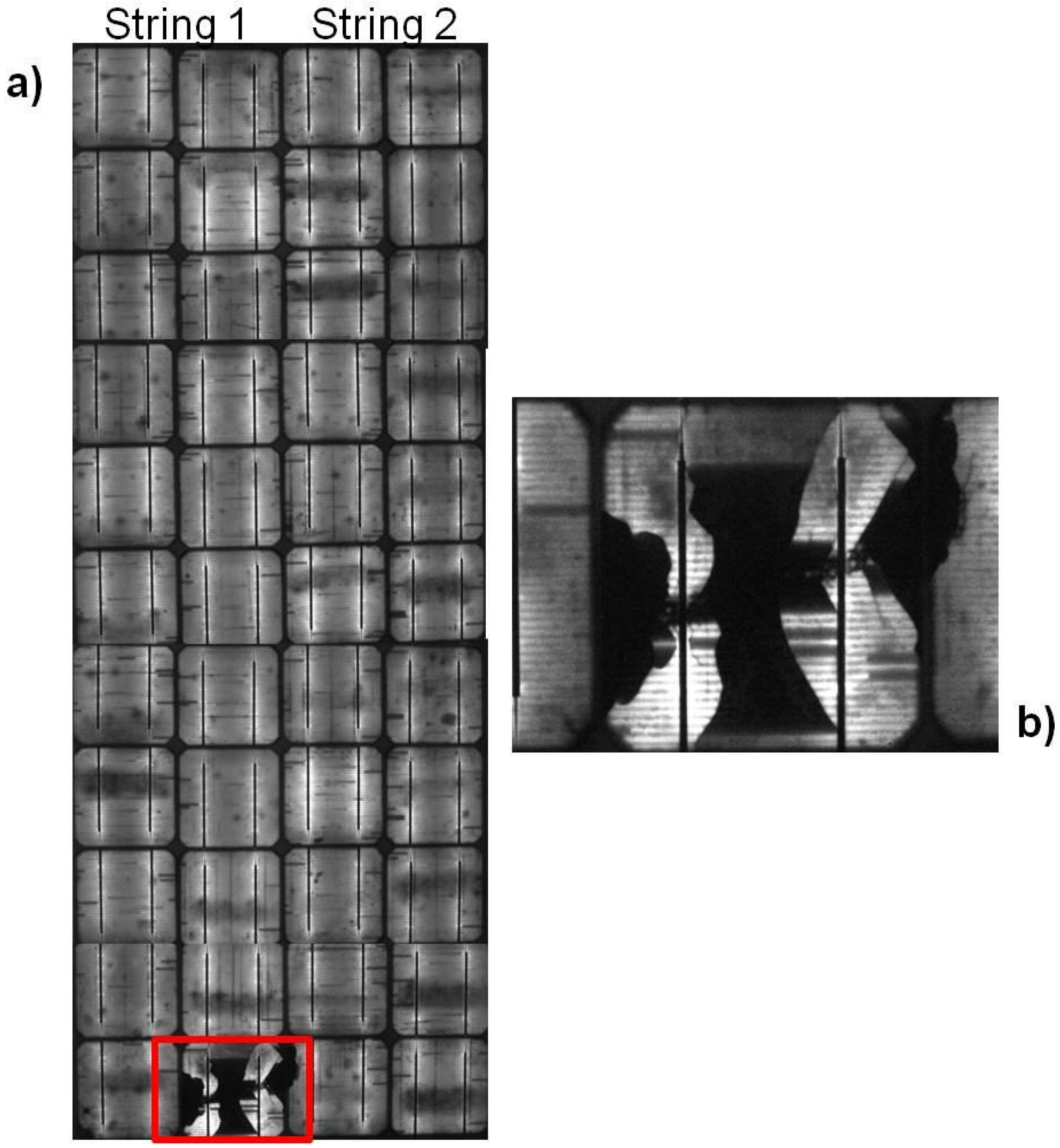

Figure 5.26: The EL image of the (a) entire module 6 with (b) the most damaged cell highlighted.

5.5.5. Comparison of Modules 4, 5 and 6

5.5.5.1. Outdoor I-V curve

Figure 5.27 shows the I-V curves of modules 4, 5 and 6 compared without the bypass diodes included in the configuration. The reference module 4 has the best power and current output as expected and has a measured P_{max} of 63W. The variation from the specified 65W is due to the defects that were only visible in the EL image.

The I-V curves of module 5 and 6 look very similar even though module 5 has a greater number of severely cracked cells. Since these I-V curves were taken without bypass diodes the current output is limited by the weakest cell in each string and this implies that the weakest cell in both modules have a similarly poor photoresponse.

The shape of the I-V curve in the low voltage region before the knee is influenced by the shunt resistance in the module. The slope present in this region of the I-V curves of modules 5 and 6 indicates that losses occur due to shunt resistances.

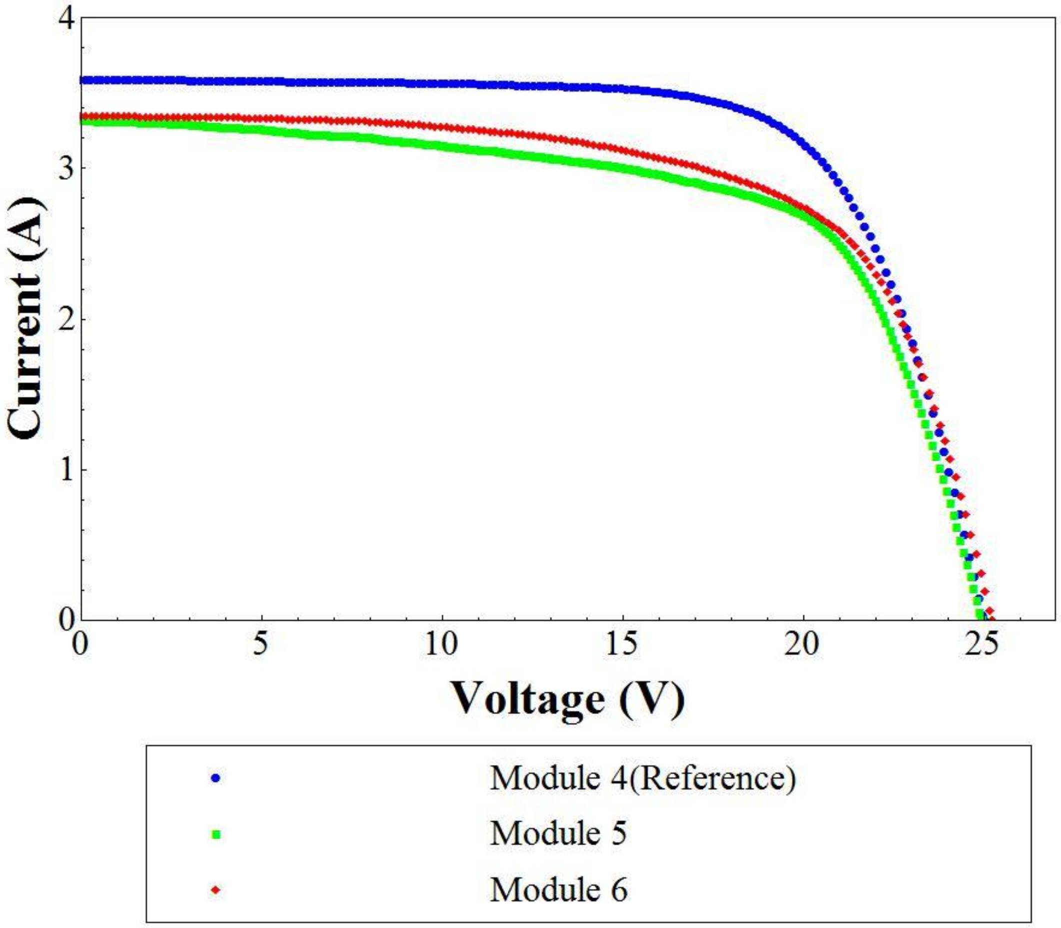

Figure 5.27: The I-V curves of modules 4, 5 and 6 without bypass diodes.

The PSO extracted parameters for a cell in the three modules are listed in table 5.7. The parameters confirm the observation made from the I-V curves as module 5 has the lowest shunt resistance corresponding with the steeper slope in the low voltage region of the I-V curve. Modules 5 and 6 have higher series resistance due to the module degradation.

Table 5.7: The extracted series and shunt resistances for Modules 4, 5 and 6.

	Rs (Ω)	Rsh (Ω)
Module 4	0.13	99.
Module 5	0.23	760
Module 6	0.29	816

5.5.5.2. Dark I-V curves

The Dark I-V curve of module 4, 5 and 6 are shown in figure 5.28. The curves of the three modules are similar in the high voltage region above the inflection point. This region is affected by the series resistance indicating the modules have series resistance values are in a similar range. The three curves vary in the low voltage region governed by shunt resistance. Module 4 has the highest shunt resistance value of the three modules which is expected considering the lack of damage to the module and resulting losses through shunting mechanisms. However modules 5 and 6 have lower shunt resistance value indicating greater losses from shunting. This was also observed in the illuminated I-V curves of the modules.

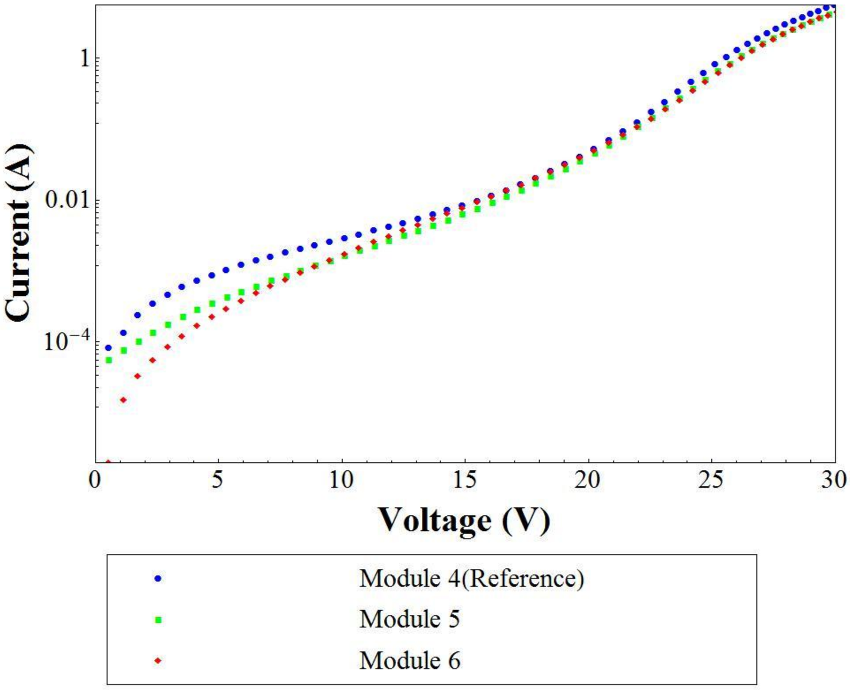

Figure 5.28: Dark I-V curves of modules 4, 5 and 6.

5.5.6. Discussion of results

Electroluminescence is used as a fast and effective technique in identifying defects and degradation in these three PV modules. It is able to quickly detect cell defects that would not be detected in visual module inspections. These defects can account for a decrease in the module performance in a module that would otherwise appear to be undamaged such as module 4. Defects in a module can be detected at the manufacturing stage enabling manufacturers to increase the reliability of PV modules. Cell mismatch can be observed in the I-V curves of a module but the EL image of the module allows the identification of cell defects and the exact nature of the defects may also be determined.

The EL images of module 5 clearly indicate the causes of the cell mismatch which is seen in the I-V curve of the module. The cracked cells and inactive areas in one string result in a lower current output and lower shunt resistance which is visible in the I-V curve. Similarly, a damaged cell in module 6 results in a lower current output and shunt resistance visible in the I-V curve of the module.

The comparison of the dark and light I-V curves of the modules allow the effects of the damaged cells and degradation of modules 5 and 6 on the module performance to be seen. The degradation in the anti-reflective coating results in lower EL intensity in the affected areas. Modules 5 and 6 both are more affected by shunt resistances than module 4.

Correlation of the I-V characteristics and EL images allows the lower power output of a module compared to the manufacturer’s specification to be fully explained.

5.6. Conclusions

The characterisation of PV modules and cell mismatch uses several techniques each highlighting different properties of the modules. The I-V characteristic of a module indicates the current, voltage and power output. A drop in these parameters occurs with time and any damage to the module also results in performance degradation. A tell-tale sign of cell mismatch is a step due to the activation of the bypass diode. This is observed in the I-V curves of modules 1, 2 and 5 indicating that one string is operating at a lower current output causing the string to be reverse biased by a voltage equal to the activation voltage of the bypass diode. Reverse biasing results in hot spots which can be detected using infrared imaging techniques. An observed hot spot in a module gives a good indication of damage in that cell which can be confirmed using EL imaging. In module 3 a hot spot over two cells is determined by EL imaging to be caused by poor contacts to the cell. EL imaging is used successfully to identify cell defects which cause mismatch in a module. LA-LBIC techniques are used to give an indication of the photoresponse of the cells in a module. The results and conclusions of the different modules will be compared and summarised in the following chapter.

Chapter 6

Summary

Cell mismatch occurs in a PV module when the cells in the module do not produce the same current output. The lower performance of a weak cell can be due to shading, accumulation of dirt or damage. A shaded cell receives less incident irradiance than the other cells in the module which results in it producing smaller photogenerated current. This shading can be caused by shadows falling on a module or from degradation in the module's encapsulant. A cell can be damaged due to micro-cracks which prevent electrical contact between areas of the cell. If a cell is producing less current than the other cells in the series string it is reverse biased under short circuit conditions which may result in hot spot formation. Hot spots cause further damage to the module as an area of localised heating degrades the cell material and the encapsulant resulting in delamination. Hot spots can be prevented by the use of bypass diodes which are connected in parallel over the strings and activated when the string is reverse biased by more than the activation voltage of the bypass diode. The activation of the bypass diode results in an increase in the short circuit current of the module.

The modules used in this study each have cell mismatch resulting from different causes and with varying degrees of degradation of the performance of the module. The modules were characterised using several different characterisation techniques.

The current-voltage characteristic curve is measured experimentally and provides information about the performance parameters of a module such as current, voltage and power output. Cell mismatch or damage in a module may be visible in the I-V curve of the module as the activation of bypass diodes results in a step in the I-V curve. The I-V curve can be modelled using the one- or two-diode equation which then allows parameters such as series and shunt resistance to be determined. The series and shunt resistances affect the shape of the I-V curve and limit the current generation capability of the module. The I-V characteristics can also be determined in dark conditions by applying a voltage and measuring the current. This removes the effect of variations in the irradiance and the series and shunt resistance can be evaluated. The current generation ability of individual cells can be determined by measuring an I-V curve while shading each cell in turn. This technique, called worst-case cell determination, identifies a poor current producing cell by the minimal effect shading it has on the module's I-V curve.

Electroluminescence (EL) imaging is very effective in identifying cell mismatch in PV modules as cracks, finger defects and material variations are quickly and non-destructively identified. When a silicon solar cell is forward biased, carriers are injected into the junction and EL radiation is emitted when the carriers recombine. The EL is not in a visible region of the electromagnetic spectrum so a cooled CCD camera is used to detect the signal. The rate at which the carriers recombine and the intensity of the EL signal are related to material properties, such as minority carrier lifetime and diffusion length. Micro cracks can be clearly identified and can be a significant cause of performance degradation if the cracks develop which may result in areas of the cell without electrical contact. Thermal imaging is effectively used to identify hot spots in the module which can be confirmed as damaged cells by using EL imaging.

Large-area light beam induced current (LA-LBIC) line scans give an indication of the relative photoresponse of the cells in the module. This is done by measuring the current generated by the module in the dark as a laser beam is scanned across it. The measured current can be attributed to the specific cell area that is illuminated by the laser beam and thus the relative photoresponse map of each cell can be determined. The laser beam has a spot size of about 1mm and a penetration depth of 3.5μm. Due to the shallow penetration depth only the effects of shallow defects are detected. However, the LA-LBIC system is not able to identify specific cell defects or to raster scan entire cells and is rather used as a means of comparing the relative photoresponse of cells in a module.

Six defective modules are evaluated in this study. Module 1 has sustained mechanical damage resulting in cracks and delamination of cells in two of the three strings. The strings affected have a lower current and power output then the unaffected string resulting in cell mismatch. The current mismatch is evident in the I-V curve of the module where a step is triggered by the activation of the bypass diode. The thermal image indicates the hot spot over the damaged cells which has caused the delamination and cracks to spread.

In module 2 the encapsulant has delaminated around the edges of the modules allowing air and moisture to infiltrate between the cell material and encapsulant layer. The LA-LBIC line scans of the module confirm that the delamination, visible as a grey-white discolouration, lowers the photoresponse in the affected areas. The delamination partially shades these areas lowering the current generation potential of the cells on the edges of the module. This results in a slight current mismatch between the two strings visible as a bypass diode activation step in the I-V curve of the module. The cells affected by the delamination have a lower intensity EL signal confirming the partial shading of the cells and the lower photoresponse of the affected areas. The EL image also reveals micro cracks in the cell material which do not significantly affect the power output of the module but could with time result in more severe damage. The damage to module 2 could be prevented by careful lamination and module construction techniques as once moisture and air are allowed to infiltrate the module performance will significantly degrade.

Module 3 is a custom-made laminate with 36 multi-crystalline silicon cells. The module configuration is such that bypass diodes are not used so the cell mismatch in the module has a significant effect on the module performance. The EL imaging of the module allowed weak current generating cells and performance limiting features like micro cracks and poor contacts to be identified. Poorly soldered contacts with high series resistance gave a reason why some cells were identified in the LA-LBIC line scan with high photoresponse but according to the worst-case cell determination method were poor current generating cells. Inactive cells were also identified as cells with very low intensity EL signal. The I-V characteristic of the module indicated the lowered performance and the current losses due to series resistance. The poorly soldered contacts in a series connected string module can contribute significantly to the performance degradation of the module.

Modules 4, 5 and 6 all have the same cell configuration and cell material which allows the degradation in the modules to be compared. Module 4 serves as a reference module as it has no visible damage and the EL images indicate no severely damaged cells. Modules 5 and 6 have a visible degradation in the anti-reflective coating that contributes to a lower module performance. The EL image showed cracked cells also contributing to lower current generation of the modules. Module 5 had several severely cracked areas resulting in cell mismatch visible as a step in the I-V curve. The parameters extracted from these I-V curves show that degradation in the cell material of module 5 and 6 has resulted in lower shunt resistance limiting the current generation of the module.

This study has shown the effects of cell mismatch on the performance and I-V curves of the PV modules. The different causes of cell mismatch are discussed and modules with different cell configuration and damage are characterised. The characterisation techniques used on each module provide information about the photoresponse, current generation, material properties and cell defects. A comprehensive understanding of these techniques allows the cell mismatch in the modules to be fully characterised.

Chapter 7

References

[1] M.A. Green, *Solar Cells.* (Artech House, Boston, 1992).

[2] BP, 2011. Statistical Review of World Energy 2011. BP, http://www.bp.com/sectionbodycopy.do?categoryId=7500&contentId=7068481S, Accessed: 19 Dec. 11.

[3] E.L. Meyer, E.E. van Dyk, "Assessing the reliability and degradation of PV module performance parameters", (IEEE Transactions on Reliability, 53, No.1, March 2004).

[4] J. Decker, "Performance of 170 grid connected PV plants in northern Germany-analysis of yields and optimization potentials." (Solar Energy 59 1997) 127-133.

[5] R.J. Overstraeten, R.P. Mertens, Physics, Technology and Use of Photovoltaics. (Adam Hilger, Bristol, 1986).

[6] J. Nelson, *The physics of Solar Cells*,(Imperial College Press, London, 2003).

[7] W. Shockley and W. T. Read, " Statistics of the Recombination of Holes and Electrons", Physics Review 87,No. 5, 835-842 (1952)

[8] J.W. Bishop, "Computer simulation of the effects of electrical mismatches in photovoltaic cell interconnection circuits," Solar Cells 25, 73-89 (1988).

[9] M.C. Alonso-Garcia and J.M. Rui, "Analysis and modelling the reverse characteristic of photovoltaic cells", Solar Energy Materials & Solar Cells 90, 1105-1120(2006).

[10] V.Quasching, R. Hanitsch, "Numerical simulation of current-voltage characteristics of photovoltaic systems with shaded cells," Solar Energy 56, No. 5, 513-520 (1996).

[11] M.A. Green, K. Emery, Y. Hishikawa and W. Warta, " Solar Efficiency tables(version 36)", Progress in Photovoltaics: Research and Applications 18,346-352 (2010)

[12] J. A. Mazer, Solar Cells: An Introduction to Crystalline Photovoltaic Technology. (Kluwer Academic Pub, Boston, 1996).

[13] E.E. van Dyk, B.J. Scott, E.L. Meyer and A.W.R. Leitch, "Temperature dependence of performance of crystalline silicon photovoltaic modules," South African Journal of Science 96, 198-200 (2000).

[14] M. Chegaar, Z Ouennought, A. Hoffmann, "A new method for evaluating solar cell parameters," Solid-State Electronics 45, 293-296 (2001).

[15] V.Quasching, R. Hanitsch, “Numerical simulation of current-voltage characteristics of photovoltaic systems with shaded cells,” Solar Energy 56, No. 5, 513-520 (1996).

[16] S. Silvestre, A. Boronat, A Chouder, “ Study of bypass diodes configuration on PV modules,” Applied Energy 86, 1632-1940 (2009).

[17] M.K. Munji, W. Okullo, E.E. van Dyk, and F.J. Vorster, “Local device parameter extraction of a concentrator photovoltaic cell under solar spot illumination,” Solar Energy Materials and Solar Cells 94, 2129–2136 (2010).

[18] R.C. Eberhart, J. Kennedy, “ A new optimizer using particle swarm theory,” In the proceeding of the Sixth International Symposium on Micro Machine and Human Science, Nagoya, Japan, 4-6 Oct 1995, pp 39-43.

[19] E. Q. B. Macabebe, Investigation of device performance parameters of photovoltaic devices, Ph.D. thesis, Nelson Mandela Metropolitan University (2009).

[20] M. K. Munji, Characterisation of concentrator solar cell devices and materials using Light-Beam Induced Current measurements, Ph.D. thesis, Nelson Mandela Metropolitan University (2011).

[21] D. L. King, J. K Dudley, W. E. Boyson, “PVSIM: A Simulation Program for Photovoltaic Cells, Modules, and Arrays,” In the proceedings of the 25th IEEE PVSC, Washington, DC, May 13-17, 1996

[22] C. Honsenberg and S. Bowden, “Photovoltaic CDRom,” (Accessed on 08/09/2011), http://pveducation.org/pvcdrom/modules/mismatch-for-cells-connected-in-series

[23] E.L. Meyer, E.E. van Dyk, “Assessing the reliability and degradation of photovoltaic module performance parameters,” IEEE Transactions on Reliability 53, 83-92(2004).

[24] F. J. Vorster and E.E. van Dyk, “Current-Voltage characteristics of high-concentration, photovoltaic arrays,” Progress in Photovoltaics: Research and Applications 13, 55-66(2005).

[25] N. Martin, M.C. Alsonso-Garcia, F. Chenlo, P. Sánchez-Friera, “ Electrical and thermal characterisation of PV modules under partial shadowing”, In the proceedings of the 23rd EU PVSEC, Valencia, Spain,1-5 September, 2008

[26] M.C. Alonso-Garcia and J.M. Rui, “Analysis and modelling the reverse characteristic of photovoltaic cells”, Solar Energy Materials & Solar Cells 90, 1105‑1120(2006).

[27] W. Herrmann, W. Wiesner, W. Vaaben, “ Hot Spot investigations on PV modules-New concepts for a test standard and consequences for module design with respect to bypass diodes,” in the proceedings of the 26th IEEE Photovoltaic Specialists Conference, Anaheim, California (1997) pp. 1129–1132.

[28] R. Hussein, D. Borchert, G. Grabosch, W.R. Fahrner, “ Dark I-V-T measurements and characteristics of (n) a-Si/ (p) c-Si heterojunction solar cells,” Solar Energy Materials & Solar Cells 69, 123-129 (2001)

[29] J. Carstensen, G. Popkirov, J. Bahr, H. Föll, " CELLO: an advanced LBIC measurement technique for solar cell local characterization," Solar Energy Materials & Solar Cells 76, 599-611(2003)

[30] P. Vorasayan, T.R. Betts, A.N. Tiwari, R. Gottschalg, "Multi-laser LBIC system for thin film PV module characterisation," Solar Energy Materials and Solar Cells 93, 917–921(2009).

[31] J. Marek, " Light-beam-induced current characterisation of grain boundaries," Journal of Applied Physics 55, 318-326(1984)

[32] N. M. Thantsha, Spatially resolved opto-electric measurements of photovoltaic materials and devices, Ph.D. thesis, Nelson Mandela Metropolitan University (2011).

[33] N. M. Thantsha, E. Q. B. Macabebe, F. J. Vorster, and E. E. van Dyk, "Optoelectronic analysis of silicon cells by LBIC investigation and current-voltage characterization," Physica B 404, 4445–4448 (2009).

[34] C. Donolato, "Theory of beam induced current characterisation of grain boundaries in polycrystalline solar cells," Journal of Applied Physics 54, 1314-1322 (1983)

[35] T. Fuyuki, H. Kondo, T. Yamazaki, Y. Takahashi, Y. Uraoka, " Photographic surveying of minority carrier diffusion length in polycrystalline silicon solar cells by electroluminescence," Applied Physics Letters 86, 262108 (2005)

[36] T. Fuyuki, H. Kondo, Y. Kaji, A. Ogane, and Y. Takahashi, "Analytic findings in the electroluminescence characterization of crystalline silicon solar cells", Journal of Applied Physics 101, 023711 (2007)

[37] P. Würfel, T. Trupke, T. Puzzer, E. Schäffer, W. Warta, S.W. Glunz, " Diffusion lengths of silicon solar cells from luminescence images," Journal of Applied Physics 101, 123110 (2007)

[38] D. Hinken, K. Ramspeck, K. Bothe, B. Fischer, and R. Brendel, "Series resistance imaging of solar cells by voltage dependent electroluminescence," Applied Physics Letters 91, 182104(2007)

[39] T. Fuyuki, A. Kitiyanan, "Photographic diagnosis of crystalline silicon solar cells utilizing Electroluminescence," Applied Physics A. 963, 189-196(2009)

[40] M. Kőntges, I.Kunze, S.Kajari-Schrőder, X.Breitenmoser, B.Bjørneklett, "The risk of power loss in crystalline silicon based photovoltaic modules due to micro-cracks," Solar Energy Materials & Solar Cells 95 (2011) 1131–1137

[41] S. Kajari-Schrőder, I. Kunze, U. Eitner, M. Kőntges, "Spatial and orientational distribution of cracks in crystalline photovoltaic modules generated by mechanical load tests," Solar Energy Materials & Solar Cells 95 (2011) 3054–3059

[42] ImageJ, 2011, ImageJ, Available at http://rsbweb.nih.gov/ij/ [Accessed 22 November 2011]

[43] E.E. van Dyk, J.B. Chamel, A.R. Gxasheka , “Investigation of delamination in an edge-defined film-fed growth photovoltaic module,” Solar Energy Materials & Solar Cells 88, 403-411(2005)

Appendix A

Research outputs associated with this work

A.1 List of Publications

J.L. Crozier, E.E. van Dyk, F.J. Vorster, "Characterization of cell mismatch in a multi-crystalline silicon photovoltaic module", Physica B (2011), Article in Press: doi:10.1016/j.physb.2011.09.090

A.2. National Conferences Attended

55th Annual Conference of the South African Institute of Physics, 27 Sept- 1 Oct 2010, Pretoria.

4th International Conference on Women in Physics, 6-8 April 2011, Stellenbosch.

4th South African Conference on Photonic Materials, 2-6 May 2011, Kariega Game Reserve.

56th Annual Conference of the South African Institute of Physics, 12 July- 15 July 2011, Pretoria.

2nd Postgraduate Renewable Energy Symposium, 17-18 November 2011, Lynedoch.

Appendix B

Appendix B.1: Mathematica Modelling Routine

```
(* Input parameters*)
    Ip1=1.27;
    Ip2=1.0;
    Io1=2.4*10^-10;
    Io2=3.6*10^-6;
    m1=1;
    m2=3.73;
    a=0.005;
    Vbr=-5;
    n=1;
    Rs= 0.016;
    Rp=34;
    k=1.388*10^-23;
    T=298;
    q=1.602*10^-19;
    Vt=(k*T)/q;
(*The interval or step size*)
    inter=0.01;
```

```
(* Determine Voltage at given currents using FindRoot Function*)

    voltage1=Table[0+V/.FindRoot[Ip1

-Io1*(Exp[(V+x*Rs)/(m1*Vt)]-1)

    -Io2*(Exp[(V+x*Rs)/(m2*Vt)]-1)

    -((V+x*Rs)/Rp)*(1+a*(1-(V+x*Rs)/Vbr))^-n

    -x ==0,{V,0.1}],{x,0,5,inter}];

(* Determine voltage for a second cell with a different photogenerated current*)

    voltage2=Table[0+V/.FindRoot[Ip2

    -Io1*(Exp[(V+x*Rs)/(m1*Vt)]-1)

    -Io2*(Exp[(V+x*Rs)/(m2*Vt)]-1)

    -((V+x*Rs)/Rp)*(1+a*(1-(V+x*Rs)/Vbr))^-n

    -x ==0,{V,0.1}],{x,0,5,inter}];



    current=Flatten[Table[x,{x,0,5,inter}]];

    iv1=Transpose[{voltage1,current}];

    iv2=Transpose[{voltage2,current}];

(* Plot the I-V curve of both cells*)

ListPlot[{iv1,iv2}, PlotRange-> {{-1,2},{0,2}}]
```

Appendix B.2: PSO Parameter Extraction

The Particle Swarm Optimization (PSO) was developed as a parameter extraction technique for I-V curves by Macabebe et al. [1]. This technique was further developed Munji et.al.[20]

With the PSO method the parameters of the diode equation are considered a population of potential solutions. The particles search for values of the parameters that best fit the diode equation. The particle moves through the solution space at a velocity (V). After each iteration the particles assess and adjust their position in relation to the position of the other particles. The movement and velocity of the particle is adjusted according to the best solution it has achieved so far (*pbest*) and by the best solutions obtained by the rest of the population (*gbest*). After each iteration the velocity is determined and calculated according to equation B2.1 [1]. The weighing factor (W) allows for global exploration and prevents the solution getting stuck in a local minimum [20].

$$V_i(j+1) = W(j)V_i(j)+c_1r_1(j)[pbest_i(j)- x_i(j)]+c_2r_2(j)[gbest_i(j) - x_i(j)] \qquad \text{A2.1}$$

The first term of the equation is the inertia term, responsible for keeping the particle moving in the same direction. The second term is a cognitive term allowing the particle to "remember" the areas where it experienced good fit. The third term is a social term causing the particle to move towards the area where the rest of the particles have experienced good fit.

The flow chart shows the steps involved in the PSO curve fitting algorithm [20].

References:

[1] E. Q. B. Macabebe, C. J. Sheppard, E. E. van Dyk, "Parameter extraction from I–V characteristics of PV devices", Solar Energy **85**, 12-18(2011).

[2] M. K. Munji, *Characterisation of concentrator solar cell devices and materials using Light-Beam Induced Current measurements,* Ph.D. thesis, Nelson Mandela Metropolitan University (2011).

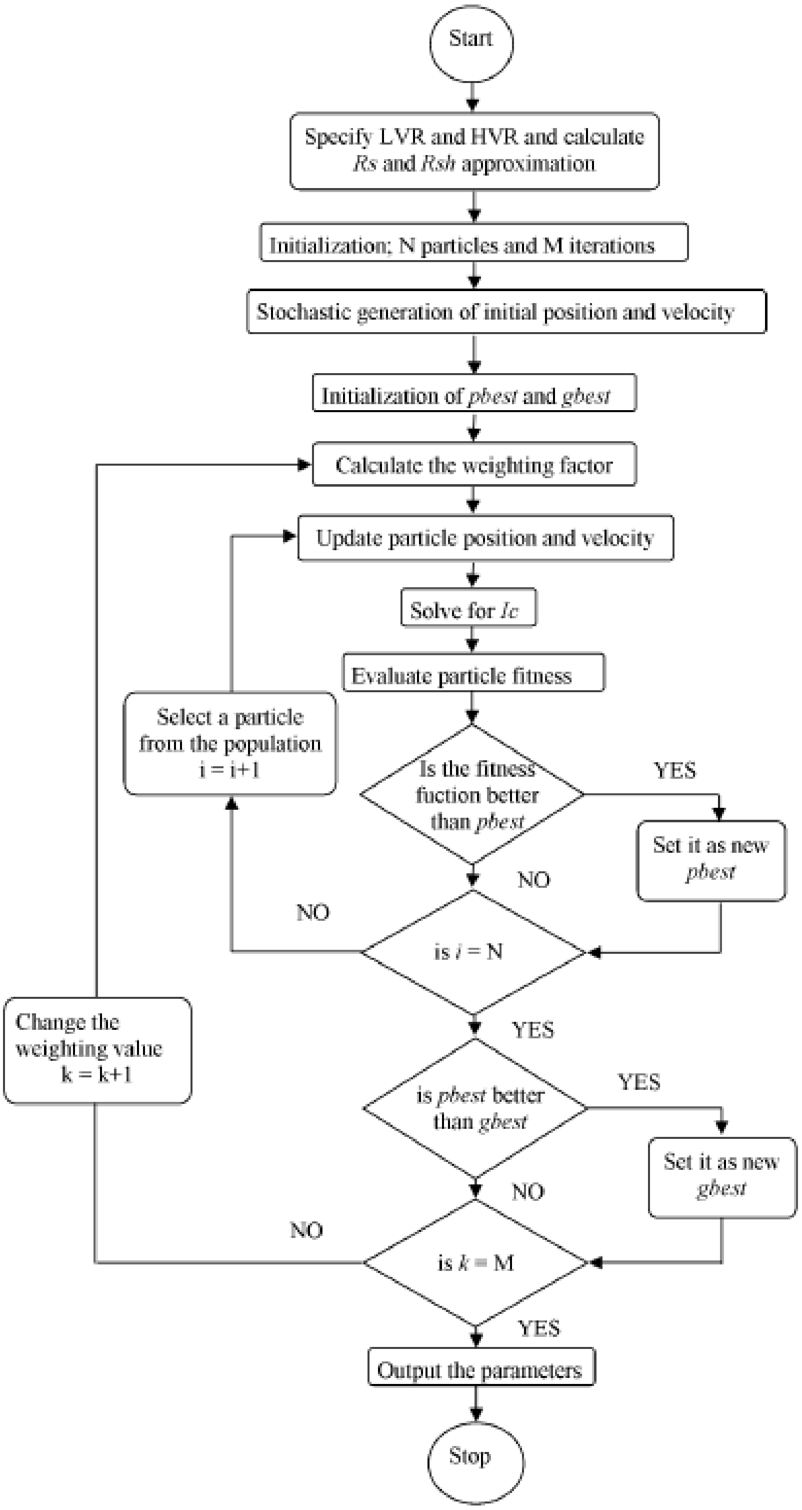

Figure B2.1: The flow chart illustrating the PSO curve fitting process [20].